STRAIN GRADIENT SOLUTIONS OF ESHELBY-TYPE PROBLEMS FOR POLYGONAL AND POLYHEDRAL INCLUSIONS

A Dissertation

by

MENGQI LIU

Submitted to the Office of Graduate Studies of
Texas A&M University
in partial fulfillment of the requirements for the degree of

DOCTOR OF PHILOSOPHY

December 2011

Major Subject: Mechanical Engineering

Strain Gradient Solutions of Eshelby-Type Problems for Polygonal and Polyhedral Inclusions

STRAIN GRADIENT SOLUTIONS OF ESHELBY-TYPE PROBLEMS FOR POLYGONAL AND POLYHEDRAL INCLUSIONS

A Dissertation

by

MENGQI LIU

Submitted to the Office of Graduate Studies of
Texas A&M University
in partial fulfillment of the requirements for the degree of

DOCTOR OF PHILOSOPHY

Approved by:

Chair of Committee,	Xin-Lin Gao
Committee Members,	Amine Benzerga
	Ibrahim Karaman
	Christian Schwartz
Head of Department,	Jerald Caton

December 2011

Major Subject: Mechanical Engineering

ABSTRACT

Strain Gradient Solutions of Eshelby-Type Problems for Polygonal and Polyhedral Inclusions. (December 2011)

Mengqi Liu, B.Eng., Beijing Institute of Technology, Beijing, China;

M.S., Southern Methodist University

Chair of Advisory Committee: Dr. Xin-Lin Gao

The Eshelby-type problems of an arbitrary-shape polygonal or polyhedral inclusion embedded in an infinite homogeneous isotropic elastic material are analytically solved using a simplified strain gradient elasticity theory (SSGET) that contains a material length scale parameter. The Eshelby tensors for a plane strain inclusion with an arbitrary polygonal cross section and for an arbitrary-shape polyhedral inclusion are analytically derived in general forms in terms of three potential functions. These potential functions, as area integrals over the polygonal cross section and volume integrals over the polyhedral inclusion, are evaluated. For the polygonal inclusion problem, the three area integrals are first transformed to three line integrals using the Green's theorem, which are then evaluated analytically by direct integration. In the polyhedral inclusion case, each of the three volume integrals is first transformed to a surface integral by applying the divergence theorem, which is then transformed to a contour (line) integral based on Stokes' theorem and using an inverse approach. In addition, the Eshelby tensor for an anti-plane strain inclusion with an arbitrary polygonal

cross section embedded in an infinite homogeneous isotropic elastic material is analytically solved. Each of the newly derived Eshelby tensors is separated into a classical part and a gradient part. The latter includes the material length scale parameter additionally, thereby enabling the interpretation of the inclusion size effect. For homogenization applications, the area or volume average of each newly derived Eshelby tensor over the polygonal cross section or the polyhedral inclusion domain is also provided in a general form. To illustrate the newly obtained Eshelby tensors and their area or volume averages, different types of polygonal and polyhedral inclusions are quantitatively studied by directly using the general formulas derived. The numerical results show that the components of the each SSGET-based Eshelby tensor for all inclusion shapes considered vary with both the position and the inclusion size. It is also observed that the components of each averaged Eshelby tensor based on the SSGET change with the inclusion size.

ACKNOWLEDGEMENTS

I would like to sincerely express my deepest gratitude to my advisor, Dr. Xin-Lin Gao, for his help, support, patience and guidance throughout of my graduate studies. I have been so fortunate to have an advisor, who taught me how to explore ideas in depth and instilled in me essential qualities of being successful in research work. His knowledgeability and consistence deeply affected me and helped me with completion of the dissertation. I am also thankful to him for suggestions of writing with articulation and accuracy.

I wish to thank my committee members, Dr. Amine Benzerga, Dr. Ibrahim Karaman, and Dr. Cris Schwartz, and Dr. Rashid Abu Al-Rub, for their questions and valuable suggestions on my work.

The completion of the dissertation obviously is not possible without the personal and emotional support either. Thus my sincere gratitude goes to my family members and friends for their love, support, and patience over the last few years. Thank you!

TABLE OF CONTENTS

LIST OF FIGURES

Page

Page

Page

CHAPTER I

INTRODUCTION

Eshelby's equivalent eigenstrain method (Eshelby, 1957) has been widely used in studying the effective properties and elastic fields of heterogeneous materials (i.e., Hill, 1965; Mori and Tanaka 1973; Huang et al., 1994). Eshelby's tensor was originally derived for an ellipsoidal inclusion by using the classical elasticity theory, and the components of this fourth-order tensor depend only on the inclusion shape and the Poisson's ratio of the material (Mura, 1987; Qu and Cherkaoui, 2005). For composites containing nano-sized inclusions, the inclusion size effect becomes significant and needs to be considered in order to provide accurate predictions. Classical elasticity cannot be applied to account for such size effects due to a lack of any material length scale parameter. Hence, Eshelby-type inclusion problems have recently been studied using higher order elasticity theories, including a simplified strain gradient elasticity theory, a micropolar theory, a microstretch theory and a modified couple stress theory (e.g., Gao and Ma, 2009, 2010a, 2010b, 2011; Ma and Gao, 2010, 2011; Cheng and He, 1995, 1997; Liu and Hu, 2004; Ma and Hu, 2006; Zheng and Zhao, 2004).

This dissertation follows the style of Journal of the Mechanics and Physics of Solids.

Closed-form expressions of the Eshelby tensor have been obtained for the spherical, cylindrical, and anti-plane strain circular inclusions embedded in an infinite or finite homogeneous isotropic elastic material and prescribed a uniform eigenstrain and a uniform eigenstrain gradient (Gao and Ma, 2009, 2010a, 2011; Ma and Gao, 2010, 2011). The Eshelby tensor for an ellipsoidal inclusion has also been analytically obtained in terms of one line integral (Gao and Ma, 2010b).

Eshelby's eigenstrain method has also been used to investigate elastic deformations of semiconductor devices induced by quantum dots and quantum wires embedded in the devices. Many quantum dots and quantum wires possess polyhedral shapes and polygonal cross sections and often exhibit the size effect. Hence, Eshelby tensor for polyhedral and polygonal inclusions based on higher-order elasticity theories are needed for accurately describing the elastic responses of the devices embedded with quantum dots and wires. However, existing analytical studies on Eshelby's problems for polyhedral and polygonal inclusions are all based on classical elasticity (e.g., Rodin, 1996; Nozaki and Taya, 1997, 2001; Kaeashita ans Nozaki, 2001; Pan, 2004; Xu and Wang, 2005, 2007a; Zheng et al, 2006; Zou et al, 2010), and the resulting Eshelby tensor cannot capture the inclusion size effect. This motivated the current dissertation work, in which the Eshelby tensor for a polygonal or a polyhedral inclusion embedded in an infinite homogeneous isotropic elastic material is analytically derived using a simplified strain gradient theory which contains a material length scale parameter.

In Chapter II, the Eshelby-type problem of a polyhedral inclusion of arbitrarily shape embedded in an infinite elastic body is analytically solved. The Eshelby tensor is

derived in terms of three potential functions, which, as three volume integrals over the polyhedral inclusion, are analytically evaluated. The volume integral of the Eshelby tensor over the polyhedral inclusion is also obtained in a general form. The numerical results are presented by using the general formulas derived to illustrate the position and inclusion size dependency of the Eshelby tensor for the polyhedral inclusion.

In Chapter III, the Eshelby tensor for an arbitrary shape polygonal inclusion and its area average over the inclusion cross sectional area are analytically derived, which is accompanied by the numerical results based on the newly obtained Eshelby tensor forms.

In Chapter IV, the Eshelby-type anti-plane strain polygonal inclusion problem is analytically solved, and the explicit expressions of the Eshelby tensor components are provided. Numerical results are also presented to illustrate how the Eshelby tensor varies with the position, inclusion size and shape of the polygonal inclusion.

In Chapter V, a summary of the major findings of the dissertation research is provided.

CHAPTER II

STRAIN GRADIENT SOLUTION FOR THE ESHELBY-TYPE POLYHEDRAL INCLUSION PROBLEM

2.1 Introduction

Eshelby's (1957, 1959) solution for the problem of an infinite homogeneous isotropic elastic material containing an ellipsoidal inclusion prescribed with a uniform eigenstrain is a milestone in micromechanics. The solution for the dynamic Eshelby ellipsoidal inclusion problem was obtained by Michelitsch *et al*. (2003), which reduces to the Eshelby solution in the static limiting case. Both of these solutions are based on classical elasticity. Recently, the Eshelby ellipsoidal inclusion problem was solved by Gao and Ma (2010b) using a simplified strain gradient elasticity theory, which recovers Eshelby's (1957, 1959) solution when the strain gradient effect is not considered.

A remarkable property of Eshelby's (1957) solution is that the Eshelby tensor, which is a fourth-order strain transformation tensor directly linking the induced strain to the prescribed uniform eigenstrain, is constant inside the inclusion. However, this property is true only for ellipsoidal inclusions (and when classical elasticity is used), which is known as the Eshelby conjecture (e.g., Eshelby, 1961; Rodin, 1996; Markenscoff, 1998a,b; Lubarda and Markenscoff, 1998; Liu, 2008; Li and Wang, 2008; Gao and Ma, 2010b; Ammari *et al.*, 2010).

For non-ellipsoidal polyhedral inclusions, Rodin (1996) provided an algorithmic analytical solution and showed that Eshelby's tensor cannot be constant inside a

polyhedral inclusion, thereby proving the Eshelby conjecture in the case of polyhedral inclusions. The expressions of Eshelby's tensor for two-dimensional (2-D) polygonal inclusions were included in Rodin (1996). The explicit expressions of the Eshelby tensor for three-dimensional (3-D) polyhedral inclusions were later derived by Nozaki and Taya (2001), where an exact solution for the stress field inside and outside an arbitrary-shape polyhedral inclusion was obtained and numerical results for five regular polyhedral inclusion shapes and three other shapes of the icosidodeca family were presented. Both Rodin (1996) and Nozaki and Taya (2001) made use of an algorithm developed by Waldvogel (1979) for evaluating the Newtonian (harmonic) potential over a polyhedral body. A more compact form of the Eshelby tensor than that presented in Nozaki and Taya (2001) for a polyhedral inclusion in an infinite elastic space was proposed by Kuvshinov (2008) using a coordinate-invariant formulation, where problems of polyhedral inclusions in an elastic half-space and bi-materials were also investigated. In addition, specific analytical solutions have been obtained for polyhedral inclusions of simple shapes such as cuboids (e.g., Chiu, 1977; Lee and Johnson, 1978; Liu and Wang, 2005) and pyramids (e.g., Pearson and Faux, 2000; Glas, 2001; Nenashev and Dvurechenskil, 2010). Also, illustrative results have been provided for dynamic Eshelby problems of cubic and triangularly prismatic inclusions along with spherical and ellipsoidal ones by Wang et al. (2005) using their general solution for the dynamic Eshelby problem for inclusions of various shapes.

However, these existing studies on polyhedral inclusion problems are all based on the classical elasticity theory, which does not contain any material length scale

parameter. As a result, the Eshelby tensors obtained in these studies and the subsequent homogenization methods cannot capture the inclusion (particle) size effect on elastic properties exhibited by particle-matrix composites (e.g., Vollenberg and Heikens 1989; Cho *et al*., 2006; Marcadon *et al*., 2007). Solutions for polyhedral inclusion problems are also important for describing interpenetrating phase composites reinforced by 3-D networks (e.g., Poniznik *et al.*, 2008; Jhaver and Tippur, 2009) and for understanding semiconductor materials buried with quantum dots that are typically polyhedral-shaped (e.g., Kuvshinov, 2008; Nenashev and Dvurechenskil, 2010). These materials often exhibit microstructure-dependent size effects whose interpretation requires the use of higher-order continuum theories.

In this chapter, the Eshelby-type inclusion problem of a polyhedral inclusion prescribed with a uniform eigenstrain and a uniform eigenstrain gradient and embedded in an infinite homogeneous isotropic elastic material is solved using a simplified strain gradient elasticity theory (SSGET) (e.g., Gao and Park, 2007), which contains a material length scale parameter and can describe size-dependent elastic deformations. The Eshelby tensor is analytically obtained in terms of three potential functions, two of which are the same as the ones involved in the counterpart Eshelby tensor based on classical elasticity. These potential functions, as three volume integrals over the polyhedral inclusion, are evaluated by dividing the polyhedral inclusion domain into tetrahedral duplexes. Each duplex and the associated local coordinate system are constructed using a procedure similar to that developed by Rodin (1996) based on the algorithm proposed in Waldvogel (1979). Each of the three volume integrals is first

transformed to a surface integral by applying the divergence theorem, which is then transformed to a contour (line) integral based on Stokes' theorem and using an inverse approach different from those employed in the existing studies for evaluating the two integrals involved in the classical elasticity-based Eshelby tensor for a polyhedral inclusion.

The rest of this chapter is organized as follows. In Section 2.2, the general form of the Eshelby tensor for a 3-D arbitrary-shape inclusion based on the SSGET is presented in terms of three potential functions (volume integrals). The expressions of the SSGET-based Eshelby tensor for a polyhedral inclusion of arbitrary shape are analytically derived in Section 2.3, which is separated into a classical part and a gradient part. The averaged Eshelby tensor over the inclusion volume is also analytically evaluated there. Numerical results are provided in Section 2.4 to quantitatively illustrate the position and inclusion size dependence of the newly obtained Eshelby tensor for the polyhedral inclusion problem. The chapter concludes in Section 2.5 with a summary.

2.2 Eshelby Tensor Based on the SSGET

The SSGET is the simplest strain gradient elasticity theory evolving from Mindlin's pioneering work. It is also known as the first gradient elasticity theory of Helmholtz type and the dipolar gradient elasticity theory (e.g., Gao and Ma, 2010a).

According to the SSGET (Gao and Park, 2007; Gao and Ma, 2010a), the Navier-like displacement equations of equilibrium are given by

$$(\lambda+\mu)u_{i,ij}+\mu u_{j,kk}-L^2\left[(\lambda+\mu)u_{i,ij}+\mu u_{j,kk}\right]_{,mm}+f_j=0 \text{ in } \Omega, \tag{2.1}$$

and the boundary conditions have the form:

$$\left.\begin{array}{l} \sigma_{ij}n_j - (\mu_{ijk}n_k)_{,j} + (\mu_{ijk}n_k n_l)_{,l}n_j = \overline{t}_i \quad \text{or} \quad u_i = \overline{u}_i \\ \mu_{ijk}n_j n_k = \overline{q}_i \quad \text{or} \quad u_{i,l}n_l = \overline{\dfrac{\partial u_i}{\partial n}} \end{array}\right\} \text{ on } \partial\Omega, \tag{2.2}$$

where λ and μ are the Lamé constants in classical elasticity, L is a material length scale parameter, u_i are the components of the displacement vector, f_i are the components of the body force vector (force per unit volume), σ_{ij} are the components of the total stress, $\boldsymbol{\sigma} = \sigma_{ij}\mathbf{e}_i\otimes\mathbf{e}_j$, μ_{ijk} are the components of the double stress, $\boldsymbol{\mu} = \mu_{ijk}\mathbf{e}_i\otimes\mathbf{e}_j\otimes\mathbf{e}_k$, and t_i and q_i are, respectively, the components of the Cauchy traction vector and double stress traction vector. Also, in Eqs. (2.1) and (2.2), Ω is the region occupied by the elastically deformed material, $\partial\Omega$ is the smooth bounding surface of Ω, n_i is the outward unit normal vector on $\partial\Omega$, and the overhead bar represents the prescribed value. In addition,

$$\mu_{ijk} = L^2\tau_{ij,k} = \mu_{jik}, \quad \sigma_{ij} \equiv \tau_{ij} - \mu_{ijk,k} = \tau_{ij} - L^2\tau_{ij,kk} = \sigma_{ji}, \tag{2.3}$$

where τ_{ij} are the components of the Cauchy stress, $\boldsymbol{\tau} = \tau_{ij}\mathbf{e}_i\otimes\mathbf{e}_j$.

When the strain gradient effect is not considered (i.e., $L = 0$), $\mu_{ijk} = 0$ and $\sigma_{ij} = \tau_{ij}$ (see Eq. (2.3)), and Eqs. (2.1) and (2.2) reduce to the governing equations and the boundary conditions in terms of displacement in classical elasticity (e.g., Timoshenko and Goodier, 1970; Gao and Rowlands, 2000).

Note that the standard index notation, together with the Einstein summation convention, is used in Eqs. (2.1)–(2.3) and throughout this chapter, with each Latin index (subscript) ranging from 1 to 3 unless otherwise stated.

Solving Eq. (2.1), subject to the boundary conditions of u_i and their first, second and third derivatives vanishing at infinity, gives the fundamental solution and Green's function based on the SSGET. By using 3-D Fourier and inverse Fourier transforms, the fundamental solution of Eq. (2.1) has been obtained as (Gao and Ma, 2009)

$$u_i(\mathbf{x}) = \iint_{-\infty}^{+\infty} G_{ij}(\mathbf{x}-\mathbf{y}) f_j(\mathbf{y}) d\mathbf{y}, \tag{2.4}$$

where $\mathbf{x}$ is the position vector of a point in the infinite 3-D space, $\mathbf{y}$ is the integration point, and $G_{ij}(\cdot)$ is the Green's function (a second-order tensor) given by

$$G_{ij}(\mathbf{x}) = \frac{1}{16\pi\mu(1-\nu)}\left[A(x)\delta_{ij} - B(x)_{,ij} \right], \tag{2.5}$$

with

$$A(x) \equiv 4(1-\nu)\frac{1}{x}\left(1 - e^{-\frac{x}{L}}\right), \quad B(x) \equiv x + \frac{2L^2}{x} - \frac{2L^2}{x} e^{-\frac{x}{L}}. \tag{2.6}$$

when $L = 0$, Eqs. (2.5) and (2.6) reduce to the Green's function for 3-D problems in classical elasticity (e.g., Li and Wang, 2008). In Eqs. (2.5) and (2.6), ν is Poisson's ratio, which is related to the Lamé constants λ and μ through (e.g., Timoshenko and Goodier, 1970)

$$\lambda = \frac{E\nu}{(1+\nu)(1-2\nu)}, \quad \mu = \frac{E}{2(1+\nu)}, \tag{2.7}$$

where E is Young's modulus.

By using the Green's function method entailing Eqs. (2.4)–(2.6), the general expressions of the Eshelby tensor based on the SSGET can then be obtained, as summarized below.

Consider the problem of a 3-D inclusion of arbitrary shape embedded in an infinite homogenous isotropic elastic body. The inclusion is prescribed with a uniform eigenstrain **ε*** and a uniform eigenstrain gradient **κ***. There is no body force or any other external force acting on the elastic body. The disturbed strain, ε_{ij}, induced by **ε*** and **κ*** can be shown to be (Gao and Ma, 2009, 2010b)

$$\varepsilon_{ij} = S_{ijkl}\varepsilon^*_{kl} + T_{ijklm}\kappa^*_{klm}\,, \tag{2.8}$$

where S_{ijkl} is the fourth-order Eshelby tensor having 36 independent components, and T_{ijklm} is a fifth-order Eshelby-like tensor with 108 independent components. Eq. (2.8) shows that **ε** (= $\varepsilon_{ij}\mathbf{e}_i\otimes\mathbf{e}_j$) is solely linked to **ε*** in the absence of **κ*** (i.e., the classical case) and is fully related to **κ*** when **ε*** = **0**. The fourth-order Eshelby tensor has been obtained as

$$S_{ijkl} = S^C_{ijkl} + S^G_{ijkl}\,, \tag{2.9a}$$

$$S^C_{ijkl} = \frac{1}{8\pi(1-\nu)}\Big[\Phi_{,ijkl} - 2\nu\Lambda_{,ij}\delta_{kl} - (1-\nu)(\Lambda_{,lj}\delta_{ik} + \Lambda_{,kj}\delta_{il} + \Lambda_{,li}\delta_{jk} + \Lambda_{,ki}\delta_{jl})\Big], \tag{2.9b}$$

$$S^G_{ijkl} = \frac{1}{8\pi(1-\nu)}\Big[2\nu\Gamma_{,ij}\delta_{kl} + (1-\nu)(\Gamma_{,jl}\delta_{ik} + \Gamma_{,il}\delta_{jk} + \Gamma_{,jk}\delta_{il} + \Gamma_{,ik}\delta_{jl}) + 2L^2(\Lambda_{,ijkl} - \Gamma_{,ijkl})\Big], \tag{2.9c}$$

where S^C_{ijkl} is the classical part, S^G_{ijkl} is the gradient part, δ_{ij} is the Kronecker delta, and

$$\Phi(\mathbf{x}) = \int_\Omega |\mathbf{x}-\mathbf{y}|d\mathbf{y}, \quad \Lambda(\mathbf{x}) = \int_\Omega \frac{1}{|\mathbf{x}-\mathbf{y}|}d\mathbf{y}, \quad \Gamma(\mathbf{x}) = \int_\Omega \frac{e^{-|\mathbf{x}-\mathbf{y}|/L}}{|\mathbf{x}-\mathbf{y}|}d\mathbf{y} \tag{2.10a–c}$$

are three scalar-valued potential functions that can be obtained analytically or numerically by evaluating the volume integrals over the domain Ω occupied by the inclusion, with $|\mathbf{x}| = x = (x_k x_k)^{1/2}$ and **y** (∈ Ω) being the integration variable. Note that the

first two potential functions given in Eqs. (2.10a,b) are the same as the ones involved in the Eshelby tensor based on classical elasticity (e.g., Mura, 1987; Nemat-Nasser and Hori, 1999; Li and Wang, 2008), whereas the third one defined in Eq. (2.10c) results from the use of the SSGET. It should be mentioned that $\Phi(\mathbf{x})$ in Eq. (2.10a) and $\Lambda(\mathbf{x})$ in Eq. (2.10b) are, respectively, known to be a biharmonic potential and a Newtonian potential (e.g., Li and Wang, 2008), while a variant of $\Gamma(\mathbf{x})$ in Eq. (2.10c) is called the Yukawa potential in physics (e.g., Rowlinson, 1989).

Equations (2.10a–c) show that among the three potential functions, only the third one, $\Gamma(\mathbf{x})$, involves the length scale parameter L. It then follows from Eqs. (2.9c) and (2.10b,c) that S^G_{ijkl} depends on L, while S^C_{ijkl}, expressed in terms of $\Lambda(\mathbf{x})$ and $\Phi(\mathbf{x})$ only according to Eqs. (2.9b) and (2.10a,b), is independent of L. Also, it is seen from Eqs. (2.9c) and (2.10b,c) that $S^G_{ijkl} = 0$ when $L = 0$ (and thus $\Gamma(\mathbf{x}) \equiv 0$), thereby giving $S_{ijkl} = S^C_{ijkl}$ (from Eq. (2.9a)). That is, the Eshelby tensor derived using the SSGET reduces to that based on classical elasticity when the strain gradient effect is not considered.

The fifth-order Eshelby-like tensor $\mathbf{T}$, which relates the eigenstrain gradient $\boldsymbol{\kappa}^*$ to the disturbed strain $\boldsymbol{\varepsilon}$ in the elastic body (see Eq. (2.8)), can be shown to be

$$T_{ijklm} = \frac{L^2}{8\pi(1-\nu)}\left[2\nu\Psi_{,ijm}\delta_{kl} + (1-\nu)(\Psi_{,lmi}\delta_{jk} + \Psi_{,lmj}\delta_{ik} + \Psi_{,kmi}\delta_{jl} + \Psi_{,kmj}\delta_{il}) - \Pi_{,ijklm}\right], \quad (2.11)$$

where

$$\Psi(\mathbf{x}) \equiv \Lambda - \Gamma, \quad \Pi(\mathbf{x}) \equiv \Phi + 2L^2(\Lambda - \Gamma), \quad (2.12a,b)$$

with the scalar-valued potential functions $\Phi(\mathbf{x})$, $\Lambda(\mathbf{x})$ and $\Gamma(\mathbf{x})$ defined in Eqs. (2.10a–c). It is clear from Eq. (2.11) that $\mathbf{T}$ vanishes when $L = 0$. Then, with $S_{ijkl} = S^C_{ijkl}$ as discussed above, Eq. (2.8) simply becomes $\varepsilon_{ij} = S^C_{ijkl}\varepsilon^*_{kl}$ when $L = 0$, which is the defining relation for the Eshelby tensor based on classical elasticity (Eshelby, 1957), as expected.

Equations (2.9a–c) and (2.11) provide the general formulas for determining S_{ijkl} ($= S^C_{ijkl} + S^G_{ijkl}$) and T_{ijklm} for an inclusion of arbitrary shape in terms of the potential functions $\Lambda(\mathbf{x})$, $\Phi(\mathbf{x})$ and $\Gamma(\mathbf{x})$ defined in Eqs. (2.10a-c). For the cases of a spherical inclusion, a cylindrical inclusion and an ellipsoidal inclusion in an infinite elastic medium, analytical expressions have been obtained for $\Lambda(\mathbf{x})$, $\Phi(\mathbf{x})$ and $\Gamma(\mathbf{x})$ and thus for the Eshelby tensor (Gao and Ma, 2009, 2010b; Ma and Gao, 2010). The more complex case of a polyhedral inclusion of arbitrary shape, for which $\Lambda(\mathbf{x})$, $\Phi(\mathbf{x})$ and $\Gamma(\mathbf{x})$ are difficult to evaluate analytically, is examined in this study.

2.3 Polyhedral Inclusion

The problem of an arbitrary-shape polyhedral inclusion in an infinite elastic body has been analytically studied by Rodin (1996), Nozaki and Taya (2001) and Kuvshinov (2008) using classical elasticity. The Eshelby tensor for this problem is derived here using the SSGET-based general formulas and a new method for evaluating the potential functions $\Lambda(\mathbf{x})$, $\Phi(\mathbf{x})$ and $\Gamma(\mathbf{x})$.

2.3.1 Eshelby tensor

Consider an arbitrarily shaped polyhedral inclusion embedded in an infinite homogeneous isotropic elastic material. The polyhedral inclusion has p faces and is prescribed with a uniform eigenstrain $\boldsymbol{\varepsilon}^*$ and a uniform eigenstrain gradient $\boldsymbol{\kappa}^*$.

The p-faced polyhedral domain occupied by the inclusion can be divided into tetrahedral duplexes originated from a chosen (arbitrary) point $\mathbf{x}$ (Waldvogel, 1979; Rodin, 1996). Each duplex can be further divided into two simplexes, each of which is a tetrahedron with three of its four faces being right triangles (see Fig. 2.1). The four vertices of each of the duplexes are, respectively, the projection point of $\mathbf{x}$ on a polyhedral surface (i.e., $\mathbf{x}_I$), two adjacent vertices on this surface (i.e., V_{JI}^{+} and V_{JI}^{-}), and the point $\mathbf{x}$ itself. For each of these duplexes, a local Cartesian coordinate system is constructed, with point $\mathbf{x}$ being set as the origin. The three orthogonal axes of the local coordinate system are denoted by λ, η and ζ, respectively. The coordinates of the two vertices V_{JI}^{+} and V_{JI}^{-} on the Jth edge of the Ith surface are, respectively, given by $(b_{JI},\, l_{JI}^{+},\, a_I)$ and $(b_{JI}, l_{JI}^{-}, a_I)$, as shown in Fig. 2.2.

In Fig. 2.2, $\boldsymbol{\lambda}_{JI}^{0}$, $\boldsymbol{\eta}_{JI}^{0}$ and $\boldsymbol{\zeta}_{I}^{0}$ are the unit vectors associated with the local coordinates λ_{JI}, η_{JI} and ζ_I, $\mathbf{y}$ is an arbitrary point on the Jth edge of the Ith surface, $\mathbf{r}$ is the position vector of $\mathbf{y}$ relative to the origin $\mathbf{x}$ (i.e., $\mathbf{r} = \mathbf{y} - \mathbf{x}$), and $\mathbf{r}_I^s$ is the projection of $\mathbf{r}$ on the Ith surface. The usual Cartesian coordinates (x_1, x_2, x_3) are used in the global coordinate system having $(\mathbf{e}_1, \mathbf{e}_2, \mathbf{e}_3)$ as the associated base vectors.

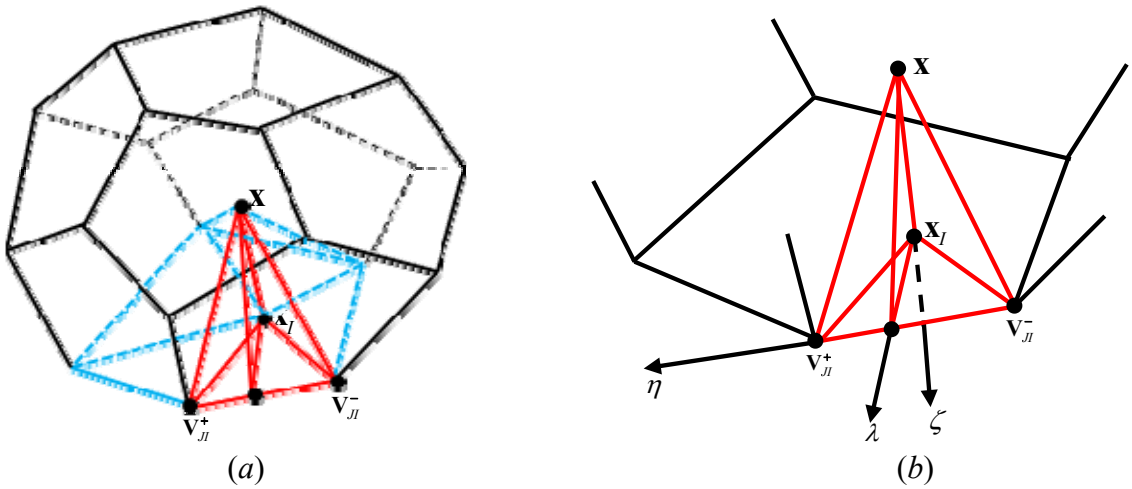

Fig. 2.1 A polyhedron represented by duplexes: (*a*) A polyhedron (with five duplexes shown); (*b*) a duplex and the associated local coordinate system constructed from an arbitrary point **x**.

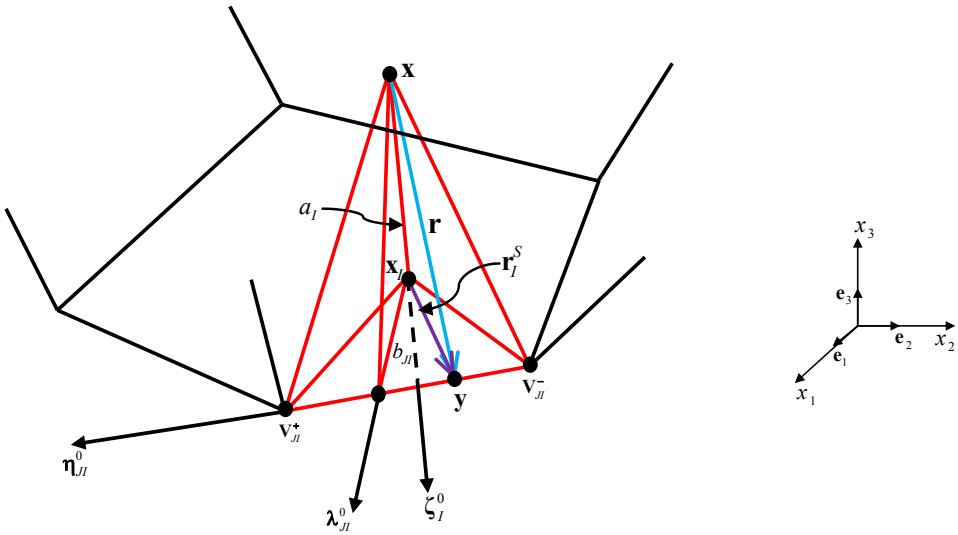

Fig. 2.2 A duplex with its base on the *I*th surface and one local coordinate axis (η) along the *J*th edge of the *I*th surface.

To obtain the Eshelby tensor for the polyhedral inclusion using Eqs. (2.9a-c), the three potential functions $\Phi(\mathbf{x})$, $\Lambda(\mathbf{x})$, and $\Gamma(\mathbf{x})$ defined in Eqs. (2.10a-c) are first

evaluated over the polyhedral domain Ω using an approach different from those employed in Rodin (1996), Nozaki and Taya (2001) and Kuvshinov (2008) for evaluating $\Phi(\mathbf{x})$ and $\Lambda(\mathbf{x})$ involved in the classical elasticity-based Eshelby tensor, as shown next.

For a sufficiently smooth function $M(\mathbf{x}-\mathbf{y})$, the use of the divergence theorem gives

$$\frac{\partial}{\partial x_k}\iiint_\Omega M dV(\mathbf{y}) = -\iiint_\Omega \frac{\partial M}{\partial y_k} dV(\mathbf{y}) = -\sum_{I=1}^{p} (\zeta_I^0)_k \iint_{\partial\Omega_I} M dS(\mathbf{y}), \tag{2.13}$$

where p is the number of the surfaces of the polyhedron, and $(\zeta_I^0)_k$ is the kth component of the unit outward normal vector on the Ith surface $\partial\Omega_I$, $\boldsymbol{\zeta}_I^0$.

To transform the surface integral in Eq. (2.13) to a contour (line) integral, let

$$M = (\nabla \times \mathbf{m}) \bullet \boldsymbol{\zeta}_I^0, \tag{2.14}$$

where $\mathbf{m}$ is a yet-unknown vector located on the Ith surface of the polyhedron, and $\nabla\times\mathbf{m}$ denotes the curl of **m.** Using the Stokes theorem then yields, upon applying Eq. (2.14),

$$\iint_{\partial\Omega_I} M dS(\mathbf{y}) = \sum_{J=1}^{q} \int_{C_{JI}} \mathbf{m} \bullet \boldsymbol{\eta}_{JI}^0 dl, \tag{2.15}$$

where $\boldsymbol{\eta}_{JI}^0$ is the unit vector along the Jth boundary edge C_{JI} of the Ith surface.

Now, write

$$\mathbf{m} = \boldsymbol{\zeta}_I^0 \times [\frac{\mathbf{r}_I^S}{r_I^S} g(r)], \tag{2.16}$$

where $r_I^S (= \sqrt{r^2 - a_I^2} = |\mathbf{r}_I^S|)$ is the length of the projection of **r** on the *I*th surface, and $g(r)$ is a function of r ($=|\mathbf{r}|$) yet to be determined. Substituting Eq. (2.16) into Eq. (2.15) leads to

$$\iint_{\partial\Omega_I} M dS(\mathbf{y}) = \sum_{J=1}^{q} b_{JI} \int_{C_{JI}} \frac{g(r)}{r_I^S} dl, \tag{2.17}$$

where $b_{JI} \equiv \mathbf{r}_I^S \bullet \boldsymbol{\lambda}_{JI}^0$ is the distance from point $\mathbf{x}_I$ (the projection of point **x** on the *I*th surface) to the *J*th edge C_{JI} (see Fig. 2.2). For each specific function *M*, a different expression of $g(r)$ and thus **m** can be determined, as shown next for the three cases representing the integrands of the potential functions $\Phi(\mathbf{x})$, $\Lambda(\mathbf{x})$ and $\Gamma(\mathbf{x})$ defined in Eqs. (2.10a–c).

For $M = r = |\mathbf{y} - \mathbf{x}|$ (corresponding to $\Phi(\mathbf{x})$), Eqs. (2.14) and (2.16) gives

$$r = g(r)(\nabla \bullet \frac{\mathbf{r}_I^S}{r_I^S}) + [\nabla g(r)] \bullet \frac{\mathbf{r}_I^S}{r_I^S}, \tag{2.18}$$

where ∇ is the gradient operator, and use has been made of the identity: $\mathbf{a} \times \mathbf{b} \times \mathbf{c} = (\mathbf{a} \bullet \mathbf{c})\mathbf{b} - (\mathbf{a} \bullet \mathbf{b})\mathbf{c}$, with **a**, **b**, **c** being arbitrary vectors and "×", "•" representing the cross, dot products, respectively. After carrying out the differentiation and dot product operations, Eq. (2.18) can be further simplified to

$$r = \frac{g(r)}{r_I^S} + g'(r)\frac{r_I^S}{r}, \tag{2.19}$$

where $g'(= dg/dr)$ is the first derivative of g with respect to r. The solution of Eq. (2.19) reads

$$g_{\Phi}(r)=\frac{r^3-a_I^3}{3r_I^S}, \tag{2.20}$$

where $a_I\,(=\mathbf{r}\bullet\boldsymbol{\zeta}_I^0)$ is the distance from point $\mathbf{x}$ to the Ith surface (see Fig. 2.2), and $g_{\Phi}(r)$ denotes the function $g(r)$ for the case with $M=r$.

Similarly, it can be shown that

$$g_{\Lambda}(r)=\frac{r_I^S}{r+a_I} \tag{2.21}$$

when $M=1/r=1/\left|\mathbf{y}-\mathbf{x}\right|$ (corresponding to $\Lambda(\mathbf{x})$), and

$$g_{\Gamma}(r)=\frac{L(e^{-a_I/L}-e^{-r/L})}{r_I^S} \tag{2.22}$$

when $M=e^{-r/L}/r=e^{-\left|\mathbf{y}-\mathbf{x}\right|/L}/\left|\mathbf{y}-\mathbf{x}\right|$ (corresponding to $\Gamma(\mathbf{x})$).

Using Eqs. (2.13), (2.17) and (2.20)–(2.22) in Eqs. (2.10a–c) then leads to, with the local coordinate axis η being along the Jth edge,

$$\Phi_{,i}=-\sum_{I=1}^{p}\sum_{J=1}^{q}(\zeta_I^0)_i b_{JI}\int_{l_{JI}^-}^{l_{JI}^+}\frac{(a_I^2+b_{JI}^2+\eta^2)^{3/2}-a_I^3}{3(b_{JI}^2+\eta^2)}d\eta, \tag{2.23}$$

$$\Lambda_{,i}=-\sum_{I=1}^{p}\sum_{J=1}^{q}(\zeta_I^0)_i b_{JI}\int_{l_{JI}^-}^{l_{JI}^+}\frac{1}{\sqrt{a_I^2+b_{JI}^2+\eta^2}+a_I}d\eta, \tag{2.24}$$

$$\Gamma_{,i}=-\sum_{I=1}^{p}\sum_{J=1}^{q}(\zeta_I^0)_i b_{JI}\int_{l_{JI}^-}^{l_{JI}^+}\frac{L(e^{-a_I/L}-e^{-\sqrt{a_I^2+b_{JI}^2+\eta^2}/L})}{b_{JI}^2+\eta^2}d\eta, \tag{2.25}$$

where l_{JI}^+ and l_{JI}^- are, respectively, the coordinates of the two vertices V_{JI}^+ and V_{JI}^- on the Jth edge, with l_{JI}^+ being positive and l_{JI}^- negative (see Fig. 2.2).

The integrals in Eqs. (2.23) and (2.24) can be exactly evaluated by direct integration to obtain the following closed-form expressions:

$$\Phi_{,i} = -\sum_{I=1}^{p}\sum_{J=1}^{q}(\zeta_I^0)_i \left\{ \frac{l_{JI}^+ b_{JI}}{6}\sqrt{a_I^2+b_{JI}^2+(l_{JI}^+)^2} + \frac{a_I^3}{3}\tan^{-1}\left[\frac{a_I l_{JI}^+}{b_{JI}\sqrt{a_I^2+b_{JI}^2+(l_{JI}^+)^2}}\right] - \frac{a_I^3}{3}\tan^{-1}\left(\frac{l_{JI}^+}{b_{JI}}\right) \right.$$
$$+ \frac{3a_I^2 b_{JI}+b_{JI}^3}{6}\ln\left[\frac{l_{JI}^+ + \sqrt{a_I^2+b_{JI}^2+(l_{JI}^+)^2}}{\sqrt{a_I^2+b_{JI}^2}}\right] - \frac{l_{JI}^- b_{JI}}{6}\sqrt{a_I^2+b_{JI}^2+(l_{JI}^-)^2}$$
$$\left. - \frac{a_I^3}{3}\tan^{-1}\left[\frac{a_I l_{JI}^-}{b_{JI}\sqrt{a_I^2+b_{JI}^2+(l_{JI}^-)^2}}\right] + \frac{a_I^3}{3}\tan^{-1}\left(\frac{l_{JI}^-}{b_{JI}}\right) - \frac{3a_I^2 b_{JI}+b_{JI}^3}{6}\ln\left[\frac{l_{JI}^- + \sqrt{a_I^2+b_{JI}^2+(l_{JI}^-)^2}}{\sqrt{a_I^2+b_{JI}^2}}\right] \right\}$$
$$\equiv -\sum_{I=1}^{p}\sum_{J=1}^{q}(\zeta_I^0)_i \Phi_1^{JI} = -\sum_{I=1}^{p}\sum_{J=1}^{q}(\zeta_I^0)_i [(\Phi_1^{JI})^+ - (\Phi_1^{JI})^-], \tag{2.26}$$

$$\Lambda_{,i} = -\sum_{I=1}^{p}\sum_{J=1}^{q}(\zeta_I^0)_i \left\{ a_I \tan^{-1}\left[\frac{a_I l_{JI}^+}{b_{JI}\sqrt{a_I^2+b_{JI}^2+(l_{JI}^+)^2}}\right] - a_I\tan^{-1}\left(\frac{l_{JI}^+}{b_{JI}}\right) + b_{JI}\ln\left[\frac{l_{JI}^+ + \sqrt{a_I^2+b_{JI}^2+(l_{JI}^+)^2}}{\sqrt{a_I^2+b_{JI}^2}}\right] \right.$$
$$\left. - a_I \tan^{-1}\left[\frac{a_I l_{JI}^-}{b_{JI}\sqrt{a_I^2+b_{JI}^2+(l_{JI}^-)^2}}\right] + a_I\tan^{-1}\left(\frac{l_{JI}^-}{b_{JI}}\right) - b_{JI}\ln\left[\frac{l_{JI}^- + \sqrt{a_I^2+b_{JI}^2+(l_{JI}^-)^2}}{\sqrt{a_I^2+b_{JI}^2}}\right] \right\}$$
$$\equiv -\sum_{I=1}^{p}\sum_{J=1}^{q}(\zeta_I^0)_i \Lambda_1^{JI} = -\sum_{I=1}^{p}\sum_{J=1}^{q}(\zeta_I^0)_i [(\Lambda_1^{JI})^+ - (\Lambda_1^{JI})^-], \tag{2.27}$$

where Φ_1^{JI}, $(\Phi_1^{JI})^+$, $(\Phi_1^{JI})^-$, Λ_1^{JI}, $(\Lambda_1^{JI})^+$ and $(\Lambda_1^{JI})^-$ are functions defined by

$$\Phi_1^{JI} = \Phi_1^{JI}(a_I, b_{JI}, l_{JI}^+, l_{JI}^-) = (\Phi_1^{JI})^+(a_I, b_{JI}, l_{JI}^+) - (\Phi_1^{JI})^-(a_I, b_{JI}, l_{JI}^-),$$
$$(\Phi_1^{JI})^+ = \frac{l_{JI}^+ b_{JI}}{6}\sqrt{a_I^2+b_{JI}^2+(l_{JI}^+)^2} + \frac{a_I^3}{3}\tan^{-1}\left[\frac{a_I l_{JI}^+}{b_{JI}\sqrt{a_I^2+b_{JI}^2+(l_{JI}^+)^2}}\right] - \frac{a_I^3}{3}\tan^{-1}\left(\frac{l_{JI}^+}{b_{JI}}\right)$$
$$+ \frac{3a_I^2 b_{JI}+b_{JI}^3}{6}\ln\left[\frac{l_{JI}^+ + \sqrt{a_I^2+b_{JI}^2+(l_{JI}^+)^2}}{\sqrt{a_I^2+b_{JI}^2}}\right],$$

$$
\begin{aligned}
(\Phi_1^{JI})^- &= \frac{l_{JI}^- b_{JI}}{6}\sqrt{a_I^2+b_{JI}^2+(l_{JI}^-)^2}+\frac{a_I^3}{3}\tan^{-1}\left[\frac{a_I l_{JI}^-}{b_{JI}\sqrt{a_I^2+b_{JI}^2+(l_{JI}^-)^2}}\right]-\frac{a_I^3}{3}\tan^{-1}\left(\frac{l_{JI}^-}{b_{JI}}\right)\\
&\quad+\frac{3a_I^2 b_{JI}+b_{JI}^3}{6}\ln\left[\frac{l_{JI}^-+\sqrt{a_I^2+b_{JI}^2+(l_{JI}^-)^2}}{\sqrt{a_I^2+b_{JI}^2}}\right],\\
\Lambda_1^{JI} &= \Lambda_1^{JI}(a_I,b_{JI},l_{JI}^+,l_{JI}^-)=(\Lambda_1^{JI})^+(a_I,b_{JI},l_{JI}^+)-(\Lambda_1^{JI})^-(a_I,b_{JI},l_{JI}^-),\\
(\Lambda_1^{JI})^+ &= a_I\tan^{-1}\left[\frac{a_I l_{JI}^+}{b_{JI}\sqrt{a_I^2+b_{JI}^2+(l_{JI}^+)^2}}\right]-a_I\tan^{-1}\left(\frac{l_{JI}^+}{b_{JI}}\right)+b_{JI}\ln\left[\frac{l_{JI}^++\sqrt{a_I^2+b_{JI}^2+(l_{JI}^+)^2}}{\sqrt{a_I^2+b_{JI}^2}}\right],\\
(\Lambda_1^{JI})^- &= a_I\tan^{-1}\left[\frac{a_I l_{JI}^-}{b_{JI}\sqrt{a_I^2+b_{JI}^2+(l_{JI}^-)^2}}\right]-a_I\tan^{-1}\left(\frac{l_{JI}^-}{b_{JI}}\right)+b_{JI}\ln\left[\frac{l_{JI}^-+\sqrt{a_I^2+b_{JI}^2+(l_{JI}^-)^2}}{\sqrt{a_I^2+b_{JI}^2}}\right].
\end{aligned}
\tag{2.28}
$$

Note that $e^{-r/L}$ can be written as a power series:

$$
e^{-r/L}=\sum_{n=0}^{\infty}\frac{(-1)^n}{n!}\left(\frac{r}{L}\right)^n. \tag{2.29}
$$

Using Eq. (2.29) in Eq. (2.25) then leads to

$$
\begin{aligned}
\Gamma_{,i} &= -\sum_{I=1}^{p}\sum_{J=1}^{q}(\zeta_I^0)_i L\left\{e^{-a_I/L}\left[\tan^{-1}\left(\frac{l_{JI}^+}{b_{JI}}\right)-\tan^{-1}\left(\frac{l_{JI}^-}{b_{JI}}\right)\right]\right.\\
&\quad+\sum_{n=0}^{\infty}\frac{(-1)^{n+1}}{L^n n!}\frac{l_{JI}^+[a_I^2+b_{JI}^2+(l_{JI}^+)^2]^{n/2}}{b_{JI}}\left[1+\frac{(l_{JI}^+)^2}{a_I^2+b_{JI}^2}\right]^{-n/2}F_1\left[\frac{1}{2},-\frac{n}{2},1,\frac{3}{2},-\frac{(l_{JI}^+)^2}{a_I^2+b_{JI}^2},-\frac{(l_{JI}^+)^2}{b_{JI}^2}\right]\\
&\quad\left.-\sum_{n=0}^{\infty}\frac{(-1)^{n+1}}{L^n n!}\frac{l_{JI}^-[a_I^2+b_{JI}^2+(l_{JI}^-)^2]^{n/2}}{b_{JI}}\left[1+\frac{(l_{JI}^-)^2}{a_I^2+b_{JI}^2}\right]^{-n/2}F_1\left[\frac{1}{2},-\frac{n}{2},1,\frac{3}{2},-\frac{(l_{JI}^-)^2}{a_I^2+b_{JI}^2},-\frac{(l_{JI}^-)^2}{b_{JI}^2}\right]\right\}\\
&\equiv -\sum_{I=1}^{p}\sum_{J=1}^{q}(\zeta_I^0)_i\Gamma_1^{JI}=-\sum_{I=1}^{p}\sum_{J=1}^{q}(\zeta_I^0)_i[(\Gamma_1^{JI})^+-(\Gamma_1^{JI})^-],
\end{aligned}
\tag{2.30}
$$

where Γ_1^{JI}, $(\Gamma_1^{JI})^+$ and $(\Gamma_1^{JI})^-$ are functions defined by

$$\Gamma_1^{JI} = \Gamma_1^{JI}(a_I, b_{JI}, l_{JI}^+, l_{JI}^-) = (\Gamma_1^{JI})^+(a_I, b_{JI}, l_{JI}^+) - (\Gamma_1^{JI})^-(a_I, b_{JI}, l_{JI}^-),$$

$$(\Gamma_1^{JI})^+ = L\left\{ e^{-a_I/L}\tan^{-1}\left(\frac{l_{JI}^+}{b_{JI}}\right) + \sum_{n=0}^{\infty}\frac{(-1)^{n+1}}{L^n n!}\frac{l_{JI}^+[a_I^2 + b_{JI}^2 + (l_{JI}^+)^2]^{n/2}}{b_{JI}}\left[1 + \frac{(l_{JI}^+)^2}{a_I^2 + b_{JI}^2}\right]^{-n/2} \right.$$

$$\left. F_1\left[\frac{1}{2}, -\frac{n}{2}, 1, \frac{3}{2}, -\frac{(l_{JI}^+)^2}{a_I^2 + b_{JI}^2}, -\frac{(l_{JI}^+)^2}{b_{JI}^2}\right]\right\}, \tag{2.31}$$

$$(\Gamma_1^{JI})^- = L\left\{ e^{-a_I/L}\tan^{-1}\left(\frac{l_{JI}^-}{b_{JI}}\right) + \sum_{n=0}^{\infty}\frac{(-1)^{n+1}}{L^n n!}\frac{l_{JI}^-[a_I^2 + b_{JI}^2 + (l_{JI}^-)^2]^{n/2}}{b_{JI}}\left[1 + \frac{(l_{JI}^-)^2}{a_I^2 + b_{JI}^2}\right]^{-n/2} \right.$$

$$\left. F_1\left[\frac{1}{2}, -\frac{n}{2}, 1, \frac{3}{2}, -\frac{(l_{JI}^-)^2}{a_I^2 + b_{JI}^2}, -\frac{(l_{JI}^-)^2}{b_{JI}^2}\right]\right\},$$

and F_1 is the first Appell hypergeometric function of two variables given by

$$F_1(a, b, c, d; x, y) = \sum_{m,n=0}^{\infty}\frac{(a)_{m+n}(b)_m(c)_n}{(d)_{m+n}m!n!}x^m y^n, \tag{2.32}$$

with $(f)_m$ being the Pochhammer symbol representing the following rising factorial:

$$(f)_m = \frac{\Gamma(f+m)}{\Gamma(f)} = f(f+1)(f+2)\cdots(f+m-1). \tag{2.33}$$

Note that Eqs. (2.26), (2.27) and (2.30) are applicable to both the interior case with **x** being inside the polyhedral inclusion (i.e., $\mathbf{x} \in \Omega$) and the exterior case with **x** being outside the inclusion (i.e., $\mathbf{x} \notin \Omega$). For the former a_I is a positive value, while for the latter a_I is a negative value. The similarity and difference identified here between the interior and exterior cases can be seen from Fig. 2.3, where how the duplex in each case is constructed is schematically shown.

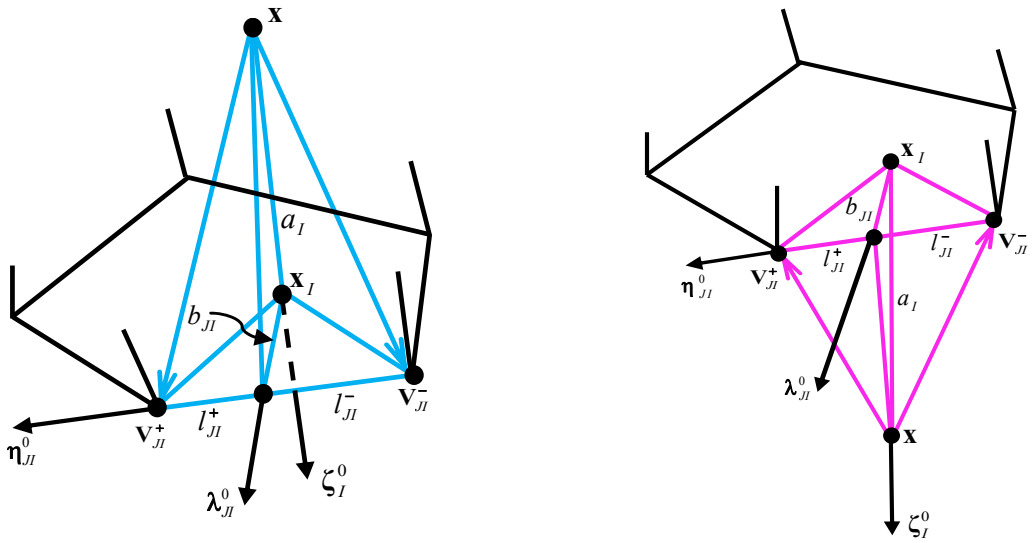

Fig. 2.3 Duplex and parameters a_I, b_{JI}, l^+_{JI}, l^-_{JI} for (*a*) $\mathbf{x} \in \Omega$ and (*b*) $\mathbf{x} \notin \Omega$.

It should be mentioned that no attempt is made here to obtain the expressions of the potential functions $\Phi(\mathbf{x})$, $\Lambda(\mathbf{x})$ and $\Gamma(\mathbf{x})$ from Eqs. (2.26), (2.27) and (2.30), since only the second and/or fourth derivatives of these functions are involved in the general expressions of the Eshelby tensor given in Eqs. (2.9a–c).

Note that for a smooth function

$F(\mathbf{x}) \equiv F(a_I, b_{JI}, l^+_{JI}, l^-_{JI}) = F^+(a_I, b_{JI}, l^+_{JI}) - F^-(a_I, b_{JI}, l^-_{JI})$ the use of chain rule gives

$$F_{,i} \equiv \frac{\partial F}{\partial x_i} = \frac{\partial F}{\partial a_I}\frac{\partial a_I}{\partial x_i} + \frac{\partial F}{\partial b_{JI}}\frac{\partial b_{JI}}{\partial x_i} + \frac{\partial F^+}{\partial l^+_{JI}}\frac{\partial l^+_{JI}}{\partial x_i} - \frac{\partial F^-}{\partial l^-_{JI}}\frac{\partial l^-_{JI}}{\partial x_i}, \tag{2.34}$$

where the parameters a_I, b_{JI}, l^+_{JI}, l^-_{JI} are related to $\mathbf{x}$ through

$$a_I = (v^+_k - x_k)(\zeta^0_I)_k, \tag{2.35a}$$

$$b_{JI} = (v^+_k - x_k)(\lambda^0_{JI})_k, \tag{2.35b}$$

$$l_{JI}^{+} = (v_k^{+} - x_k)(\eta_{JI}^0)_k, \tag{2.35c}$$

$$l_{JI}^{-} = (v_k^{-} - x_k)(\eta_{JI}^0)_k, \tag{2.35d}$$

where x_k, v_k^{+} and v_k^{-} are, respectively, the coordinates of the points $\mathbf{x}, \mathrm{V}_{JI}^{+}$ and V_{JI}^{-} in the global coordinate system, and $(\zeta_I^0)_k$, $(\lambda_{JI}^0)_k$ and $(\eta_{JI}^0)_k$ are the components of the unit base vectors $\boldsymbol{\zeta}_I^0$, $\boldsymbol{\lambda}_{JI}^0$ and $\boldsymbol{\eta}_{JI}^0$ in the global coordinate system.

It then follows from Eqs. (2.34) and (2.35a–d) that

$$F_{,i} = -\frac{\partial F}{\partial a_I}(\zeta_I^0)_i - \frac{\partial F}{\partial b_{JI}}(\lambda_{JI}^0)_i - (\frac{\partial F^{+}}{\partial l_{JI}^{+}} - \frac{\partial F^{-}}{\partial l_{JI}^{-}})(\eta_{JI}^0)_i, \tag{2.36a}$$

$$\begin{aligned}
F_{,ijk} = & -\frac{\partial^3 F}{\partial a_I^3}(\zeta_I^0)_i(\zeta_I^0)_j(\zeta_I^0)_k - \frac{\partial^3 F}{\partial b_{JI}^3}(\lambda_{JI}^0)_i(\lambda_{JI}^0)_j(\lambda_{JI}^0)_k - [\frac{\partial^3 F^{+}}{\partial (l_{JI}^{+})^3} - \frac{\partial^3 F^{-}}{\partial (l_{JI}^{-})^3}](\eta_{JI}^0)_i(\eta_{JI}^0)_j(\eta_{JI}^0)_k \\
& - \frac{\partial^3 F}{\partial a_I^2 \partial b_{JI}}[(\lambda_{JI}^0)_i(\zeta_I^0)_j(\zeta_I^0)_k + (\zeta_I^0)_i(\lambda_{JI}^0)_j(\zeta_I^0)_k + (\zeta_I^0)_i(\zeta_I^0)_j(\lambda_{JI}^0)_k] \\
& - [\frac{\partial^3 F^{+}}{\partial a_I^2 \partial l_{JI}^{+}} - \frac{\partial^3 F^{-}}{\partial a_I^2 \partial l_{JI}^{-}}][(\eta_{JI}^0)_i(\zeta_I^0)_j(\zeta_I^0)_k + (\zeta_I^0)_i(\eta_{JI}^0)_j(\zeta_I^0)_k + (\zeta_I^0)_i(\zeta_I^0)_j(\eta_{JI}^0)_k] \\
& - \frac{\partial^3 F}{\partial a_I \partial b_{JI}^2}[(\zeta_I^0)_i(\lambda_{JI}^0)_j(\lambda_{JI}^0)_k + (\lambda_{JI}^0)_i(\zeta_I^0)_j(\lambda_{JI}^0)_k + (\lambda_{JI}^0)_i(\lambda_{JI}^0)_j(\zeta_I^0)_k] \\
& - (\frac{\partial^3 F^{+}}{\partial b_{JI}^2 \partial l_{JI}^{+}} - \frac{\partial^3 F^{-}}{\partial b_{JI}^2 \partial l_{JI}^{-}})[(\eta_{JI}^0)_i(\lambda_{JI}^0)_j(\lambda_{JI}^0)_k + (\lambda_{JI}^0)_i(\eta_{JI}^0)_j(\lambda_{JI}^0)_k + (\lambda_{JI}^0)_i(\lambda_{JI}^0)_j(\eta_{JI}^0)_k] \\
& - [\frac{\partial^3 F^{+}}{\partial a_I \partial (l_{JI}^{+})^2} - \frac{\partial^3 F^{-}}{\partial a_I \partial (l_{JI}^{-})^2}][(\zeta_I^0)_i(\eta_{JI}^0)_j(\eta_{JI}^0)_k + (\eta_{JI}^0)_i(\zeta_I^0)_j(\eta_{JI}^0)_k + (\eta_{JI}^0)_i(\eta_{JI}^0)_j(\zeta_I^0)_k] \\
& - [\frac{\partial^3 F^{+}}{\partial b_{JI} \partial (l_{JI}^{+})^2} - \frac{\partial^3 F^{-}}{\partial b_{JI} \partial (l_{JI}^{-})^2}][(\lambda_{JI}^0)_i(\eta_{JI}^0)_j(\eta_{JI}^0)_k + (\eta_{JI}^0)_i(\lambda_{JI}^0)_j(\eta_{JI}^0)_k + (\eta_{JI}^0)_i(\eta_{JI}^0)_j(\lambda_{JI}^0)_k] \\
& - (\frac{\partial^3 F^{+}}{\partial a_I \partial b_{JI} \partial l_{JI}^{+}} - \frac{\partial^3 F^{-}}{\partial a_I \partial b_{JI} \partial l_{JI}^{-}})[(\zeta_I^0)_i(\lambda_{JI}^0)_j(\eta_{JI}^0)_k + (\zeta_I^0)_i(\eta_{JI}^0)_j(\lambda_{JI}^0)_k + (\lambda_{JI}^0)_i(\zeta_I^0)_j(\eta_{JI}^0)_k \\
& + (\lambda_{JI}^0)_i(\eta_{JI}^0)_j(\zeta_I^0)_k + (\eta_{JI}^0)_i(\zeta_I^0)_j(\lambda_{JI}^0)_k + (\eta_{JI}^0)_i(\lambda_{JI}^0)_j(\zeta_I^0)_k].
\end{aligned} \tag{2.36b}$$

Using Eqs. (2.26), (2.27), (2.30) and (2.36a,b) in Eqs. (2.9b–c) will lead to the final expressions of the Eshelby tensor for the *p*-faced polyhedral inclusion as

$$
\begin{aligned}
S^C_{ijkl} = \frac{1}{8\pi(1-\nu)} \sum_{I=1}^{p} \sum_{J=1}^{q} \Big\{ & (S^C_1)_{JI} (\zeta^0_I)_i (\zeta^0_I)_j \delta_{kl} + (S^C_2)_{JI} [(\zeta^0_I)_i (\zeta^0_I)_k \delta_{jl} + (\zeta^0_I)_i (\zeta^0_I)_l \delta_{jk}] \\
& + (S^C_3)_{JI} [(\zeta^0_I)_k (\zeta^0_I)_j \delta_{il} + (\zeta^0_I)_l (\zeta^0_I)_j \delta_{ik}] + (S^C_4)_{JI} (\zeta^0_I)_i (\lambda^0_{JI})_j \delta_{kl} \\
& + (S^C_5)_{JI} [(\zeta^0_I)_i (\lambda^0_{JI})_k \delta_{jl} + (\zeta^0_I)_i (\lambda^0_{JI})_l \delta_{jk}] + (S^C_6)_{JI} [(\lambda^0_{JI})_k (\zeta^0_I)_j \delta_{il} + (\lambda^0_{JI})_l (\zeta^0_I)_j \delta_{ik}] \\
& + (S^C_7)_{JI} (\zeta^0_I)_i (\eta^0_{JI})_j \delta_{kl} + (S^C_8)_{JI} [(\zeta^0_I)_i (\eta^0_{JI})_k \delta_{jl} + (\zeta^0_I)_i (\eta^0_{JI})_l \delta_{jk}] \\
& + (S^C_9)_{JI} [(\eta^0_{JI})_k (\zeta^0_I)_j \delta_{il} + (\eta^0_{JI})_l (\zeta^0_I)_j \delta_{ik}] + (S^C_{10})_{JI} [(\zeta^0_I)_i (\lambda^0_{JI})_j (\zeta^0_I)_k (\zeta^0_I)_l \\
& + (\zeta^0_I)_i (\zeta^0_I)_j (\lambda^0_{JI})_k (\zeta^0_I)_l + (\zeta^0_I)_i (\zeta^0_I)_j (\zeta^0_I)_k (\lambda^0_{JI})_l] + (S^C_{11})_{JI} [(\zeta^0_I)_i (\eta^0_{JI})_j (\zeta^0_I)_k (\zeta^0_I)_l \\
& + (\zeta^0_I)_i (\zeta^0_I)_j (\eta^0_{JI})_k (\zeta^0_I)_l + (\zeta^0_I)_i (\zeta^0_I)_j (\zeta^0_I)_k (\eta^0_{JI})_l] + (S^C_{12})_{JI} [(\zeta^0_I)_i (\zeta^0_I)_j (\lambda^0_{JI})_k (\lambda^0_{JI})_l \\
& + (\zeta^0_I)_i (\lambda^0_{JI})_j (\zeta^0_I)_k (\lambda^0_{JI})_l + (\zeta^0_I)_i (\lambda^0_{JI})_j (\lambda^0_{JI})_k (\zeta^0_I)_l] + (S^C_{13})_{JI} [(\zeta^0_I)_i (\zeta^0_I)_j (\eta^0_{JI})_k (\eta^0_{JI})_l \\
& + (\zeta^0_I)_i (\eta^0_{JI})_j (\zeta^0_I)_k (\eta^0_{JI})_l + (\zeta^0_I)_i (\eta^0_{JI})_j (\eta^0_{JI})_k (\zeta^0_I)_l] + (S^C_{14})_{JI} [(\zeta^0_I)_i (\lambda^0_{JI})_j (\eta^0_{JI})_k (\eta^0_{JI})_l \\
& + (\zeta^0_I)_i (\eta^0_{JI})_j (\lambda^0_{JI})_k (\eta^0_{JI})_l + (\zeta^0_I)_i (\eta^0_{JI})_j (\eta^0_{JI})_k (\lambda^0_{JI})_l] + (S^C_{15})_{JI} [(\zeta^0_I)_i (\eta^0_{JI})_j (\lambda^0_{JI})_k (\lambda^0_{JI})_l \\
& + (\zeta^0_I)_i (\lambda^0_{JI})_j (\eta^0_{JI})_k (\lambda^0_{JI})_l + (\zeta^0_I)_i (\lambda^0_{JI})_j (\lambda^0_{JI})_k (\eta^0_{JI})_l] + (S^C_{16})_{JI} [(\zeta^0_I)_i (\zeta^0_I)_j (\lambda^0_{JI})_k (\eta^0_{JI})_l \\
& + (\zeta^0_I)_i (\zeta^0_I)_j (\eta^0_{JI})_k (\lambda^0_{JI})_l + (\zeta^0_I)_i (\lambda^0_{JI})_j (\eta^0_{JI})_k (\zeta^0_I)_l + (\zeta^0_I)_i (\lambda^0_{JI})_j (\zeta^0_I)_k (\eta^0_{JI})_l \\
& + (\zeta^0_I)_i (\eta^0_{JI})_j (\zeta^0_I)_k (\lambda^0_{JI})_l + (\zeta^0_I)_i (\eta^0_{JI})_j (\lambda^0_{JI})_k (\zeta^0_I)_l] \Big\},
\end{aligned}
\tag{2.37a}
$$

where

$$
\begin{aligned}
& (S^C_1)_{JI} = \frac{1}{3} \frac{\partial^3 \Phi^{JI}_1}{\partial a^3_I} - 2\nu \frac{\partial \Lambda^{JI}_1}{\partial a_I}, \quad (S^C_2)_{JI} = \frac{1}{3} \frac{\partial^3 \Phi^{JI}_1}{\partial a^3_I} - (1-\nu) \frac{\partial \Lambda^{JI}_1}{\partial a_I}, \\
& (S^C_3)_{JI} = -(1-\nu) \frac{\partial \Lambda^{JI}_1}{\partial a_I}, \quad (S^C_4)_{JI} = \frac{1}{3} \frac{\partial^3 \Phi^{JI}_1}{\partial b^3_{JI}} - 2\nu \frac{\partial \Lambda^{JI}_1}{\partial b_{JI}}, \\
& (S^C_5)_{JI} = \frac{1}{3} \frac{\partial^3 \Phi^{JI}_1}{\partial b^3_{JI}} - (1-\nu) \frac{\partial \Lambda^{JI}_1}{\partial b_{JI}}, \quad (S^C_6)_{JI} = -(1-\nu) \frac{\partial \Lambda^{JI}_1}{\partial b_{JI}}, \\
& (S^C_7)_{JI} = \frac{1}{3} \left[\frac{\partial^3 (\Phi^{JI}_1)^+}{\partial (l^+_{JI})^3} - \frac{\partial^3 (\Phi^{JI}_1)^-}{\partial (l^-_{JI})^3} \right] - 2\nu \left[\frac{\partial (\Lambda^{JI}_1)^+}{\partial l^+_{JI}} - \frac{\partial (\Lambda^{JI}_1)^-}{\partial l^-_{JI}} \right], \\
& (S^C_8)_{JI} = \frac{1}{3} \left[\frac{\partial^3 (\Phi^{JI}_1)^+}{\partial (l^+_{JI})^3} - \frac{\partial^3 (\Phi^{JI}_1)^-}{\partial (l^-_{JI})^3} \right] - (1-\nu) \left[\frac{\partial (\Lambda^{JI}_1)^+}{\partial l^+_{JI}} - \frac{\partial (\Lambda^{JI}_1)^-}{\partial l^-_{JI}} \right],
\end{aligned}
$$

$$(S_9^C)_{JI} = -(1-v)[\frac{\partial(\Lambda_1^{JI})^+}{\partial l_{JI}^+} - \frac{\partial(\Lambda_1^{JI})^-}{\partial l_{JI}^-}],\ (S_{10}^C)_{JI} = \frac{\partial^3\Phi_1^{JI}}{\partial a_I^2\partial b_{JI}} - \frac{1}{3}\frac{\partial^3\Phi_1^{JI}}{\partial b_{JI}^3},$$

$$(S_{11}^C)_{JI} = \frac{\partial^3(\Phi_1^{JI})^+}{\partial a_I^2\partial l_{JI}^+} - \frac{\partial^3(\Phi_1^{JI})^-}{\partial a_I^2\partial l_{JI}^-} - \frac{1}{3}[\frac{\partial^3(\Phi_1^{JI})^+}{\partial(l_{JI}^+)^3} - \frac{\partial^3(\Phi_1^{JI})^-}{\partial(l_{JI}^-)^3}],$$

$$(S_{12}^C)_{JI} = \frac{\partial^3\Phi_1^{JI}}{\partial b_{JI}^2\partial a_I} - \frac{1}{3}\frac{\partial^3\Phi_1^{JI}}{\partial a_I^3},$$

$$(S_{13}^C)_{JI} = [\frac{\partial^3(\Phi_1^{JI})^+}{\partial(l_{JI}^+)^2\partial a_I} - \frac{\partial^3(\Phi_1^{JI})^-}{\partial(l_{JI}^-)^2\partial a_I}] - \frac{1}{3}\frac{\partial^3\Phi_1^{JI}}{\partial a_I^3},$$

$$(S_{14}^C)_{JI} = [\frac{\partial^3(\Phi_1^{JI})^+}{\partial(l_{JI}^+)^2\partial b_{JI}} - \frac{\partial^3(\Phi_1^{JI})^-}{\partial(l_{JI}^-)^2\partial b_{JI}}] - \frac{1}{3}\frac{\partial^3\Phi_1^{JI}}{\partial b_{JI}^3},$$

$$(S_{15}^C)_{JI} = \frac{\partial^3(\Phi_1^{JI})^+}{\partial b_{JI}^2\partial l_{JI}^+} - \frac{\partial^3(\Phi_1^{JI})^-}{\partial b_{JI}^2\partial l_{JI}^-} - \frac{1}{3}[\frac{\partial^3(\Phi_1^{JI})^+}{\partial(l_{JI}^+)^3} - \frac{\partial^3(\Phi_1^{JI})^-}{\partial(l_{JI}^-)^3}],$$

$$(S_{16}^C)_{JI} = \frac{\partial^3(\Phi_1^{JI})^+}{\partial a_I\partial b_{JI}\partial l_{JI}^+} - \frac{\partial^3(\Phi_1^{JI})^-}{\partial a_I\partial b_{JI}\partial l_{JI}^-},$$

(2.37b)

and

$$\begin{aligned}
S_{ijkl}^G = \frac{1}{8\pi(1-v)}\sum_{J=1}^{q}\sum_{I=1}^{p}\Big\{&(S_1^G)_{JI}(\zeta_I^0)_i(\zeta_I^0)_j\delta_{kl} + (S_2^G)_{JI}[(\zeta_I^0)_i(\zeta_I^0)_k\delta_{jl} + (\zeta_I^0)_i(\zeta_I^0)_l\delta_{jk}]\\
&+ (S_3^G)_{JI}[(\zeta_I^0)_k(\zeta_I^0)_j\delta_{il} + (\zeta_I^0)_l(\zeta_I^0)_j\delta_{ik}] + (S_4^G)_{JI}(\zeta_I^0)_i(\lambda_{JI}^0)_j\delta_{kl}\\
&+ (S_5^G)_{JI}[(\zeta_I^0)_i(\lambda_{JI}^0)_k\delta_{jl} + (\zeta_I^0)_i(\lambda_{JI}^0)_l\delta_{jk}] + (S_6^G)_{JI}[(\lambda_{JI}^0)_k(\zeta_I^0)_j\delta_{il} + (\lambda_{JI}^0)_l(\zeta_I^0)_j\delta_{ik}]\\
&+ (S_7^G)_{JI}(\zeta_I^0)_i(\eta_{JI}^0)_j\delta_{kl} + (S_8^G)_{JI}[(\zeta_I^0)_i(\eta_{JI}^0)_k\delta_{jl} + (\zeta_I^0)_i(\eta_{JI}^0)_l\delta_{jk}]\\
&+ (S_9^G)_{JI}[(\eta_{JI}^0)_k(\zeta_I^0)_j\delta_{il} + (\eta_{JI}^0)_l(\zeta_I^0)_j\delta_{ik}] + (S_{10}^G)_{JI}[(\zeta_I^0)_i(\lambda_{JI}^0)_j(\zeta_I^0)_k(\zeta_I^0)_l\\
&+ (\zeta_I^0)_i(\zeta_I^0)_j(\lambda_{JI}^0)_k(\zeta_I^0)_l + (\zeta_I^0)_i(\zeta_I^0)_j(\zeta_I^0)_k(\lambda_{JI}^0)_l] + (S_{11}^G)_{JI}[(\zeta_I^0)_i(\eta_{JI}^0)_j(\zeta_I^0)_k(\zeta_I^0)_l\\
&+ (\zeta_I^0)_i(\zeta_I^0)_j(\eta_{JI}^0)_k(\zeta_I^0)_l + (\zeta_I^0)_i(\zeta_I^0)_j(\zeta_I^0)_k(\eta_{JI}^0)_l] + (S_{12}^G)_{JI}[(\zeta_I^0)_i(\zeta_I^0)_j(\lambda_{JI}^0)_k(\lambda_{JI}^0)_l\\
&+ (\zeta_I^0)_i(\lambda_{JI}^0)_j(\zeta_I^0)_k(\lambda_{JI}^0)_l + (\zeta_I^0)_i(\lambda_{JI}^0)_j(\lambda_{JI}^0)_k(\zeta_I^0)_l] + (S_{13}^G)_{JI}[(\zeta_I^0)_i(\zeta_I^0)_j(\eta_{JI}^0)_k(\eta_{JI}^0)_l\\
&+ (\zeta_I^0)_i(\eta_{JI}^0)_j(\zeta_I^0)_k(\eta_{JI}^0)_l + (\zeta_I^0)_i(\eta_{JI}^0)_j(\eta_{JI}^0)_k(\zeta_I^0)_l] + (S_{14}^G)_{JI}[(\zeta_I^0)_i(\lambda_{JI}^0)_j(\eta_{JI}^0)_k(\eta_{JI}^0)_l\\
&+ (\zeta_I^0)_i(\eta_{JI}^0)_j(\lambda_{JI}^0)_k(\eta_{JI}^0)_l + (\zeta_I^0)_i(\eta_{JI}^0)_j(\eta_{JI}^0)_k(\lambda_{JI}^0)_l] + (S_{15}^G)_{JI}[(\zeta_I^0)_i(\eta_{JI}^0)_j(\lambda_{JI}^0)_k(\lambda_{JI}^0)_l
\end{aligned}$$

$$+(\zeta_I^0)_i(\lambda_{JI}^0)_j(\eta_{JI}^0)_k(\lambda_{JI}^0)_l+(\zeta_I^0)_i(\lambda_{JI}^0)_j(\lambda_{JI}^0)_k(\eta_{JI}^0)_l]+(S_{16}^G)_{JI}[(\zeta_I^0)_i(\zeta_I^0)_j(\lambda_{JI}^0)_k(\eta_{JI}^0)_l$$
$$+(\zeta_I^0)_i(\zeta_I^0)_j(\eta_{JI}^0)_k(\lambda_{JI}^0)_l+(\zeta_I^0)_i(\lambda_{JI}^0)_j(\eta_{JI}^0)_k(\zeta_I^0)_l+(\zeta_I^0)_i(\lambda_{JI}^0)_j(\zeta_I^0)_k(\eta_{JI}^0)_l$$
$$+(\zeta_I^0)_i(\eta_{JI}^0)_j(\zeta_I^0)_k(\lambda_{JI}^0)_l+(\zeta_I^0)_i(\eta_{JI}^0)_j(\lambda_{JI}^0)_k(\zeta_I^0)_l]\Big\},$$

(2.37c)

where

$$(S_1^G)_{JI}=\frac{2L^2}{3}\frac{\partial^3(\Lambda_1^{JI}-\Gamma_1^{JI})}{\partial a_I^3}+\frac{4\nu(1-\nu)}{(1-2\nu)}\frac{\partial\Gamma_1^{JI}}{\partial a_I}+\frac{2\nu L^2}{(1-2\nu)}\left\{\frac{\partial^3(\Lambda_1^{JI}-\Gamma_1^{JI})}{\partial a_I^3}+\frac{\partial^3(\Lambda_1^{JI}-\Gamma_1^{JI})}{\partial a_I\partial b_{JI}^2}\right.$$
$$\left.+\frac{\partial^3[(\Lambda_1^{JI})^+-(\Gamma_1^{JI})^+]}{\partial a_I\partial(l_{JI}^+)^2}-\frac{\partial^3[(\Lambda_1^{JI})^--(\Gamma_1^{JI})^-]}{\partial a_I\partial(l_{JI}^-)^2}\right\},$$
$$(S_2^G)_{JI}=\frac{2L^2}{3}\frac{\partial^3(\Lambda_1^{JI}-\Gamma_1^{JI})}{\partial a_I^3}+(1-\nu)\frac{\partial\Gamma_1^{JI}}{\partial a_I},\qquad(S_3^G)_{JI}=(1-\nu)\frac{\partial\Gamma_1^{JI}}{\partial a_I},$$
$$(S_4^G)_{JI}=\frac{2L^2}{3}\frac{\partial^3(\Lambda_1^{JI}-\Gamma_1^{JI})}{\partial b_{JI}^3}+\frac{4\nu(1-\nu)}{(1-2\nu)}\frac{\partial\Gamma_1^{JI}}{\partial b_{JI}}+\frac{2\nu L^2}{(1-2\nu)}\left\{\frac{\partial^3(\Lambda_1^{JI}-\Gamma_1^{JI})}{\partial a_I^2\partial b_{JI}}+\frac{\partial^3(\Lambda_1^{JI}-\Gamma_1^{JI})}{\partial b_{JI}^3}\right.$$
$$\left.+\frac{\partial^3[(\Lambda_1^{JI})^+-(\Gamma_1^{JI})^+]}{\partial b_{JI}\partial(l_{JI}^+)^2}-\frac{\partial^3[(\Lambda_1^{JI})^--(\Gamma_1^{JI})^-]}{\partial b_{JI}\partial(l_{JI}^-)^2}\right\},$$
$$(S_5^G)_{JI}=\frac{2L^2}{3}\frac{\partial^3(\Lambda_1^{JI}-\Gamma_1^{JI})}{\partial b_{JI}^3}+(1-\nu)\frac{\partial\Gamma_1^{JI}}{\partial b_{JI}},\qquad(S_6^G)_{JI}=(1-\nu)\frac{\partial\Gamma_1^{JI}}{\partial b_{JI}},$$
$$(S_7^G)_{JI}=\frac{2L^2}{3}\left\{\frac{\partial^3[(\Lambda_1^{JI})^+-(\Gamma_1^{JI})^+]}{\partial(l_{JI}^+)^3}-\frac{\partial^3[(\Lambda_1^{JI})^--(\Gamma_1^{JI})^-]}{\partial(l_{JI}^-)^3}\right\}+\frac{4\nu(1-\nu)}{(1-2\nu)}\left[\frac{\partial(\Gamma_1^{JI})^+}{\partial l_{JI}^+}-\frac{\partial(\Gamma_1^{JI})^-}{\partial l_{JI}^-}\right]$$
$$+\frac{2\nu L^2}{(1-2\nu)}\left\{\frac{\partial^3[(\Lambda_1^{JI})^+-(\Gamma_1^{JI})^+]}{\partial a_I^2\partial l_{JI}^+}-\frac{\partial^3[(\Lambda_1^{JI})^--(\Gamma_1^{JI})^-]}{\partial a_I^2\partial l_{JI}^-}+\frac{\partial^3[(\Lambda_1^{JI})^+-(\Gamma_1^{JI})^+]}{\partial b_{JI}^2\partial l_{JI}^+}\right.$$
$$\left.-\frac{\partial^3[(\Lambda_1^{JI})^--(\Gamma_1^{JI})^-]}{\partial b_{JI}^2\partial l_{JI}^-}+\frac{\partial^3[(\Lambda_1^{JI})^+-(\Gamma_1^{JI})^+]}{\partial(l_{JI}^+)^3}-\frac{\partial^3[(\Lambda_1^{JI})^--(\Gamma_1^{JI})^-]}{\partial(l_{JI}^-)^3}\right\},$$
$$(S_8^G)_{JI}=\frac{2L^2}{3}\left\{\frac{\partial^3[(\Lambda_1^{JI})^+-(\Gamma_1^{JI})^+]}{\partial(l_{JI}^+)^3}-\frac{\partial^3[(\Lambda_1^{JI})^--(\Gamma_1^{JI})^-]}{\partial(l_{JI}^-)^3}\right\}+(1-\nu)\left[\frac{\partial(\Gamma_1^{JI})^+}{\partial l_{JI}^+}-\frac{\partial(\Gamma_1^{JI})^-}{\partial l_{JI}^-}\right],$$
$$(S_9^G)_{JI}=(1-\nu)\left[\frac{\partial(\Gamma_1^{JI})^+}{\partial l_{JI}^+}-\frac{\partial(\Gamma_1^{JI})^-}{\partial l_{JI}^-}\right],$$

$$
\begin{aligned}
(S_{10}^{G})_{JI} &= 2L^2[\frac{\partial^3(\Lambda_1^{JI}-\Gamma_1^{JI})}{\partial a_I^2\partial b_{JI}}-\frac{1}{3}\frac{\partial^3(\Lambda_1^{JI}-\Gamma_1^{JI})}{\partial b_{JI}^3}],\\
(S_{11}^{G})_{JI} &= 2L^2\{\frac{\partial^3[(\Lambda_1^{JI})^{+}-(\Gamma_1^{JI})^{+}]}{\partial a_I^2\partial l_{JI}^{+}}-\frac{\partial^3[(\Lambda_1^{JI})^{-}-(\Gamma_1^{JI})^{-}]}{\partial a_I^2\partial l_{JI}^{-}}-\frac{1}{3}\frac{\partial^3[(\Lambda_1^{JI})^{+}-(\Gamma_1^{JI})^{+}]}{\partial(l_{JI}^{+})^3}\\
&\quad+\frac{1}{3}\frac{\partial^3[(\Lambda_1^{JI})^{-}-(\Gamma_1^{JI})^{-}]}{\partial(l_{JI}^{-})^3}\},\\
(S_{12}^{G})_{JI} &= 2L^2\left[\frac{\partial^3(\Lambda_1^{JI}-\Gamma_1^{JI})}{\partial b_{JI}^2\partial a_I}-\frac{1}{3}\frac{\partial^3(\Lambda_1^{JI}-\Gamma_1^{JI})}{\partial a_I^3}\right],\\
(S_{13}^{G})_{JI} &= 2L^2\left\{\frac{\partial^3[(\Lambda_1^{JI})^{+}-(\Gamma_1^{JI})^{+}]}{\partial a_I\partial(l_{JI}^{+})^2}-\frac{\partial^3[(\Lambda_1^{JI})^{-}-(\Gamma_1^{JI})^{-}]}{\partial a_I\partial(l_{JI}^{-})^2}-\frac{1}{3}\frac{\partial^3(\Lambda_1^{JI}-\Gamma_1^{JI})}{\partial a_I^3}\right\},\\
(S_{14}^{G})_{JI} &= 2L^2\left\{\frac{\partial^3[(\Lambda_1^{JI})^{+}-(\Gamma_1^{JI})^{+}]}{\partial b_{JI}\partial(l_{JI}^{+})^2}-\frac{\partial^3[(\Lambda_1^{JI})^{-}-(\Gamma_1^{JI})^{-}]}{\partial b_{JI}\partial(l_{JI}^{-})^2}-\frac{1}{3}\frac{\partial^3(\Lambda_1^{JI}-\Gamma_1^{JI})}{\partial b_{JI}^3}\right\},\\
(S_{15}^{G})_{JI} &= 2L^2\left\{\frac{\partial^3[(\Lambda_1^{JI})^{+}-(\Gamma_1^{JI})^{+}]}{\partial b_{JI}^2\partial l_{JI}^{+}}-\frac{\partial^3[(\Lambda_1^{JI})^{-}-(\Gamma_1^{JI})^{-}]}{\partial b_{JI}^2\partial l_{JI}^{-}}-\frac{1}{3}\frac{\partial^3[(\Lambda_1^{JI})^{+}-(\Gamma_1^{JI})^{+}]}{\partial(l_{JI}^{+})^3}\right.\\
&\quad\left.+\frac{1}{3}\frac{\partial^3[(\Lambda_1^{JI})^{-}-(\Gamma_1^{JI})^{-}]}{\partial(l_{JI}^{-})^3}\right\},\\
(S_{16}^{G})_{JI} &= 2L^2\left\{[\frac{\partial^3[(\Lambda_1^{JI})^{+}-(\Gamma_1^{JI})^{+}]}{\partial a_I\partial b_{JI}\partial l_{JI}^{+}}-\frac{\partial^3[(\Lambda_1^{JI})^{-}-(\Gamma_1^{JI})^{-}]}{\partial a_I\partial b_{JI}\partial l_{JI}^{-}}]\right\}.
\end{aligned}
\tag{2.37d}
$$

In Eqs. (2.37b,d), Φ_1^{JI}, $(\Phi_1^{JI})^{+}$, $(\Phi_1^{JI})^{-}$, Λ_1^{JI}, $(\Lambda_1^{JI})^{+}$, $(\Lambda_1^{JI})^{-}$, Γ_1^{JI}, $(\Gamma_1^{JI})^{+}$ and $(\Gamma_1^{JI})^{-}$ are defined in Eqs. (2.28) and (2.31).

It should be mentioned that the classical part S_{ijkl}^{C} in Eqs. (2.37a,b) depends only on Poisson's ratio ν and cannot account for the inclusion size effect, noting that Φ_1^{JI}, $(\Phi_1^{JI})^{+}$, $(\Phi_1^{JI})^{-}$, Λ_1^{JI}, $(\Lambda_1^{JI})^{+}$ and $(\Lambda_1^{JI})^{-}$ involved in Eq. (2.37b) do not contain the material length scale parameter L (see Eq. (2.28)). However, the gradient part S_{ijkl}^{G} in Eqs. (2.37c,d) can capture the inclusion size effect, since Eqs. (2.37c,d) as well as the expressions of Γ_1^{JI}, $(\Gamma_1^{JI})^{+}$ and $(\Gamma_1^{JI})^{-}$ (see Eq. (2.31)) contain the parameter L in addition

to Poisson's ratio ν. Clearly, when $L = 0$ (i.e., in the absence of the strain gradient effect), $S^G_{ijkl} \equiv 0$ according to Eqs. (2.37c,d) and (2.31), thereby resulting in $S_{ijkl} = S^C_{ijkl}$ from Eq. (2.9a). That is, the SSGET-based Eshelby tensor reduces to its counterpart based on classical elasticity when the strain gradient effect is not considered. Also, it is seen that the expressions of the classical elasticity-based Eshelby tensor in Eqs. (2.37a,b) and (2.28) derived here are more compact than those given in Nozaki and Taya (2001). The expressions of the Eshelby tensor S_{ijkl} in Eqs. (2.9a) and (2.37a–d) are derived for a p-faced polyhedral inclusion of arbitrary shape. For simple-shape inclusions, more explicit expressions can be obtained for S_{ijkl}.

2.3.2 Averaged Eshelby tensor

The volume average of the position-dependent Eshelby tensor, $\overline{S}_{ijkl}$, is given by

$$\overline{S}_{ijkl} = \frac{1}{V_\Omega} \sum_{M=1}^{p} \sum_{N=1}^{n} \sum_{I=1}^{p} \sum_{J=1}^{q} \iiint_{\Omega_{NM}} (S_{NM})_{ijkl}(a_I, b_{JI}, l^+_{JI}, l^-_{JI}) dV, \tag{2.38}$$

where $(S_{NM})_{ijkl}$ is the Eshelby tensor at point $\mathbf{x}$ inside Ω_{NM} presented in Eqs. (2.9a) and (2.37a–d), V_Ω is the volume of the polyhedral inclusion Ω, Ω_{NM} is the region occupied by the duplex formed by the origin (point **o)** of the global coordinate system, the projection of point **o** onto the Mth polygonal surface (i.e., O_M) and two vertices on the Nth edge of the Mth surface (i.e., V^+_{NM} and V^-_{NM}), and n is the number of edges on the Mth surface. Note that this duplex Ω_{NM} is different from that formed by point $\mathbf{x}$, its projection onto the Ith polygonal surface (i.e., $\mathbf{x}_I$) and two vertices on the Jth edge of the Ith surface (i.e., V^+_{JI} and V^-_{JI}), as shown in Fig. 2.4.

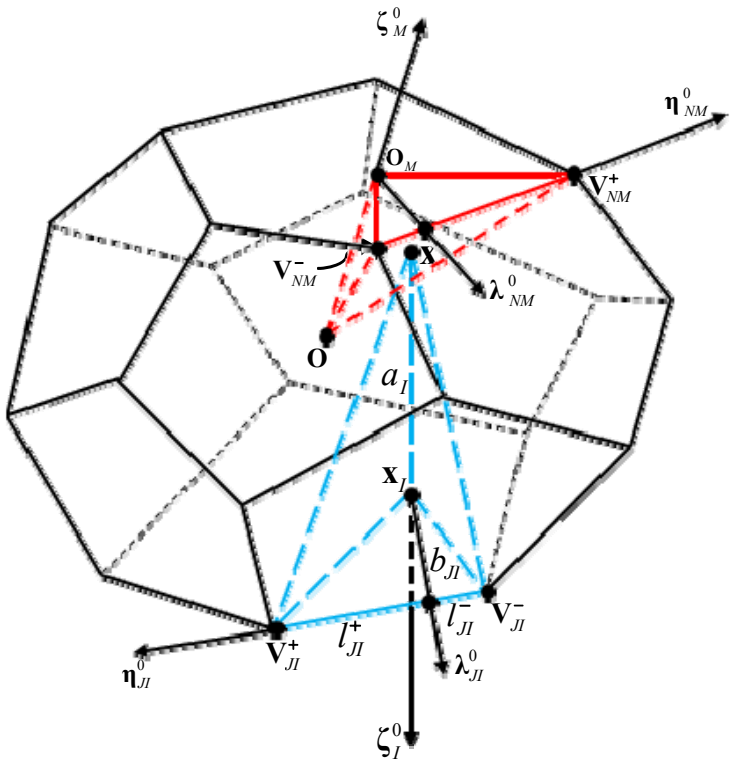

Fig. 2.4 Duplexes and the corresponding local coordinate systems constructed from an arbitrary point **x** and from the origin **o** of the global coordinate system, respectively.

For the *NM*th duplex Ω_{NM} originated from point **o**, the local Cartesian coordinate system $(\lambda_{NM}, \eta_{NM}, \zeta_M)$ can be chosen in a way similar to what was done earlier (see Fig. 2.2). Then, the coordinates of the vertices of the duplex Ω_{JI} on the *J*th edge of the *I*th surface and of an arbitrary point **x** within the *NM*th duplex Ω_{NM} in the $(\lambda_{NM}, \eta_{NM}, \zeta_M)$ local coordinate system can be identified as $(v_1^{JINM+}, v_2^{JINM+}, v_3^{JINM+})$, $(v_1^{JINM-}, v_2^{JINM-}, v_3^{JINM-})$ and $(x_1^{JINM}, x_2^{JINM}, x_3^{JINM})$, respectively.

Also, the base vectors $\boldsymbol{\lambda}_{JI}^{0}$, $\boldsymbol{\eta}_{JI}^{0}$ and $\boldsymbol{\zeta}_{I}^{0}$ of the local coordinate system attached to the duplex Ω_{JI} originated at $\mathbf{x}$ can be expressed in terms of the base vectors $\boldsymbol{\lambda}_{NM}^{0}$, $\boldsymbol{\eta}_{NM}^{0}$ and $\boldsymbol{\zeta}_{M}^{0}$. It then follows that the parameters for the duplex Ω_{JI} can be determined as

$$a_I = (v_k^{JINM+} - x_k^{JINM})(\zeta_I^0)_k^{NM} = (v_k^{JINM-} - x_k^{JINM})(\zeta_I^0)_k^{NM}, \tag{2.39a}$$

$$b_{JI} = (v_k^{JINM+} - x_k^{JINM})(\lambda_{JI}^0)_k^{NM} = (v_k^{JINM-} - x_k^{JINM})(\lambda_{JI}^0)_k^{NM}, \tag{2.39b}$$

$$l_{JI}^{+} = (v_k^{JINM+} - x_k^{JINM})(\eta_{JI}^0)_k^{NM}, \tag{2.39c}$$

$$l_{JI}^{-} = (v_k^{JINM-} - x_k^{JINM})(\eta_{JI}^0)_k^{NM}, \tag{2.39d}$$

where $(\lambda_{JI}^0)_k^{NM}$, $(\eta_{JI}^0)_k^{NM}$ and $(\zeta_I^0)_k^{NM}$ represent, respectively, the kth components of the unit vectors $\boldsymbol{\lambda}_{JI}^{0}$, $\boldsymbol{\eta}_{JI}^{0}$ and $\boldsymbol{\zeta}_{I}^{0}$ in the local coordinate system $(\lambda_{NM}, \eta_{NM}, \zeta_M)$ with the base vectors $\boldsymbol{\lambda}_{NM}^{0}$, $\boldsymbol{\eta}_{NM}^{0}$ and $\boldsymbol{\zeta}_{M}^{0}$.

Using Eqs. (2.39a–d) in Eq. (2.38) yields

$$\begin{aligned}\overline{S}_{ijkl} = \frac{1}{V_\Omega}\sum_{M=1}^{p}\sum_{N=1}^{n}\sum_{I=1}^{p}\sum_{J=1}^{q}\iiint_{\Omega_{NM}} (S_{NM})_{ijkl}[a_I(\lambda_{NM},\eta_{NM},\zeta_M), b_{JI}(\lambda_{NM},\eta_{NM},\zeta_M),\\ l_{JI}^{+}(\lambda_{NM},\eta_{NM},\zeta_M), l_{JI}^{-}(\lambda_{NM},\eta_{NM},\zeta_M)]d\lambda_{NM}d\eta_{NM}d\zeta_M.\end{aligned} \tag{2.40}$$

This general formula can be used for a polyhedral inclusion of arbitrary shape.

For a polyhedron inclusion that is symmetric about the global coordinate axes x_1, x_2 and x_3, only one eighth of the inclusion needs to be considered and the global coordinate system can be used in all computations. The one-eighth polyhedral domain can be divided into several sub-polyhedra with their top and bottom surfaces parallel to the x_1x_2-plane, and the volume integral over each sub-domain can be evaluated by direct integration using the global coordinate system. Also, only the global coordinates of all

vertices need to be determined, and the unit vectors $\boldsymbol{\lambda}_{JI}^{0}$, $\boldsymbol{\eta}_{JI}^{0}$ and $\boldsymbol{\zeta}_{I}^{0}$ in the local coordinate system can be expressed in terms of the base vectors (i.e., $\mathbf{e}_1$, $\mathbf{e}_2$, $\mathbf{e}_3$) in the global coordinate system. As a result, Eq. (2.40) can be simplified to

$$\overline{S}_{ijkl} = \frac{8}{V_\Omega} \sum_{T=1}^{t} \sum_{I=1}^{p} \sum_{J=1}^{q} \iiint_{\Omega_T} (S_T)_{ijkl} [a_I(x_1, x_2, x_3), b_{JI}(x_1, x_2, x_3), l_{JI}^{+}(x_1, x_2, x_3), l_{JI}^{-}(x_1, x_2, x_3)] dx_1 dx_2 dx_3, \tag{2.41}$$

where t is the number of sub-polyhedra in the one eighth of the polyhedral inclusion, and $(S_T)_{ijkl}$ is the Eshelby tensor at point $\mathbf{x}$ inside Ω_T given in Eqs. (2.9a) and (2.37a–d).

2.4 Numerical Results

To illustrate the general formulas of the Eshelby tensor for a p-faced polyhedral inclusion of arbitrary shape derived in Section 3, three types of polyhedral inclusions (i.e., cubic, octahedral and tetrakaidecahedral) shown in Fig. 2.5 are quantitatively studied in this section. Cuboids are the first polyhedral inclusions investigated using classical elasticity (e.g., Chiu, 1977; Lee and Johnson, 1978; Liu and Wang, 2005). A tetrakaidecahedron can be generated by uniformly truncating the six corners of an octahedron and is known to be the only polyhedron that can pack with identical units to fill space and nearly minimize the surface energy (e.g., Li *et al.*, 2003). Tetrakaidecahedral cells have been frequently used to represent foamed materials and interpenetrating phase composites (e.g., Li *et al.*, 2003, 2006; Jhaver and Tippur, 2009).

Two components, S_{1111} and S_{1212}, of the Eshelby tensor at any point $\mathbf{x}$ inside each polyhedral inclusion with various sizes are evaluated using Eqs. (2.9a), (2.37a–d), (2.28) and (2.31) and plotted to demonstrate how the components change with the position and

inclusion size. Also, how the average Eshelby tensor component $\overline{S}_{1111}$ varies with the inclusion size is presented here, which is computed using Eq. (2.41). For illustration purposes, Poisson's ratio ν is taken to be 0.3 and the material length scale parameter L to be 17.6 μm in the current numerical analysis, as was done earlier (Gao and Ma, 2009, 2010a,b; Ma and Gao, 2010, 2011).

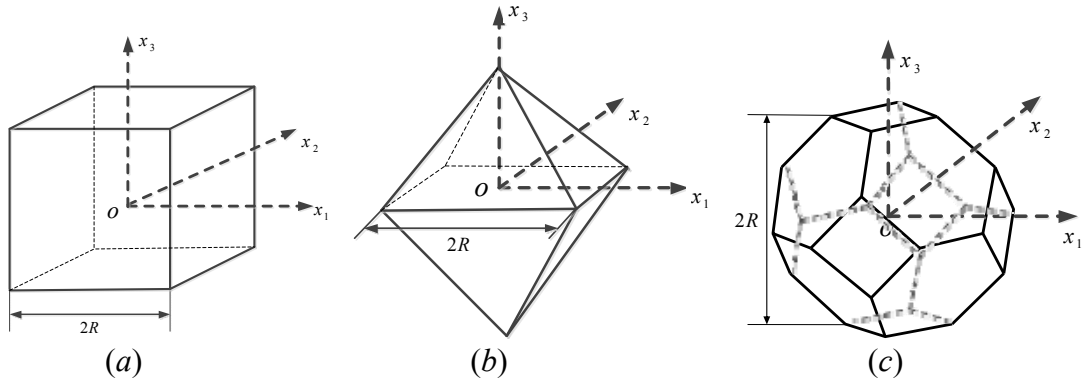

Fig. 2.5 Three types of polyhedral inclusions: (*a*) cubic, (*b*) octahedral, and (*c*) tetrakaidecahedral.

The distributions of S_{1111} for the cubic, octahedral, and tetrakaidecahedral inclusions along the x_1 axis predicted by the current model are shown in Figs. 2.6–2.8, where the values of S_{1111}^{C} are also displayed for comparison.

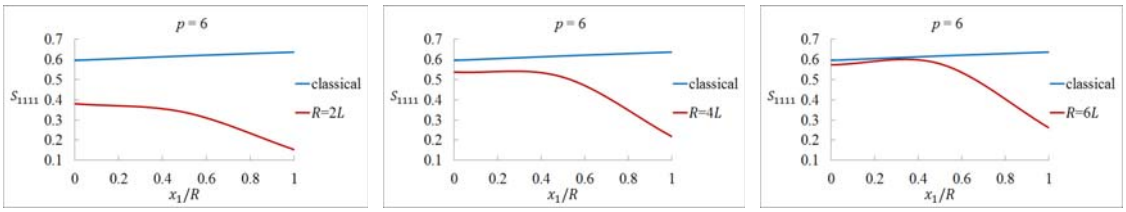

(*a*) (*b*) (*c*)

Fig. 2.6 Variation of S_{1111} along the x_1 axis inside the cubic inclusion: (*a*) $R = 2L$, (*b*) $R = 4L$, and (*c*) $R = 6L$, with R being half of the edge length (see Fig. 2.5(*a*)).

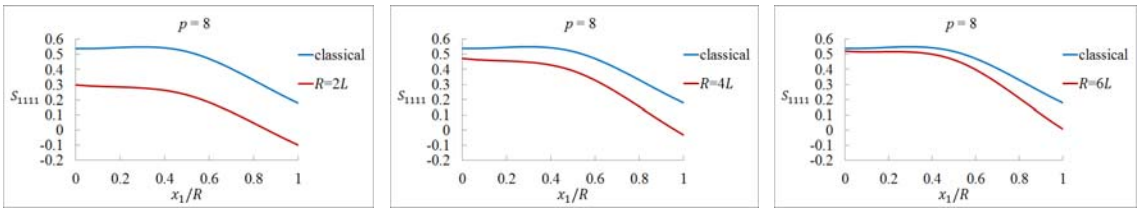

(*a*) (*b*) (*c*)

Fig. 2.7 Variation of S_{1111} along the x_1 axis inside the octahedral inclusion: (*a*) $R = 2L$, (*b*) $R = 4L$, and (*c*) $R = 6L$, with R being half of the edge length (see Fig. 2.5(*b*)).

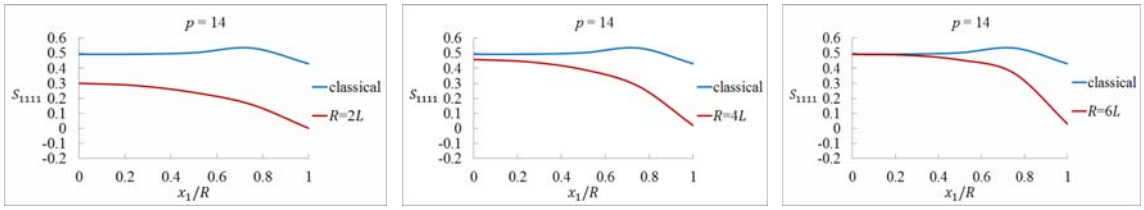

(*a*) (*b*) (*c*)

Fig. 2.8 Variation of S_{1111} along the x_1 axis inside the tetrakaidecahedral inclusion: (*a*) $R = 2L$, (*b*) $R = 4L$, and (*c*) $R = 6L$, with R being half of the cell height (see Fig. 2.5(*c*)).

It can be seen from Figs. 2.6–2.8 that the classical part S^C_{1111} (based on classical elasticity) varies with the position of **x** within each polyhedral inclusion rather than uniform, which shows that the Eshelby conjecture is true for the three polyhedral inclusion shapes considered here. Also, it is found that for each of the three inclusion

shapes S^C_{1111} at a given value of x_1/R is the same for all values of R/L, confirming the inclusion size-independence of the classical part of the Eshelby tensor, which is noted near the end of Section 2.3.1. In addition, for all three polyhedral inclusion shapes considered, it is observed from Figs. 2.6–2.8 that when the characteristic inclusion size R (see Fig. 2.5) is small (compared to the length scale parameter L, e.g., $R/L = 2$), the strain gradient part S^G_{1111}, which is the difference between S_{1111} and S^C_{1111} (i.e., $S^G_{1111} = S_{1111} - S^C_{1111}$) and is displayed as the vertical distance between the S^C_{1111} curve and each S_{1111} curve in Figs. 2.6–2.8, is significant and should not be neglected. However, as the inclusion size becomes larger, the values of S_{1111} are all getting closer to those of S^C_{1111}. This means that the inclusion size effect is less significant and may be ignored for large inclusions in some cases, which agrees with the general trend observed experimentally (e.g., Cho *et al.*, 2006).

The change of S_{1212} with the position and inclusion size is illustrated in Figs. 2.9–2.12 together with a comparison with S^C_{1212} for the three types of polyhedral inclusions. Clearly, S^C_{1212} varies with the position of $\mathbf{x}$ inside each polyhedral inclusion, which differs from that in an ellipsoidal inclusion and supports the Eshelby conjecture. But the classical part S^C_{1212} at a given value of x_1/R remains the same for all inclusion sizes, as expected from the discussion in Section 2.3.1. The gradient part S^G_{1212}, as the difference between S_{1212} and S^C_{1212} (i.e., $S^G_{1212} = S_{1212} - S^C_{1212}$), is seen to be significantly large for small inclusions (e.g., $R/L = 2$) and becomes insignificant for large inclusions for all three types of polyhedral inclusions. More specifically, it is observed from Fig. 2.9 that

for the cubic inclusion the strain gradient effect, as measured by the value of S^{G}_{1212}, is large for all inclusion sizes when $x_1/R > 0.6$. For the octahedral inclusion, the strain gradient effect is insignificant and can be neglected when $R/L > 4$, as illustrated in Fig. 2.10. For the tetrakaidecahedral inclusion, Fig. 2.11 shows that the strain gradient effect is also small, especially in the region away from the square faces.

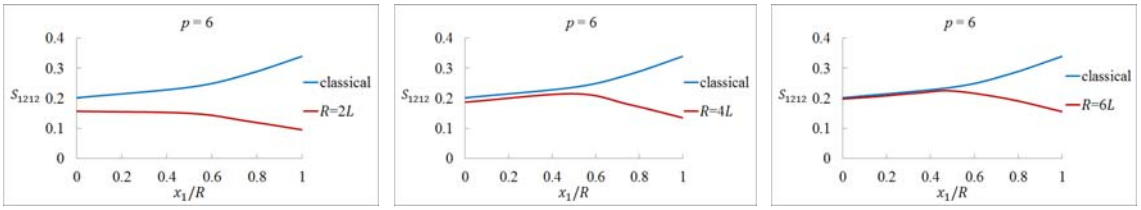

(*a*) (*b*) (*c*)

Fig. 2.9 Variation of S_{1212} along the x_1 axis inside the cubic inclusion: (*a*) $R = 2L$, (*b*) $R=4L$, and (*c*) $R = 6L$, with R being half of the edge length (see Fig. 2.5(*a*)).

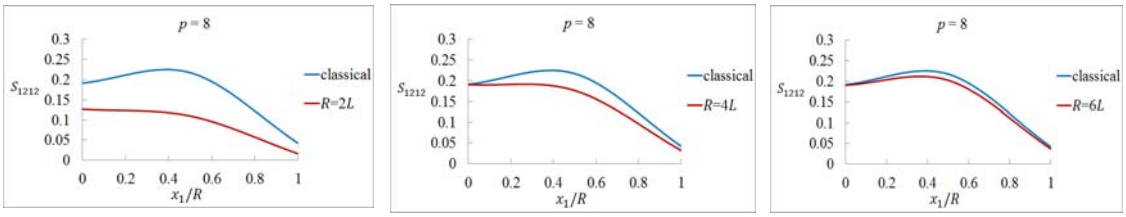

(*a*) (*b*) (*c*)

Fig. 2.10 Variation of S_{1212} along the x_1 axis inside the octahedral inclusion: (*a*) $R = 2L$, (*b*) $R = 4L$, and (*c*) $R = 6L$, with R being half of the edge length (see Fig. 2.5(*b*)).

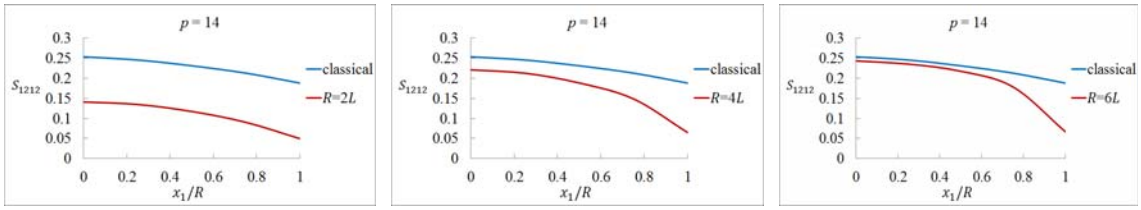

(*a*) (*b*) (*c*)

Fig. 2.11 Variation of S_{1212} along the x_1 axis inside the tetrakaidecahedral inclusion: (*a*) $R = 2L$, (*b*) $R = 4L$, and (*c*) $R = 6L$, with R being half of the cell height (see Fig. 2.5(*c*)).

The component $\overline{S}_{1111}$ of the averaged Eshelby tensor varying with the inclusion size is shown in Fig. 2.12 for the three inclusion shapes, where $\overline{S}^{C}_{1111}$ is also displayed for comparison. The values of $\overline{S}_{1111}$ shown in Fig. 2.12 are obtained using Eqs. (2.41) and (2.39a–d), which are also applied to get the values of $\overline{S}^{C}_{1111}$ with $L \to 0$.

It can be seen from Fig. 2.12 that for each polyhedral inclusion $\overline{S}^{C}_{1111}$ (based on classical elasticity) is a constant independent of the inclusion size R. However, $\overline{S}_{1111}$ predicted by the current model based on the strain gradient elasticity theory does vary with the inclusion size: the smaller the inclusion, the smaller the Eshelby tensor component. In particular, when the inclusion is small, the strain gradient effect, as measured by $\overline{S}^{G}_{1111} (= \overline{S}_{1111} - \overline{S}^{C}_{1111})$, is significantly large and should not be ignored. As the inclusion becomes large, $\overline{S}_{1111}$ approaches $\overline{S}^{C}_{1111}$ from below, indicating that the strain gradient effect gets small and may be neglected for very large inclusions.

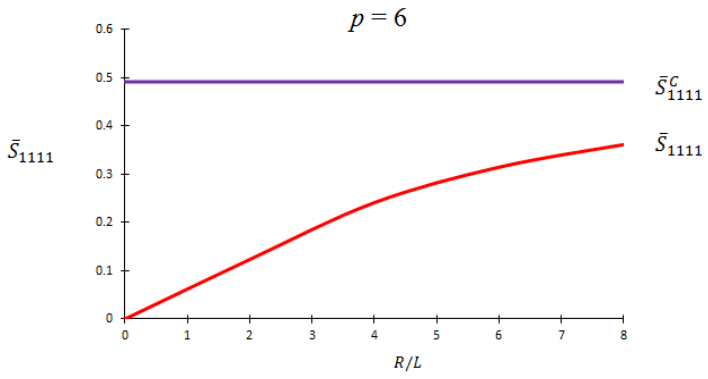

(*a*)

Fig. 2.12 Variation of $\overline{S}_{1111}$ with the inclusion size: (*a*) cubic, (*b*) octahedral, and (*c*) tetrakaidecahedral.

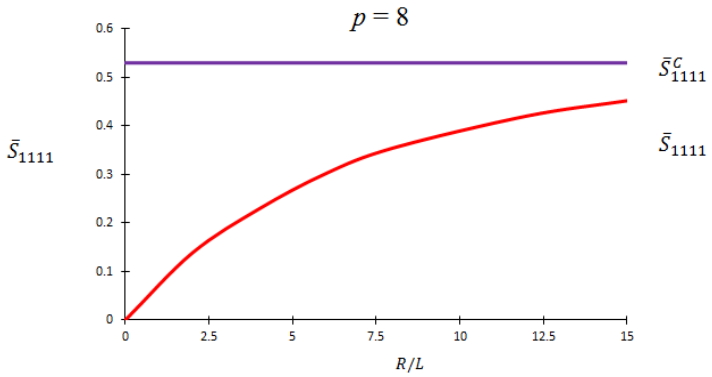

(*b*)

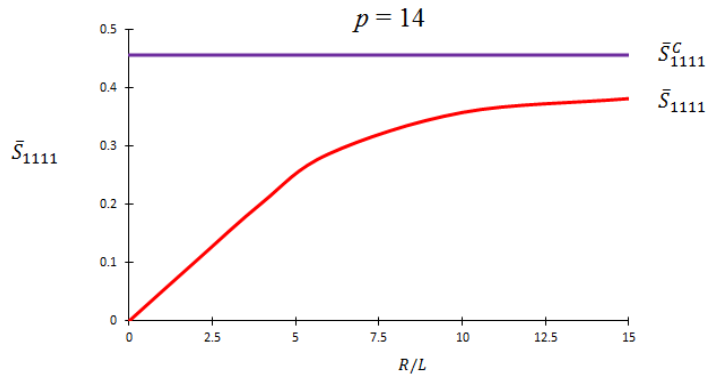

(*c*)

Fig. 2.12 Continued.

The observations made here are also true for the other components of the Eshelby tensor S_{ijkl} in Eqs. (2.9a), (2.37a–d), (2.28) and (2.31) and its volume average $\overline{S}_{ijkl}$ in Eq. (2.41).

From the numerical results presented above, it is clear that the newly obtained Eshelby tensor based on the SSGET can capture the inclusion size effect at the micron scale, while the Eshelby tensor based on classical elasticity does not have this capability.

2.5 Summary

An analytical solution is provided for the Eshelby-type problem of an arbitrarily shaped polyhedral inclusion embedded in an infinite elastic matrix by using a simplified strain gradient elasticity theory (SSGET) that contains one material length scale parameter in addition to two classical elastic constants. The SSGET-based Eshelby tensor for a polyhedral inclusion of arbitrary shape is derived in a general analytical form in terms of three potential functions, two of which are the same as the ones involved in the Eshelby tensor based on classical elasticity. These potential functions, as three volume integrals over the inclusion, are evaluated by dividing the polyhedral inclusion domain into tetrahedral duplexes. Each of the three volume integrals is first transformed into a surface integral by applying the divergence theorem, which is then transformed to a contour (line) integral based on Stokes' theorem and using an inverse approach that differs from those employed in the existing studies based on classical elasticity. The newly obtained Eshelby tensor is separated into a classical part and a gradient part. The classical part depends only on Poisson's ratio of the matrix material, while the gradient part depends on both Poisson's ratio and the material length scale parameter that enables the explanation of the inclusion size effect. This SSGET-based Eshelby tensor reduces to its counterpart based on classical elasticity when the strain gradient effect is not considered. A general form of the volume averaged Eshelby tensor over the polyhedral inclusion is also obtained, which can be used in homogenization analyses of composites containing polyhedral inclusions.

To demonstrate the newly derived Eshelby tensor, three types of polyhedral inclusions, cubic, octahedral and tetrakaidecahedral, are analyzed by applying the general formulas directly. The numerical results reveal that for each of the three inclusion shapes the components of the new Eshelby tensor change with the position and inclusion size, whereas their classical elasticity–based counterparts only vary with the position. When the inclusion is small, the gradient part is seen to contribute significantly and should not be ignored. Also, it is found that the smaller the inclusion size is, the smaller the components of the volume-averaged Eshelby tensor are. These components approach from below the values of their classical elasticity based counterparts as the inclusion size becomes large. Hence, the inclusion size effect may be neglected for large polyhedral inclusions in some cases.

CHAPTER III

STRAIN GRADIENT SOLUTION FOR THE ESHELBY-TYPE POLYGONAL INCLUSION PROBLEM

3.1 Introduction

Eshelby's eigenstrain method is widely used to study the elastic field induced by an inclusion with a uniform eigenstrain. The determination of Eshelby's tensor for the inclusion which relates disturbed strain to the eigenstrain is essential in the application of this method. The Eshelby tensor for an arbitrary-shape polygonal inclusion has been analytically obtained by Nozaki and Taya (1997), Nozaki et al (2001) and Rodin (1996). Special properties and averaged values of Eshelby tensors for polygon inclusions of regular shapes has been studied by Xu and Wang (2005, 2007a), Kawashita and Nozaki (2001), and Zheng et al (2006), and irregular-shaped polygonal inclusion problems have been analyzed by Tsukrov and Novak (2004) and Zou et al (2010). Pan (2004) solved the Eshelby problem of a polygonal inclusion in an anisotropic piezoelectric material. However, these studies are all based on the classical elasticity theory which cannot capture the inclusion size effect due to a lack of any material length scale parameter. Eshelby's tensors based on higher order elasticity theories are therefore needed.

In this chapter, the Eshelby tensor for an arbitrarily shaped polygonal inclusion prescribed with a uniform eigenstrain and a uniform eigenstrain gradient and embedded in an infinite elastic material is derived using the simplified strain gradient elasticity theory (SSGET) (Gao and Park, 2007). The Eshelby tensor obtained includes a classical

part containing Poisson's ratio only and a strain gradient part involving the length scale parameter additionally. The Eshelby tensor is expressed in terms of three potential functions which are surface (area) integrals. These surface integrals are first transformed to line integrals and then evaluated by using inverse Fourier transforms and Laplace transforms. The formulas for the averaged Eshelby tensor components are also derived in this chapter.

The numerical results are presented for the Eshelby tensor components to illustrate their variations with position and inclusion size. The averaged Eshelby tensor components changing with the inclusion size are also quantitatively studied in Section 3.4. A summary is given in the last section.

3.2 Eshelby tensor

Consider an infinite homogeneous isotropic elastic body containing an arbitrary-shape inclusion. The inclusion is prescribed with a uniform eigenstrain $\boldsymbol{\varepsilon}^*$ and a uniform eigenstrain gradient $\boldsymbol{\kappa}^*$. There is no body force or any other external force acting on the elastic body.

The disturbed strain induced by $\boldsymbol{\varepsilon}^*$ and $\boldsymbol{\kappa}^*$ can be shown to be (Gao and Ma, 2009, 2010b)

$$\varepsilon_{\beta\kappa}(\mathbf{x}) = S_{\beta\kappa\gamma o}\varepsilon^*_{\gamma o} + T_{\beta\kappa\gamma o\chi}\kappa^*_{\gamma o\chi}, \tag{3.1}$$

with

$$S_{\beta\kappa\gamma o} = -\frac{1}{2}C_{\alpha\phi\gamma o}[\langle G_{\alpha\beta}(\mathbf{x}-\mathbf{y})\rangle_{,\phi\kappa} + \langle G_{\alpha\kappa}(\mathbf{x}-\mathbf{y})\rangle_{,\phi\beta}], \tag{3.2}$$

$$T_{\beta\kappa\gamma o\chi} = \frac{L^2}{2} C_{\alpha\phi\gamma o}[\langle G_{\alpha\beta}(\mathbf{x}-\mathbf{y})\rangle_{,\chi\phi\kappa} + \langle G_{\alpha\kappa}(\mathbf{x}-\mathbf{y})\rangle_{,\chi\phi\beta}], \tag{3.3}$$

where $S_{\beta\kappa\gamma o}$ is the fourth-order Eshelby tensor having 36 independent components, $T_{\beta\kappa\gamma o\chi}$ is a fifth-order tensor having 108 independent components, and

$$\langle \bullet \rangle = \int_{\Omega} \bullet \, dS(\mathbf{y}) \tag{3.4}$$

is the area integral of $\bullet$ over the inclusion Ω. Eq. (3.1) shows that $\boldsymbol{\varepsilon}$ is solely linked to $\boldsymbol{\varepsilon}^*$ in the absence of $\boldsymbol{\kappa}^*$ (i.e., the classical case) and is fully related to $\boldsymbol{\kappa}^*$ when $\boldsymbol{\varepsilon}^* = \mathbf{0}$.

The Eshelby tensor has been obtained as

$$S_{\beta\kappa\gamma o} = S^C_{\beta\kappa\gamma o} + S^G_{\beta\kappa\gamma o}, \tag{3.5a}$$

$$S^C_{\beta\kappa\gamma o} = \frac{1}{8\pi(1-\nu)}\Big[\Phi_{,\beta\kappa\gamma o} - 2\nu\Lambda_{,\beta\kappa}\delta_{\gamma o} - (1-\nu)(\Lambda_{,o\kappa}\delta_{\beta\gamma} + \Lambda_{,\gamma\kappa}\delta_{\beta o} + \Lambda_{,o\beta}\delta_{\kappa\gamma} + \Lambda_{,\gamma\beta}\delta_{\kappa o})\Big], \tag{3.5b}$$

$$S^G_{\beta\kappa\gamma o} = \frac{1}{8\pi(1-\nu)}\Big[2\nu\Gamma_{,\beta\kappa}\delta_{\gamma o} + (1-\nu)(\Gamma_{,\kappa o}\delta_{\beta\gamma} + \Gamma_{,\beta o}\delta_{\kappa\gamma} + \Gamma_{,\kappa\gamma}\delta_{\beta o} + \Gamma_{,\beta\gamma}\delta_{\kappa o}) + 2L^2(\Lambda_{,\beta\kappa\gamma o} - \Gamma_{,\beta\kappa\gamma o})\Big], \tag{3.5c}$$

where $S^C_{\beta\kappa\gamma o}$ is the classical part, $S^G_{\beta\kappa\gamma o}$ is the strain gradient part, $\delta_{\beta\kappa}$ is the Kronecker delta, and

$$\Phi = \iint_S -|\mathbf{y}-\mathbf{x}|^2(\ln|\mathbf{y}-\mathbf{x}| - \frac{1}{2})dS(\mathbf{y}), \tag{3.6a}$$

$$\Lambda = \iint_S -\ln|\mathbf{y}-\mathbf{x}|^2 dS(\mathbf{y}), \tag{3.6b}$$

$$\Gamma = \iint_S 2K_0(\frac{|\mathbf{y}-\mathbf{x}|}{L})dS(\mathbf{y}) \tag{3.6c}$$

are three scalar-valued potential functions that can be obtained by evaluating the area integrals over Ω, with **y** ($\in \Omega$) being the integration variable and **x** being an arbitrary point inside or outside the inclusion. Note that the first two functions, which are, respectively, a biharmonic potential and a harmonic potential, are the same as the ones involved in the Eshelby tensor based on classical elasticity, while the third function defined in Eq. (3.6c) results from the use of the SSGET.

It can be seen from Eqs. (3.5c) and (3.6b,c) that $S^G_{\beta\kappa\gamma o}$ depends on L, while $S^C_{\beta\kappa\gamma o}$, expressed in terms of the first two potential functions only according to Eqs. (3.5b) and (3.6a,b), is independent of L. Also, it is found that $S^G_{\beta\kappa\gamma o} = 0$ when $L = 0$. As a result, $S_{\beta\kappa\gamma o} = S^C_{\beta\kappa\gamma o}$ when $L = 0$. That is, the current Eshelby tensor reduces to its counterpart based on classical elasticity when the strain gradient effect is not considered.

The fifth order Eshelby-like tensor **T**, which links the eigenstrain gradient $\boldsymbol{\kappa}^*$ to the disturbed strain $\boldsymbol{\varepsilon}^*$ in the elastic body (see Eq. 3.1), is given by

$$T_{\beta\kappa\gamma o\chi} = \frac{L^2}{8\pi(1-\nu)}\Big[2\nu\Psi_{,\beta\kappa\chi}\delta_{\gamma o} + (1-\nu)(\Psi_{,o\chi\beta}\delta_{\kappa\gamma} + \Psi_{,o\chi\kappa}\delta_{\beta\gamma} + \Psi_{,\gamma\chi\beta}\delta_{\kappa o} + \Psi_{,\gamma\chi\kappa}\delta_{\beta o}) - \Pi_{,\beta\kappa\gamma o\chi}\Big], \tag{3.7}$$

where

$$\Psi \equiv \Lambda - \Gamma, \quad \Pi \equiv \Phi + 2L^2(\Lambda - \Gamma), \tag{3.8a,b}$$

with Λ, Φ and Γ defined in Eqs. (3.6a-c). It can be clearly seen that **T=0** when L=0. Then, with $S_{\beta\kappa\gamma o} = S^C_{\beta\kappa\gamma o}$ as discussed above, Eq. (3.1) reduces to $\varepsilon_{\beta\kappa} = S^C_{\beta\kappa\gamma o}\varepsilon^*_{\gamma o}$ when L=0, which

is the defining relation for the Eshelby tensor based on classical elasticity (Eshelby, 1957).

3.3 Polygonal inclusion

The problem of an infinite long prismatic inclusion of an arbitrary polygonal cross-sectional shape embedded in an infinite homogeneous isotropic elastic body has been analytically studied by Rodin (1996) and Nozaki and Taya (1997) based on classical elasticity. The SSGET-based Eshelby tensor and its average for the same problem are derived here.

3.3.1 Eshelby tensor

Consider an infinitely long prismatic inclusion of polygonal cross-sectional shape embedded in an infinite homogeneous isotropic elastic material and prescribed with a uniform eigenstrain $\boldsymbol{\varepsilon}^*$ and a uniform eigenstrain gradient $\boldsymbol{\kappa}^*$. This is a plane strain problem, whose analysis can be carried out on a cross-sectional plane. In the present case, the cross section of the inclusion is a *p*-sided polygon of arbitrary shape and is located in the x_1- x_2 plane as shown in Fig. 3.1. The usual Cartesian coordinate system (x_1, x_2) is adopted as the global coordinate system. This *p*-sided polygon can be divided into *p* triangles originated from a chosen arbitrary point **x** through lines connecting **x** and one of the vertices (Waldvogel, 1979; Rodin, 1996). One side of each triangle is an edge of the polygon. For each of the triangles the local coordinate system is constructed with origin at point **x** and its two coordinate axes denoted by λ and η along and perpendicular to the polygon edge, respectively. The coordinates of two vertices $\mathrm{V}_I^+, \mathrm{V}_I^-$ on the *I*th edge

of the polygon are, respectively, given by (b_I, l_I^+) and (b_I, l_I^-) (see Fig. 3.1(b)). $\boldsymbol{\lambda}_I^0$, $\boldsymbol{\eta}_I^0$ are the unit vectors associated with the local coordinates λ_I and η_I, and **y** is an arbitrary point on the *I*th edge, as shown in Fig. 3.2.

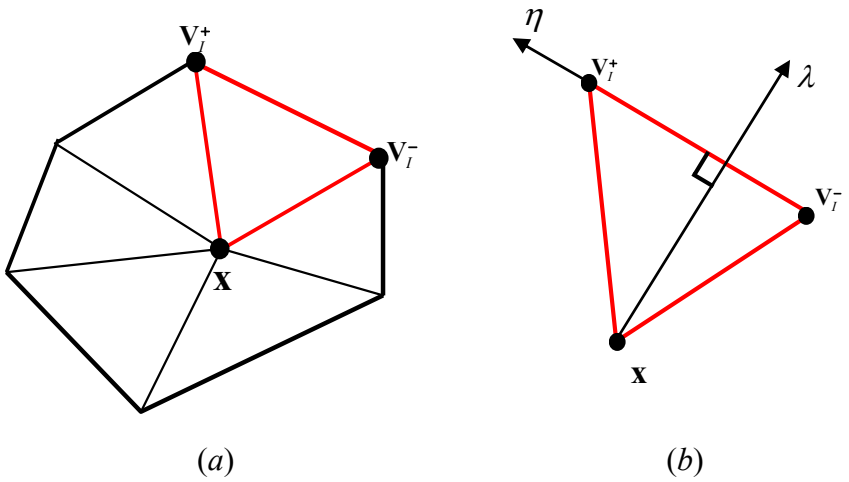

Fig. 3.1 A polygon represented by triangles: (*a*) an arbitrary polygon; (*b*) a triangle and the associated local coordinate system originated from an arbitrary point **x.**

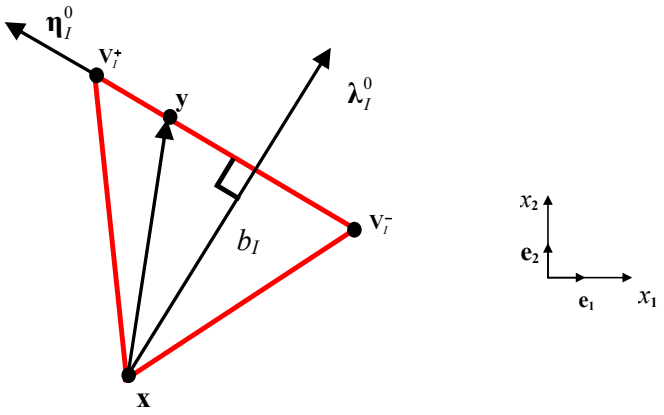

Fig. 3.2 A triangle constructed from point **x** and with its base along the *I*th edge of the *p*-sided polygon.

The three potential functions defined in Eqs. (3.6a-c) are evaluated for each of these *p* triangles. By applying the Green's theorem, the area integrals can be transformed to line integrals as

$$\Phi_{,\beta} = \sum_{I=1}^{p} (\lambda_I^0)_\beta \int_{l_I^-}^{l_I^+} \frac{1}{2}(b_I^2 + \eta^2)[\ln(b_I^2 + \eta^2) - 1] d\eta \,, \tag{3.9}$$

$$\Lambda_{,\beta} = \sum_{I=1}^{p} (\lambda_I^0)_\beta \int_{l_I^-}^{l_I^+} \ln(b_I^2 + \eta^2) d\eta \,, \tag{3.10}$$

$$\Gamma_{,\beta} = -\sum_{I=1}^{p} (\lambda_I^0)_\beta \int_{l_I^-}^{l_I^+} 2K_0(\frac{\sqrt{b_I^2 + \eta^2}}{L}) d\eta \,, \tag{3.11}$$

where $|\mathbf{y} - \mathbf{x}|^2 = b_I^2 + \eta^2$ for any $\mathbf{y}$ on the *I*th edge, $b_I \equiv (\mathbf{y} - \mathbf{x}) \bullet \boldsymbol{\lambda}_I^0$, $(\lambda_I^0)_\beta$ is the β th component of the unit normal vector on the *I*th edge, and η is the local coordinate axis along the *I*th edge.

The first two integrals can be evaluated by direct integration to obtain

$$\begin{aligned}\Phi_{,\beta} = \sum_{I=1}^{p} (\lambda_I^0)_\beta \{ &-\frac{7b_I^2(l_I^+ - l_I^-)}{6} - \frac{5[(l_I^+)^3 - (l_I^-)^3]}{18} + \frac{2b_I^3}{3}[\tan^{-1}(\frac{l_I^+}{b_I}) - \tan^{-1}(\frac{l_I^-}{b_I})] \\ &+ \frac{1}{2}\ln[b_I^2 + (l_I^+)^2][b_I^2 l_I^+ + \frac{(l_I^+)^3}{3}] - \frac{1}{2}\ln[b_I^2 + (l_I^-)^2](b_I^2 l_I^- + \frac{(l_I^-)^3}{3})\} \\ &\equiv \sum_{I=1}^{p} (\lambda_I^0)_\beta \Phi_1^I,\end{aligned} \tag{3.12}$$

$$\begin{aligned}\Lambda_{,\beta} = \sum_{I=1}^{p} (\lambda_I^0)_\beta \{ &2b_I[\tan^{-1}(\frac{l_I^+}{b_I}) - \tan^{-1}(\frac{l_I^-}{b_I})] + l_I^+ \ln[b_I^2 + (l_I^+)^2] - l_I^- \ln[b_I^2 + (l_I^-)^2] \\ &- 2l_I^+ + 2l_I^-\} \equiv \sum_{I=1}^{p} (\lambda_I^0)_\beta \Lambda_1^I.\end{aligned} \tag{3.13}$$

Note that K_0 can be expressed by using the inverse Fourier transform as

$$2K_0(\frac{r}{L}) = \frac{1}{\pi}\int_{-\infty}^{\infty}\int_{-\infty}^{\infty}\frac{e^{i\boldsymbol{\xi}\bullet\mathbf{r}}}{\xi^2+\frac{1}{L^2}}d^2\xi\,. \tag{3.14}$$

where $r = |\mathbf{r}| = (|\mathbf{y}-\mathbf{x}|)$, $\xi = |\boldsymbol{\xi}|$, and $\boldsymbol{\xi}, \mathbf{r}$ are given by

$$\boldsymbol{\xi} = \xi_1\boldsymbol{\lambda}^0 + \xi_2\boldsymbol{\eta}^0, \qquad \mathbf{r} = b_I\boldsymbol{\lambda}^0 + \eta\boldsymbol{\eta}^0\,. \tag{3.15}$$

Notice that

$$\frac{1}{\xi^2+\frac{1}{L^2}} = \int_0^{\infty} e^{-(\xi^2+\frac{1}{L^2})t}\,dt\,. \tag{3.16}$$

Substituting Eqs. (3.15) and (3.16) into Eq. (3.14) yields

$$\begin{aligned} 2K_0(\frac{\sqrt{b_I^2+\eta^2}}{L}) &= \frac{1}{\pi}\int_0^{\infty}\int_{-\infty}^{\infty}\int_{-\infty}^{\infty} e^{i(\xi_1 b_I+\xi_2\eta)} e^{-(\xi_1^2+\xi_2^2+\frac{1}{L^2})t}\,d\xi_1 d\xi_2 dt \\ &= \int_0^{\infty}\frac{e^{-\frac{(b_I^2+\eta^2)}{4t}} e^{-\frac{t}{L^2}}}{t}dt. \end{aligned} \tag{3.17}$$

Using Eq. (3.17) in Eq. (3.11) then gives

$$\begin{aligned} \Gamma_{,\beta} &= -\sum_{I=1}^{p}(\lambda_I^0)_\beta \sum_{n=0}^{\infty}\frac{(-1)^n}{n!(2n+1)2^{n-1}}(\frac{1}{b_I L})^n K_n(\frac{b_I}{L})[(l_I^+)^{2n+1}-(l_I^-)^{2n+1}] \\ &\equiv -\sum_{I=1}^{p}(\lambda_I^0)_\beta \Gamma_1^I\,. \end{aligned} \tag{3.18}$$

Note that Eqs. (3.9), (3.10) and (3.18) are applicable to both the interior case with $\mathbf{x}$ being inside the inclusion (i.e., $\mathbf{x}\in\Omega$) and the exterior case with $\mathbf{x}$ outside the inclusion (i.e., $\mathbf{x}\notin\Omega$). For $\mathbf{x}\in\Omega$, b_I is positive, while b_I is negative for $\mathbf{x}\notin\Omega$, as shown in Fig. 3.3.

Note that for a smooth function $F(b_I, l_I^+, l_I^-)$ the use of the chain rule gives

$$F_{,\beta} \equiv \frac{\partial F}{\partial x_\beta} = \frac{\partial F}{\partial b_I}\frac{\partial b_I}{\partial x_\beta} + \frac{\partial F}{\partial l_I^+}\frac{\partial l_I^+}{\partial x_\beta} + \frac{\partial F}{\partial l_I^-}\frac{\partial l_I^-}{\partial x_\beta}\,, \tag{3.19}$$

where the parameters b_I, l_I^+, l_I^- are related to $\mathbf{x}$ through

$$b_I = (v_\alpha^+ - x_\alpha)(\lambda_I^0)_\alpha, \tag{3.20a}$$

$$l_I^+ = (v_\alpha^+ - x_\alpha)(\eta_I^0)_\alpha, \tag{3.20b}$$

$$l_I^- = (v_\alpha^- - x_\alpha)(\eta_I^0)_\alpha, \tag{3.20c}$$

in which x_α, v_α^+ and v_α^- are, respectively, the coordinates of the points $\mathbf{x}, \mathbf{V}_I^+$ and $\mathbf{V}_I^-$ in the global coordinate system, and $(\lambda_I^0)_\alpha$ and $(\eta_I^0)_\alpha$ are the components of the unit base vectors $\boldsymbol{\lambda}_I^0$ and $\boldsymbol{\eta}_I^0$ in the global coordinate system.

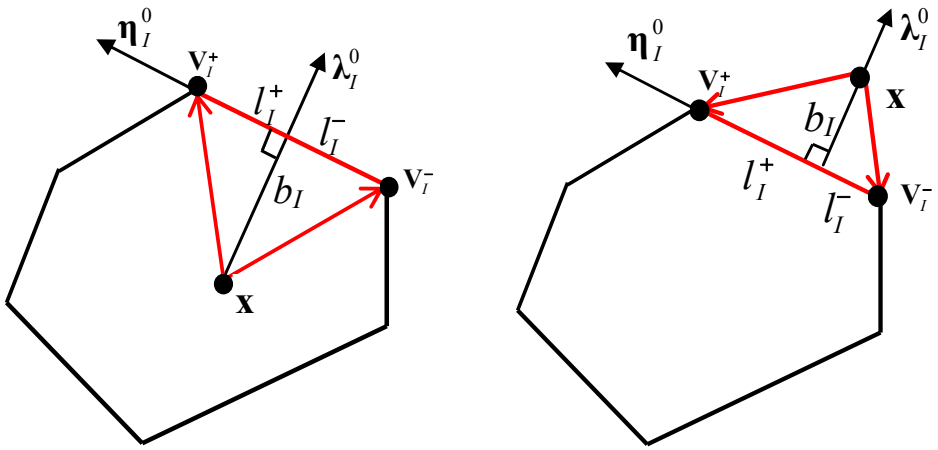

Fig. 3.3 A triangle and parameter b_I, l_I^+, l_I^- : (*a*) inside the inclusion; (*b*) outside the inclusion.

From Eqs. (3.19) and (3.20a-c), it then follows that

$$F_{,\beta} = -\frac{\partial F}{\partial b_I}(\lambda_I^0)_\beta - (\frac{\partial F}{\partial l_I^+} + \frac{\partial F}{\partial l_I^-})(\eta_I^0)_\beta , \tag{3.21}$$

$$\begin{aligned} F_{,\beta\kappa} = {} & \frac{\partial^2 F}{\partial b_I^2}(\lambda_I^0)_\beta(\lambda_I^0)_\kappa + (\frac{\partial^2 F}{\partial b_I \partial l_I^+} + \frac{\partial^2 F}{\partial b_I \partial l_I^-})[(\lambda_I^0)_\beta(\eta_I^0)_\kappa + (\eta_I^0)_\beta(\lambda_I^0)_\kappa] \\ & + [\frac{\partial^2 F}{\partial (l_I^+)^2} + \frac{\partial^2 F}{\partial (l_I^-)^2}](\eta_I^0)_\beta(\eta_I^0)_\kappa \end{aligned} \tag{3.22}$$

$$\begin{aligned} F_{,\beta\kappa\gamma} = {} & -\frac{\partial^3 F}{\partial b_I^3}(\lambda_I^0)_\beta(\lambda_I^0)_\kappa(\lambda_I^0)_\gamma - [\frac{\partial^3 F}{\partial (l_I^+)^3} + \frac{\partial^3 F}{\partial (l_I^-)^3}](\eta_I^0)_\beta(\eta_I^0)_\kappa(\eta_I^0)_\gamma \\ & - (\frac{\partial^3 F}{\partial b_I^2 \partial l_I^+} + \frac{\partial^3 F}{\partial b_I^2 \partial l_I^-})[(\eta_I^0)_\beta(\lambda_I^0)_\kappa(\lambda_I^0)_\gamma + (\lambda_I^0)_\beta(\eta_I^0)_\kappa(\lambda_I^0)_\gamma + (\lambda_I^0)_\beta(\lambda_I^0)_\kappa(\eta_I^0)_\gamma] \\ & - [\frac{\partial^3 F}{\partial (l_I^+)^2 \partial b_I} + \frac{\partial^3 F}{\partial (l_I^-)^2 \partial b_I}][(\lambda_I^0)_\beta(\eta_I^0)_\kappa(\eta_I^0)_\gamma + (\eta_I^0)_\beta(\lambda_I^0)_\kappa(\eta_I^0)_\gamma + (\eta_I^0)_\beta(\eta_I^0)_\kappa(\lambda_I^0)_\gamma]. \end{aligned} \tag{3.23}$$

Using Eqs. (3.9), (3.10), (3.18) and (3.21,3.23) in Eqs. (3.5b,c) will yield the final expressions of the classical and gradient parts of the Eshelby tensor for the *p*-sided polygonal inclusion as

$$\begin{aligned} S^C_{\beta\kappa\gamma o} = {} & \frac{1}{8\pi(1-\nu)} \sum_{I=1}^{p} \{(S_1^C)_I \lambda_\beta^0 \lambda_\kappa^0 \delta_{\gamma o} + (S_2^C)_I \lambda_\beta^0 (\lambda_\gamma^0 \delta_{\kappa o} + \lambda_o^0 \delta_{\kappa\gamma}) + (S_3^C)_I \lambda_\kappa^0 (\lambda_\gamma^0 \delta_{\beta o} + \lambda_o^0 \delta_{\beta\gamma}) \\ & + (S_4^C)_I \lambda_\beta^0 \eta_\kappa^0 \delta_{\gamma o} + (S_5^C)_I \lambda_\beta^0 (\eta_\gamma^0 \delta_{\kappa o} + \eta_o^0 \delta_{\kappa\gamma}) + (S_6^C)_I \lambda_\kappa^0 (\eta_\gamma^0 \delta_{\beta o} + \eta_o^0 \delta_{\beta\gamma}) + (S_7^C)_I \\ & (\lambda_\beta^0 \lambda_\kappa^0 \eta_\gamma^0 \eta_o^0 + \lambda_\beta^0 \eta_\kappa^0 \lambda_\gamma^0 \eta_o^0 + \lambda_\beta^0 \eta_\kappa^0 \eta_\gamma^0 \lambda_o^0) + (S_8^C)_I (\lambda_\beta^0 \eta_\kappa^0 \lambda_\gamma^0 \lambda_o^0 + \lambda_\beta^0 \lambda_\kappa^0 \eta_\gamma^0 \lambda_o^0 + \lambda_\beta^0 \lambda_\kappa^0 \lambda_\gamma^0 \eta_o^0)\}, \end{aligned} \tag{3.24a}$$

where

$$(S_1^C)_I = -\frac{1}{3}\frac{\partial^3 \Phi_1^I}{\partial b_I^3} + 2\nu \frac{\partial \Lambda_1^I}{\partial b_I}, \quad (S_2^C)_I = -\frac{1}{3}\frac{\partial^3 \Phi_1^I}{\partial b_I^3} + (1-\nu)\frac{\partial \Lambda_1^I}{\partial b_I},$$

$$(S_3^C)_I = (1-v)\frac{\partial \Lambda_1^I}{\partial b_I},\ (S_4^C)_I = -\frac{1}{3}[\frac{\partial^3 \Phi_1^I}{\partial (l_I^+)^3} + \frac{\partial^3 \Phi_1^I}{\partial (l_I^-)^3}] + 2v(\frac{\partial \Lambda_1^I}{\partial l_I^+} + \frac{\partial \Lambda_1^I}{\partial l_I^-}),$$

$$(S_5^C)_I = -\frac{1}{3}[\frac{\partial^3 \Phi_1^I}{\partial (l_I^+)^3} + \frac{\partial^3 \Phi_1^I}{\partial (l_I^-)^3}] + (1-v)(\frac{\partial \Lambda_1^I}{\partial l_I^+} + \frac{\partial \Lambda_1^I}{\partial l_I^-}),$$

$$(S_6^C)_I = (1-v)(\frac{\partial \Lambda_1^I}{\partial l_I^+} + \frac{\partial \Lambda_1^I}{\partial l_I^-}),\quad (S_7^C)_I = -\frac{\partial^3 \Phi_1^I}{\partial (l_I^+)^2 \partial b_I} - \frac{\partial^3 \Phi_1^I}{\partial (l_I^-)^2 \partial b_I} + \frac{1}{3}\frac{\partial^3 \Phi_1^I}{\partial b_I^3},$$

$$(S_8^C)_I = -\frac{\partial^3 \Phi_1^I}{\partial b_I^2 \partial l_I^+} - \frac{\partial^3 \Phi_1^I}{\partial b_I^2 \partial l_I^-} + \frac{1}{3}[\frac{\partial^3 \Phi_1^I}{\partial (l_I^+)^3} + \frac{\partial^3 \Phi_1^I}{\partial (l_I^-)^3}], \tag{3.24b}$$

and

$$\begin{aligned} S^G_{\beta\kappa\gamma o} = \frac{1}{8\pi(1-v)}\sum_{I=1}^{p} \{&(S_1^G)_I \lambda_\beta^0 \lambda_\kappa^0 \delta_{\gamma o} + (S_2^G)_I \lambda_\beta^0 (\lambda_\gamma^0 \delta_{\kappa o} + \lambda_o^0 \delta_{\kappa\gamma}) + (S_3^G)_I \lambda_\kappa^0 (\lambda_\gamma^0 \delta_{\beta o} + \lambda_o^0 \delta_{\beta\gamma}) \\ &+ (S_4^G)_I \lambda_\beta^0 \eta_\kappa^0 \delta_{\gamma o} + (S_5^G)_I \lambda_\beta^0 (\eta_\gamma^0 \delta_{\kappa o} + \eta_o^0 \delta_{\kappa\gamma}) + (S_6^G)_I \lambda_\kappa^0 (\eta_\gamma^0 \delta_{\beta o} + \eta_o^0 \delta_{\beta\gamma}) + (S_7^G)_I \\ &(\lambda_\beta^0 \lambda_\kappa^0 \eta_\gamma^0 \eta_o^0 + \lambda_\beta^0 \eta_\kappa^0 \lambda_\gamma^0 \eta_o^0 + \lambda_\beta^0 \eta_\kappa^0 \eta_\gamma^0 \lambda_o^0) + (S_8^G)_I (\lambda_\beta^0 \eta_\kappa^0 \lambda_\gamma^0 \lambda_o^0 + \lambda_\beta^0 \lambda_\kappa^0 \eta_\gamma^0 \lambda_o^0 + \lambda_\beta^0 \lambda_\kappa^0 \lambda_\gamma^0 \eta_o^0)\}, \end{aligned}$$

(3.25a)

where

$$\begin{aligned} (S_1^G)_I = &-\frac{2L^2}{3}\frac{\partial^3 (\Lambda_1^I + \Gamma_1^I)}{\partial b_I^3} + \frac{4v(1-v)}{(1-2v)}\frac{\partial \Gamma_1^I}{\partial b_I} \\ &-\frac{2vL^2}{(1-2v)}[\frac{\partial^3 (\Lambda_1^I + \Gamma_1^I)}{\partial b_I^3} + \frac{\partial^3 (\Lambda_1^I + \Gamma_1^I)}{\partial b_I \partial (l_I^+)^2} + \frac{\partial^3 (\Lambda_1^I + \Gamma_1^I)}{\partial b_I \partial (l_I^-)^2}], \end{aligned}$$

$$(S_2^G)_I = -\frac{2L^2}{3}\frac{\partial^3 (\Lambda_1^I + \Gamma_1^I)}{\partial b_I^3} + (1-v)\frac{\partial \Gamma_1^I}{\partial b_I},$$

$$(S_3^G)_I = (1-v)\frac{\partial \Gamma_1^I}{\partial b_I},$$

$$(S_4^G)_I = -\frac{2L^2}{3}[\frac{\partial^3(\Lambda_1^I+\Gamma_1^I)}{\partial(l_I^+)^3}+\frac{\partial^3(\Lambda_1^I+\Gamma_1^I)}{\partial(l_I^-)^3}]+\frac{4\nu(1-\nu)}{(1-2\nu)}(\frac{\partial\Gamma_1^I}{\partial l_I^+}+\frac{\partial\Gamma_1^I}{\partial l_I^-})$$
$$-\frac{2\nu L^2}{(1-2\nu)}[\frac{\partial^3(\Lambda_1^I+\Gamma_1^I)}{\partial b_I^2\partial l_I^+}+\frac{\partial^3(\Lambda_1^I+\Gamma_1^I)}{\partial b_I^2\partial l_I^-}+\frac{\partial^3(\Lambda_1^I+\Gamma_1^I)}{\partial(l_I^+)^3}+\frac{\partial^3(\Lambda_1^I+\Gamma_1^I)}{\partial(l_I^-)^3}],$$
$$(S_5^G)_I = -\frac{2L^2}{3}[\frac{\partial^3(\Lambda_1^I+\Gamma_1^I)}{\partial(l_I^+)^3}+\frac{\partial^3(\Lambda_1^I+\Gamma_1^I)}{\partial(l_I^-)^3}]+(1-\nu)(\frac{\partial\Gamma_1^I}{\partial l_I^+}+\frac{\partial\Gamma_1^I}{\partial l_I^-}),$$

$$(S_6^G)_I = (1-\nu)(\frac{\partial\Gamma_1^I}{\partial l_I^+}+\frac{\partial\Gamma_1^I}{\partial l_I^-}),\ (S_7^G)_I = -2L^2[\frac{\partial^3(\Lambda_1^I+\Gamma_1^I)}{\partial(l_I^+)^2\partial b_I}+\frac{\partial^3(\Lambda_1^I+\Gamma_1^I)}{\partial(l_I^-)^2\partial b_I}-\frac{1}{3}\frac{\partial^3(\Lambda_1^I+\Gamma_1^I)}{\partial b_I^3}],$$
$$(S_8^G)_I = -2L^2\{\frac{\partial^3(\Lambda_1^I+\Gamma_1^I)}{\partial b_I^2\partial l_I^+}+\frac{\partial^3(\Lambda_1^I+\Gamma_1^I)}{\partial b_I^2\partial l_I^-}-\frac{1}{3}[\frac{\partial^3(\Lambda_1^I+\Gamma_1^I)}{\partial(l_I^+)^3}+\frac{\partial^3(\Lambda_1^I+\Gamma_1^I)}{\partial(l_I^-)^3}]\}. \qquad (3.25b)$$

Note that $\Phi_1^I, \Lambda_1^I, \Gamma_1^I$ in Eqs. (3.24b) and (3.25b) are defined in Eqs. (3.9), (3.10) and (3.18).

It should be noticed that the classical part $S_{\beta\kappa\gamma o}^C$ given in Eqs. (3.24a,b) is only related to Poisson's ratio ν and cannot explain the inclusion size effect, since Φ_1^I and Λ_1^I involved in Eq. (3.24b) do not depend on material length scale parameter L (see Eqs. (3.9) and (3.10)). However, the gradient part $S_{\beta\kappa\gamma o}^G$ given in Eqs. (3.25a,b) can capture the inclusion size effect, since Eq. (3.25b) contains parameter L in addition to Poisson's ratio ν. When L=0, $S_{\beta\kappa\gamma o}^G$ becomes zero and $S_{\beta\kappa\gamma o}$ reduces to $S_{\beta\kappa\gamma o}^C$, which is the Eshelby tensor based on the classical elasticity and cannot account for the inclusion size effect.

3.3.2 Averaged Eshelby tensor

Since both $S_{\beta\kappa\gamma o}^C$ and $S_{\beta\kappa\gamma o}^G$ are position-dependent inside the polygonal inclusion, the average Eshelby tensor is evaluated here, which is needed in homogenization

analyses of composites containing polygonal inclusions. The *p*-sided polygon is divided into *p* triangles. The three vertices of each of the triangles consist of the origin **O** of the global coordinate system and two consecutive vertices of the polygon. The area integral of the Eshelby tensors is first evaluated over each of these triangles individually. The summation of these *p* area integrals will then give the area integral of **S** over the cross section of the polygon. After dividing the sum by the cross-sectional area of the inclusion will finally lead to the averaged Eshelby tensor for the *p*-sided polygonal inclusion.

That is, the averaged Eshelby tensor for a *p*-sided polygonal inclusion over the cross section of the inclusion can be obtained as

$$\overline{S}_{\beta\kappa\gamma o} = \frac{1}{A_\Omega} \sum_{N=1}^{p} \sum_{I=1}^{p} \iint_{\Omega_N} (S_N)_{\beta\kappa\gamma o}(b_I, l_I^+, l_I^-) dA \tag{3.26}$$

where $(S_N)_{\beta\kappa\gamma o}$ is the Eshelby tensor at an arbitrary **x** within Ω_N given in Eqs. (3.5a), (3.24a,b) and (3.25a,b), Ω_N is the triangle formed by the origin **O** and the two vertices on the *N*th edge (i.e., $\mathbf{V}_N^+, \mathbf{V}_N^-$) as shown in Fig. 3.4, A_Ω is the cross-sectional area of the polygonal inclusion. Note that the triangle Ω_N constructed from the origin **O** is different from Ω_I which is built from an arbitrary point **x**. The former is constructed for evaluating the average of the Eshelby tensor at all points within Ω, while the latter is used to obtain the Eshelby tensor at **x**.

For the *N*th triangle Ω_N, the local Cartesian coordinate system (λ_N, η_N) can be chosen in a way similar to what was done earlier (see Fig. 3.2). The coordinates of the

vertices of the triangle Ω_I on the Ith edge and of an arbitrary point $\mathbf{x}$ in the local coordinate system (λ_N, η_N) can be identified as (v_1^{IN+}, v_2^{IN+}), (v_1^{IN-}, v_2^{IN-}) and (x_1^{IN}, x_2^{IN}), respectively. Also, the base vectors $\boldsymbol{\lambda}_I^0$ and $\boldsymbol{\eta}_I^0$ of the local coordinate system (λ_I, η_I) attached to triangle Ω_I can be expressed in terms of the base vectors $\boldsymbol{\lambda}_N^0$ and $\boldsymbol{\eta}_N^0$. The parameters for the triangle Ω_N then can be obtained as

$$b_I = (v_\alpha^{IN+} - x_\alpha^{IN})(\lambda_I^0)_\alpha^N = (v_\alpha^{IN-} - x_\alpha^{IN})(\lambda_I^0)_\alpha^N, \tag{3.27a}$$

$$l_I^+ = (v_\alpha^{IN+} - x_\alpha^{IN})(\eta_I^0)_\alpha^N, \tag{3.27b}$$

$$l_I^- = (v_\alpha^{IN-} - x_\alpha^{IN})(\eta_I^0)_\alpha^N, \tag{3.27c}$$

where $(\lambda_I^0)_\alpha^N$ and $(\eta_I^0)_\alpha^N$ represent, respectively, the αth components of the base vectors $\boldsymbol{\lambda}_I^0$ and $\boldsymbol{\eta}_I^0$ in the local coordinate system (λ_N, η_N) with the base vectors $\boldsymbol{\lambda}_N^0$ and $\boldsymbol{\eta}_N^0$.

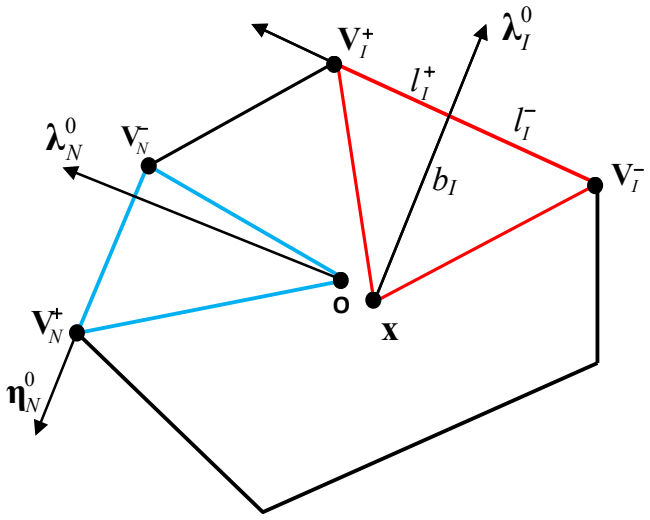

Fig. 3.4 Triangles and the related local coordinate systems originated from point **x** and from the global coordinate origin **O**.

Using Eqs. (3.27a-c) in Eq. (3.26) gives

$$\overline{S}_{\beta\kappa\gamma o} = \frac{1}{A_\Omega} \sum_{N=1}^{p} \sum_{I=1}^{p} \iint_{\Omega_N} (S_N)_{\beta\kappa\gamma o} [b_I(\lambda_N, \eta_N), l_I^+(\lambda_N, \eta_N), l_I^-(\lambda_N, \eta_N)] d\lambda_N d\eta_N . \quad (3.28)$$

This formula is applicable to a polygonal inclusion of arbitrary shape.

For an isogon inscribed to a circle of radius R and with two of its vertices on the x_1 axis (possible for $p \geq 4$) (see Fig. 3.5(a)-(c)), it is symmetric about x_1 and x_2 axes. Hence, only one fourth of the inclusion needs to be considered. This one fourth of the inclusion area can be further divided into several triangles and trapezoids by using lines parallel to the x_1 axis (see in Fig. 3.6), and the area integral can then be evaluated from these sub-areas formed by the parallel lines (rather than the triangles originated from **O**). Hence, only the global coordinates of all the vertices of the polygon need to be determined. Also, the unit vectors $\boldsymbol{\lambda}_I^0$ and $\boldsymbol{\eta}_I^0$ of each local coordinate system (λ_I, η_I) can be represented in terms of the base vectors $\mathbf{e}_1$ and $\mathbf{e}_2$ of the global coordinate system (x_1, x_2). As a result, Eq. (3.28) can be simplified to

$$\overline{S}_{\beta\kappa\gamma o} = \frac{4}{A_\Omega} \sum_{T=1}^{t} \sum_{I=1}^{p} \iint_{\Omega_T} (S_T)_{\beta\kappa\gamma o} [b_I(x_1, x_2), l_I^+(x_1, x_2), l_I^-(x_1, x_2)] dx_1 dx_2 , \quad (3.29)$$

where t is the total number of sub-areas from the one-forth of the polygonal area, $(S_T)_{\beta\kappa\gamma o}$ is the Eshelby tensor at an arbitrary point $\mathbf{x}$ inside Ω_T given in Eqs. (3.5a), (3.24a,b) and (3.25a,b), and Ω_T is the sub-area formed by the Tth edge, x_2 axis and one or two lines parallel to x_1 axis (see Fig. 3.6).

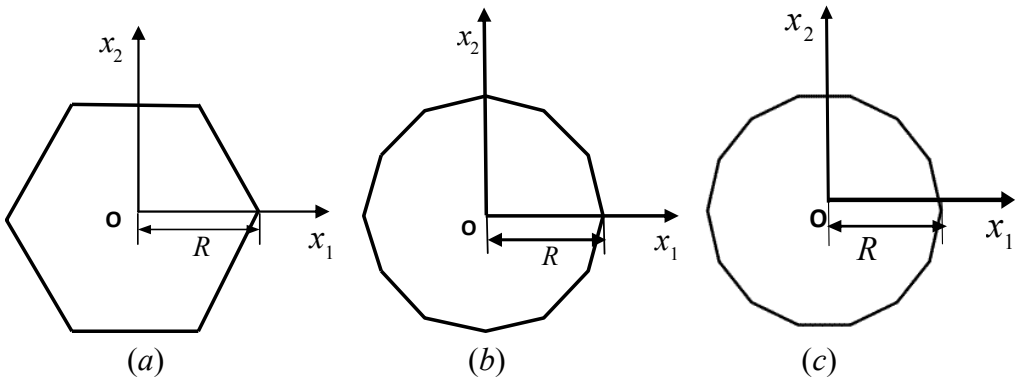

Fig. 3.5 Three kinds of polygonal inclusions of the isogon type: (*a*) hexagonal, (*b*) dodecagonal, and (*c*) tetrakaidecagonal.

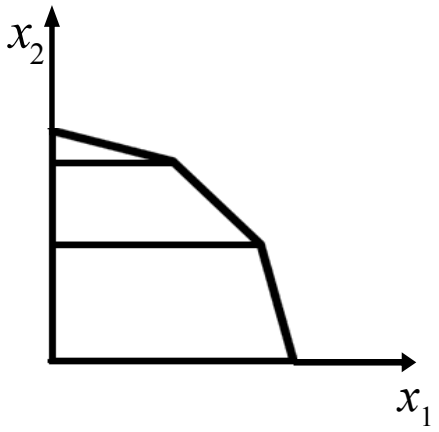

Fig. 3.6 Sub-areas of one-fourth of a dodecagonal inclusion formed by using lines parallel to the x_1 axis.

3.4 Numerical results

In this section, three kinds of polygonal inclusions, i.e., hexagonal, dodecagonal and tetrakaidecagonal (see Fig. 3.5), are quantitatively studied by using the general formulas for a *p*-sided polygonal inclusion of arbitrary shape derived in Section 3.3. The components of Eshelby's tensor at any **x** inside each of the three polygonal inclusions for various inclusion sizes are evaluated and presented to demonstrate how they change with

the position and inclusion size. Also, the averaged Eshelby tensor varying with the inclusion size is analyzed. The Poisson's ratio v and the material length scale parameter L are taken to be 0.3 and 17.6 μm, respectively, in the numerical analysis.

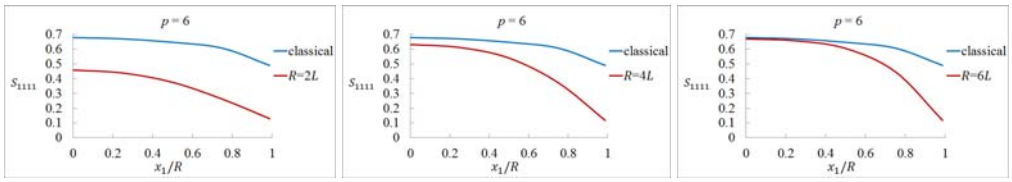

(*a*) (*b*) (*c*)

Fig. 3.7 Variation of S_{1111} along the x_1 axis inside the hexagonal inclusion: (*a*) R=2L, (*b*) R=4L, and (*c*) R=6L.

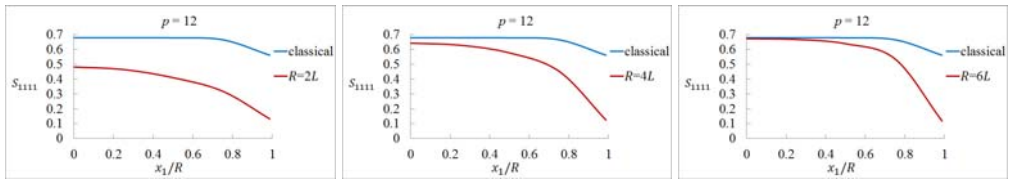

(*a*) (*b*) (*c*)

Fig. 3.8 Variation of S_{1111} along the x_1 axis inside the dodecagonal inclusion: (*a*) R=2L, (*b*) R=4L, and (*c*) R=6L.

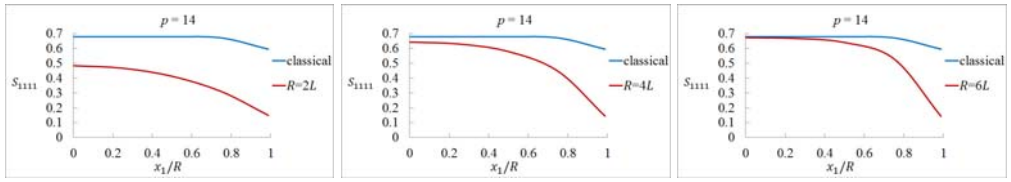

(*a*) (*b*) (*c*)

Fig. 3.9 Variation of S_{1111} along the x_1 axis inside the tetrakaidecagonal inclusion: (*a*) R=2L, (*b*) R=4L, and (*c*) R=6L.

The distributions of S_{1111} and S_{1212} for the hexagonal, dodecagonal and tetrakaidecagonal inclusions along the x_1 axis are shown in Figs. 3.7-3.9, where the values for S_{1111}^C are also provided for comparison. It can be seen from Figs. 3.7-3.9 that the classical part S_{1111}^C (based on classical elasticity) varies with the position of **x** within each polygonal inclusion, unlike that for an ellipsoidal inclusion. Also, the results for the hexagonal and dodecagonal inclusions are exactly the same as what provided in Rodin (1996). In addition, Figs.3.7-3.9 show that for each of the three inclusion shapes S_{1111}^C at a given value of x_1/R is the same for all values of R/L, confirming the inclusion size independent of the classical part of the Eshelby tensor. However, S_{1111} based on the SSGET varies with not only the position but also the inclusion size. When the inclusion size is small compared with length scale parameter L (e.g., r/L=2), the difference between S_{1111}^C and S_{1111} ($= S_{1111}^C + S_{1111}^G$), which is the gradient part S_{1111}^G, is quite large and cannot be ignored. However, this difference becomes smaller as the inclusion size increases. When the inclusion size becomes large enough (e.g., r/L=6), especially at those positions near the inclusion center, the inclusion size effect is very small and may be neglected. When **x** gets closer to the inclusion boundary, the contribution from S_{1111}^G becomes significant and can no longer be neglected. This is expected, since the region near the inclusion surface is where the largest strain gradient exists, and should exhibit the largest strain gradient effect.

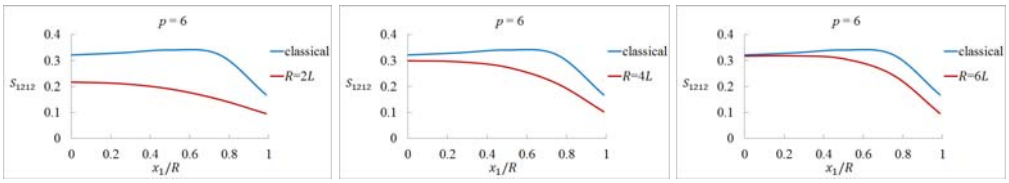

(*a*) (*b*) (*c*)

Fig. 3.10 Variation of S_{1212} along the x_1 axis inside the hexagonal inclusion: (*a*) R=2L, (*b*) R=4L, and (*c*) R=6L.

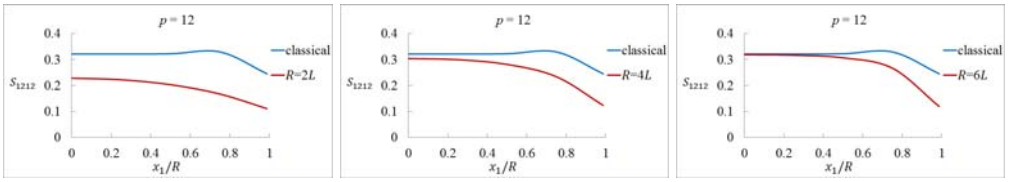

(*a*) (*b*) (*c*)

Fig. 3.11 Variation of S_{1212} along the x_1 axis inside the dodecagonal inclusion: (*a*) R=2L, (*b*) R=4L, and (*c*) R=6L.

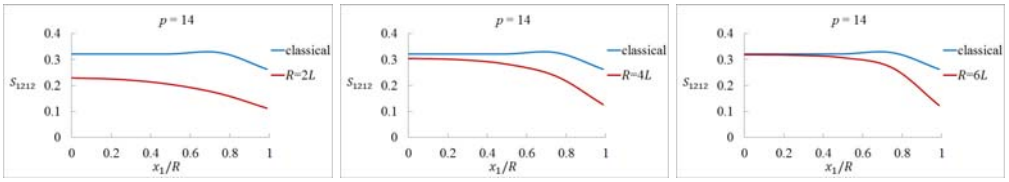

(*a*) (*b*) (*c*)

Fig. 3.12 Variation of S_{1212} along the x_1 axis inside the tetrakaidecagonal inclusion: (*a*) R=2L, (*b*) R=4L, and (*c*) R=6L.

The variations of S_{1212} with the position and inclusion size for the three polygonal inclusions are displayed in Figs. 3.10-3.12, which show similar trends to those exhibited by S_{1111}. The results for those of the classical part S_{1212}^{C} along the x_1 axis of the hexagonal and dodecagonal inclusions agree well with Rodin (1996). It is found from Figs. 3.10-3.12 that for each of the three polygonal inclusion shapes S_{1212}^{C} varies with the position

of **x** within the inclusion but does not change with the inclusion size. However, S_{1212} varies with both the position and inclusion size. The difference between S_{1212} and S_{1212}^{C} (i.e., $S_{1212}^{G} = S_{1212} - S_{1212}^{C}$), is seen to be significantly large for small inclusions. The values of S_{1212} approach to those of S_{1212}^{C} as the inclusion size increases. When the inclusion size becomes large enough (e.g., r/L = 6), the strain gradient effect becomes insignificant and the difference between S_{1212} and S_{1212}^{C} is negligible in the range x_1/L<0.5, while in the region beyond that range, the size effect is still considerable and cannot be ignored due to the large strain gradient near the inclusion boundary.

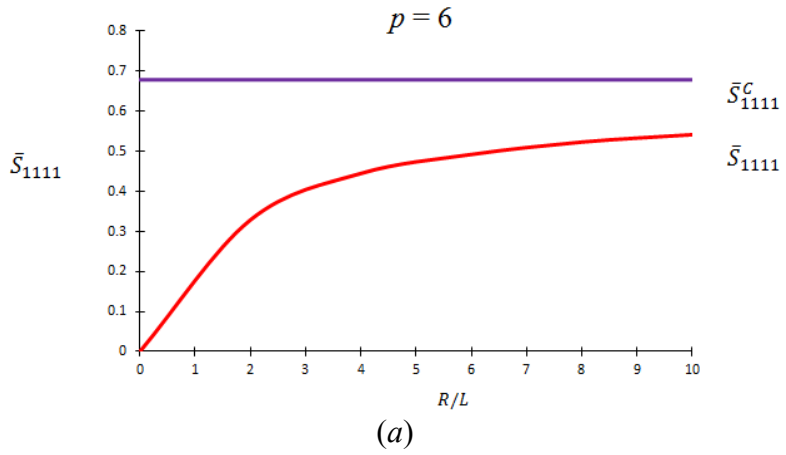

(*a*)

Fig. 3.13 Variation of $\overline{S}_{1111}$ with the inclusion size: (*a*) hexagonal, (*b*) dodecagonal, and (*c*) tetrakaidecagonal.

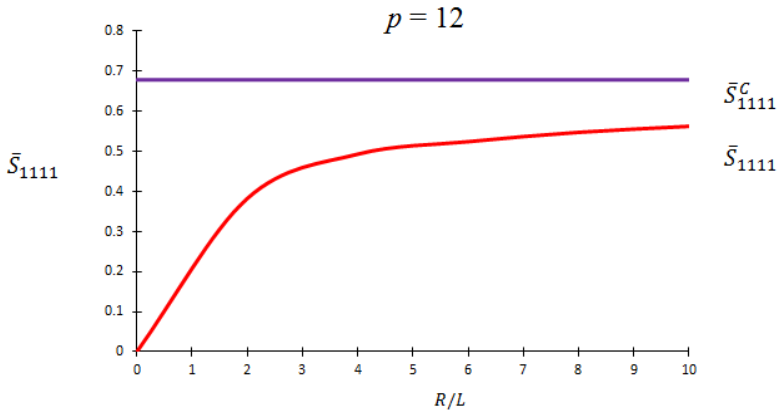

(*b*)

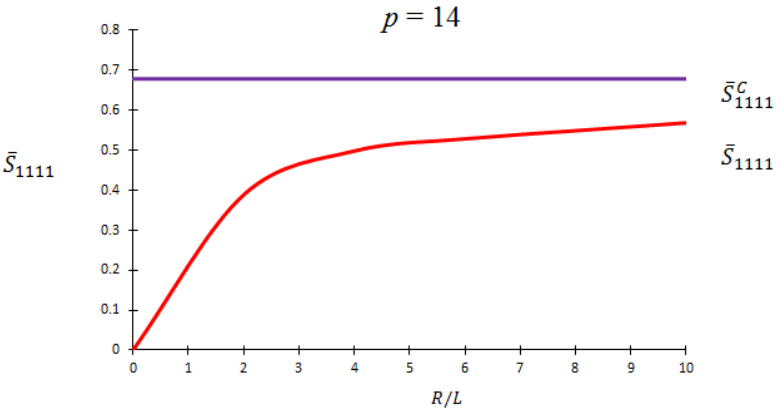

(*c*)

Fig. 3.13 Continued.

The component $\overline{S}_{1111}$ of the averaged Eshelby tensor varying with the inclusion size is shown in Fig. 3.13 for the three inclusion shapes, where $\overline{S}^C_{1111}$ is also plotted for comparison. The values of $\overline{S}_{1111}$ displayed in Fig. 3.13 are obtained using Eq. (3.29), which is also used to get the values of $\overline{S}^C_{1111}$ with $L \to 0$. It can be seen that for each polygonal inclusion the classical part $\overline{S}^C_{1111}$ (based on classical elasticity) is a constant that does not change with the inclusion size. However, $\overline{S}_{1111}$ does vary with the inclusion

size: the smaller the inclusion, the smaller the component of the area-averaged Eshelby tensor. In particular, when the inclusion is small, the strain gradient effect is significant and cannot be neglected. Nevertheless, as the inclusion becomes large, $\overline{S}_{1111}$ approaches $\overline{S}^{C}_{1111}$ from below, indicating that the strain gradient effect gets small and may be ignored for large inclusions. Also, for the same value of R/L, $\overline{S}_{1111}$ increases with the number of sides of the polygonal inclusion. When R/L is sufficiently large (i.e., $R/L \geq 9$), this effect is very small, and, as a result, $\overline{S}_{1111}$ are almost the same for the three inclusions shapes.

The numerical results presented above show that the Eshelby tensor based on the SSGET can capture the inclusion size effect at the micron scale, unlike the counterpart Eshelby tensor based on classical elasticity.

3.5 Summary

The Eshelby-type problem of an arbitrary shape polygonal inclusion embedded in an infinite homogeneous isotropic elastic material is analytically solved using the simplified strain gradient elasticity theory (SSGET). The resulting Eshelby tensor includes one material length scale parameter in addition to Poisson's ratio. The Eshelby tensor is expressed in terms of three potential functions, two of which are the same as those involved in the classical elasticity-based counterpart Eshelby tensor. This newly obtained Eshelby tensor is separated into a classical part and a gradient part. The former depends only on Poisson's ratio, while the latter depends on the material length scale parameter additionally which enables the interpretation of the size effect. When the

strain gradient is not considered, the current Eshelby tensor reduces to the counterpart based on classical elasticity. A general form of the averaged Eshelby tensor is also provided, which is needed in homogenization analyses of composite materials containing polygonal inclusions.

The numerical results for three polygonal inclusion shapes are provided by directly applying the general formulas derived. The results show that for each of the three inclusion shapes considered the components of the newly obtained Eshelby tensor vary with both the position and inclusion size, while the classical counterparts change with the position only. It is also seen that when the inclusion size is comparable to the material length scale parameter, the size effect is significant and should not be neglected. This size effect becomes small as inclusion size increases, especially at the positions near the inclusion center. The averaged Eshelby tensor components are observed to be smaller for a smaller inclusion size. These averaged components approach the values of their classical counterparts from below as the inclusion size becomes large. This indicates that the inclusion size effect can be ignored for large polygonal inclusions.

CHAPTER IV

STRAIN GRADIENT SOLUTION FOR THE ANTI-PLANE STRAIN POLYGONAL INCLUSION PROBLEM

4.1 Introduction

Anti-plane strain problems have been extensively studied due to their engineering relevance and mathematical simplicity (i.e., Gao, 1996; Gao and Li, 2005; Xu and Wang, 2007; Le Quang et al., 2008). As an example, the Eshelby-type problem of an infinite elastic body containing an anti-plane strain cylindrical inclusion has been investigated using both classical elasticity and higher-order theories (e.g., Le Quang et al., 2008; Lubarda, 2003; Gao and Ma, 2011).

In this chapter, the anti-plane strain problem of a polygonal inclusion of arbitrary shape embedded in an infinite elastic body and prescribed with a uniform eigenstrain and a uniform eigenstrain gradient is solved using the simplified strain gradient elasticity theory (SSGET). This extends the recent work of Gao and Ma (2011) on the anti-plane strain cylindrical inclusion problem.

The rest of the chapter is organized as follows. In Section 4.2, the Green's function for anti-plane strain deformations in an infinite elastic body is first reviewed. This is followed by the presentation of the general forms of the Eshelby tensor and the fifth-order Eshelby-like tensor recently derived by Gao and Ma (2011). In Section 4.3, the general form of the Eshelby tensor is applied to solve the problem of an anti-plane strain prismatic inclusion with a polygonal cross section of arbitrary shape embedded in

an infinite elastic body. The solution gives explicit expressions of the Eshelby tensor for the anti-plane strain polygonal inclusion problem. In Section 4.4, the averaged Eshelby tensor is obtained by decomposing the Eshelby tensor into two one dimensional arrays. Numerical results are provided in Section 4.5 to illustrate the newly derived Eshelby tensor and its area average for the anti-plane strain polygonal inclusion and to show how the components of the Eshelby tensors change with the position and inclusion size. The chapter concludes in Section 4.6 with a summary.

4.2 Green's function and Eshelby tensor for anti-plane strain deformations

For an anti-plane strain problem, the displacement field is given by

$$u_1 = 0, \quad u_2 = 0, \quad u_3 = w(x_1, x_2), \tag{4.1}$$

where w denotes the only non-zero displacement component which is a function of x_1 and x_2 only.

The infinitesimal strain ε_{ij} and the strain gradient κ_{ijk} are, respectively, defined by

$$\varepsilon_{ij} = \frac{1}{2}(u_{i,j} + u_{j,i}), \quad \kappa_{ijk} \equiv \varepsilon_{ij,k} = \frac{1}{2}(u_{i,jk} + u_{j,ik}). \tag{4.2a,b}$$

From Eqs. (4.2a,b) and (4.1), the non-zero strain and strain gradient components can be obtained as

$$\begin{aligned} &\varepsilon_{13} = \varepsilon_{31} = \frac{1}{2} w_{,1}, \quad \varepsilon_{23} = \varepsilon_{32} = \frac{1}{2} w_{,2}, \\ &\kappa_{131} = \kappa_{311} = \frac{1}{2} w_{,11}, \quad \kappa_{132} = \kappa_{312} = \frac{1}{2} w_{,12}, \\ &\kappa_{231} = \kappa_{321} = \frac{1}{2} w_{,21}, \quad \kappa_{232} = \kappa_{322} = \frac{1}{2} w_{,22}. \end{aligned} \tag{4.3}$$

Substituting Eq. (4.1) into the Navier-like displacement equation based on SSGET (i.e., Eq. (2.1)) yields

$$\mu w_{,\alpha\alpha} - \mu L^2 w_{,\alpha\alpha\beta\beta} + f_3 = 0 \tag{4.4}$$

along with $f_1 = 0 = f_2$.

For $f_3 = \delta(x_1)\delta(x_2)$, Eq. (4.4), subject to the boundary conditions of w and its first, second and third spatial derivatives vanishing at infinity, has been solved by Gao and Ma (2011) using Fourier transform to obtain

$$G(\mathbf{x}) = -\frac{1}{2\pi\mu}[\ln|\mathbf{x}| + K_0(\frac{|\mathbf{x}|}{L})], \tag{4.5}$$

where $K_0(\cdot)$ is the modified Bessel function of the second kind of the zeroth order, $G(\mathbf{x})$ is the Green's function for anti-plane strain deformation based on the SSGET, which represents the displacement w at point $\mathbf{x}$ induced by a unit concentrated body force, $f_3(\mathbf{y}) = \delta(\mathbf{y})$, acting at the origin in the x_1x_2-plane. When L = 0, the Green's function in Eq. (4.5) reduces to, noting that $K_0(|\mathbf{x}|/L) \to 0$ as $L \to 0$,

$$G(\mathbf{x}) = -\frac{1}{2\pi\mu}\ln|\mathbf{x}|, \tag{4.6}$$

which is the Green's function for anti-plane strain deformations in classical elasticity (e.g., Le Quang et al., 2008).

By using the Green's function given in Eq. (4.5) and following a procedure similar to that used in Gao and Ma (2009), the problem of an anti-plane strain inclusion of arbitrary shape embedded in an infinite homogeneous isotropic elastic body and

prescribed with a uniform eigenstrain $\boldsymbol{\varepsilon}^*$ and a uniform eigenstrain gradient $\boldsymbol{\kappa}^*$ has been solved by Gao and Ma (2011) to give

$$\varepsilon_{3\alpha} = S_{3\alpha 3\beta}\varepsilon^*_{3\beta} + T_{3\alpha 3\beta\gamma}\kappa^*_{3\beta\gamma}, \tag{4.7}$$

where $S_{3\alpha 3\beta}$ are the four non-vanishing components of the fourth order Eshelby tensor which are given by

$$S_{3131} = -\mu\langle G\rangle_{,11},\ \ S_{3132} = -\mu\langle G\rangle_{,21} = S_{3231} = -\mu\langle G\rangle_{,12},\ \ S_{3232} = -\mu\langle G\rangle_{,22}, \tag{4.8}$$

and $T_{3\alpha 3\beta\gamma}$ are the eight non-vanishing components of the fifth-order Eshelby-like tensor that read

$$T_{31311} = \mu L^2\langle G\rangle_{,111},\ \ T_{32311} = \mu L^2\langle G\rangle_{,112} = T_{31312} = T_{31321},$$

$$T_{32322} = \mu L^2\langle G\rangle_{,222},\ \ T_{32312} = T_{32321} = \mu L^2\langle G\rangle_{,122} = T_{31322}. \tag{4.9}$$

In Eqs. (4.8) and (4.9),

$$\langle F\rangle = \int_\Omega F dA(y) \tag{4.10}$$

is the area integral of a smooth function F over the cross-sectional area Ω of the inclusion.

From Eq. (4.7) it is seen that the disturbed strain $\boldsymbol{\varepsilon}$ is solely related to the eigenstrain $\boldsymbol{\varepsilon}^*$ if the eigenstrain gradient $\boldsymbol{\kappa}^* = 0$, and $\boldsymbol{\varepsilon}$ is linked to only $\boldsymbol{\kappa}^*$ if $\boldsymbol{\varepsilon}^* = \mathbf{0}$.

Eqs. (4.8) and (4.9) give the non-zero components of the SSGET-based Eshelby tensor **S** and the Eshelby-like fifth order tensor **T** in terms of the Green's function G in Eq. (4.5) for an anti-plane strain inclusion of arbitrary cross-sectional shape Ω. These formulas have been used to obtain closed form expressions of **S** and **T** for a circular-

shaped anti-plane strain inclusion. The more complex case of a polygonal inclusion of arbitrary shape will be studied here in the next section.

4.3 Inclusion with polygonal cross section of arbitrary shape

For anti-plane strain prismatic inclusion with an arbitrary shape polygonal cross section (Fig. 4.1), the determination of the Eshelby tensor requires the evaluation of $\langle G \rangle$ and its second derivatives, as indicated in Eq. (4.8).

From Eq. (4.5) it follows that

$$\langle G \rangle = \frac{1}{4\pi\mu}(\Lambda - \Gamma) \tag{4.11}$$

where

$$\Lambda = \iint_S -\ln|\mathbf{y}-\mathbf{x}|^2 dS(\mathbf{y}), \quad \Gamma = \iint_S 2K_0\left(\frac{|\mathbf{y}-\mathbf{x}|}{L}\right) dS(\mathbf{y}), \tag{4.12a-b}$$

which are the same as two of the three potential functions involved in the Eshelby tensor for plane strain inclusion problems discussed in Chapter III. These two area integrals can be evaluated by following the same procedure used in Chapter III.

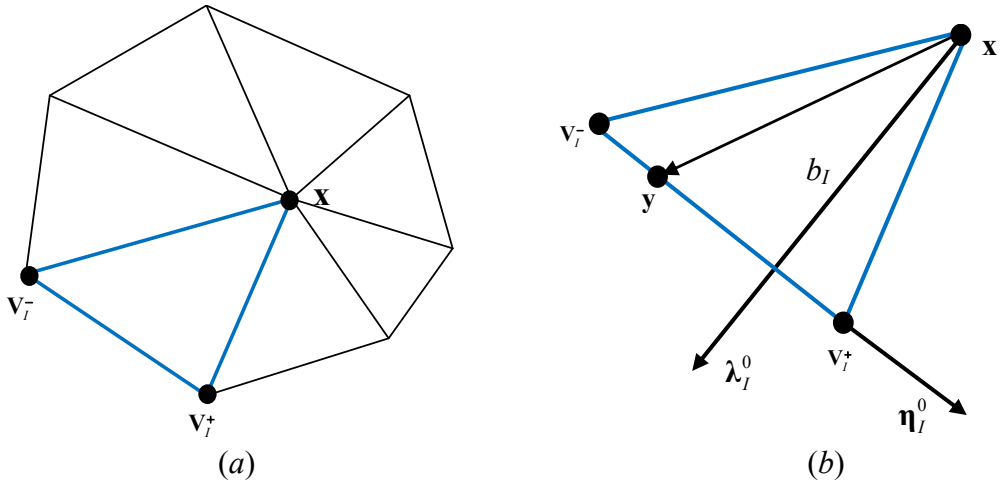

Fig. 4.1 A polygon represented by triangles: (*a*) each triangle formed by point **x** (arbitrary) and two consecutive vertices of the polygon, (*b*) one triangle with two vertices on the *I*th edge of the polygon and the associated local coordinate system.

Using Eq. (4.11) then gives

$$\langle G \rangle_{,\alpha} = \frac{1}{4\pi\mu}(\Lambda_{,\alpha} - \Gamma_{,\alpha}), \tag{4.13}$$

where

$$\Lambda_{,\alpha} = -\sum_{I=1}^{p} (\lambda_I^0)_\alpha \int_{l_I^-}^{l_I^+} -\ln(b_I^2 + \eta^2) d\eta, \tag{4.14a}$$

$$\Gamma_{,\alpha} = -\sum_{I=1}^{p} (\lambda_I^0)_\alpha \int_{l_I^-}^{l_I^+} 2K_0\left(\frac{\sqrt{b_I^2 + \eta^2}}{L}\right) d\eta. \tag{4.14b}$$

In reaching Eqs. (4.14a,b), use has been made of the Green's theorem.

Evaluating the line integrals in Eqs. (4.14a-b) yields

$$\begin{aligned} \Lambda_{,\alpha} = \sum_{I=1}^{p} (\lambda_I^0)_\alpha \{ & 2b_I \tan^{-1}\left(\frac{l_I^+}{b_I}\right) + l_I^+ \ln[b_I^2 + (l_I^+)^2] - 2l_I^+ - 2b_I \tan^{-1}\left(\frac{l_I^-}{b_I}\right) \\ & - l_I^- \ln[b_I^2 + (l_I^-)^2] + 2l_I^- \} \equiv \sum_{I=1}^{p} (\lambda_I^0)_\alpha \Lambda_1^I, \end{aligned} \tag{4.15a}$$

$$\begin{aligned}\Gamma_{,\alpha} &= -\sum_{I=1}^{p}(\lambda_I^0)_\alpha\{\sum_{n=0}^{\infty}\frac{(-1)^n}{n!(2n+1)2^{n-1}}(\frac{1}{b_I L})^n K_n(\frac{b_I}{L})[(l_I^+)^{2n+1}-(l_I^-)^{2n+1}]\} \\ &\equiv -\sum_{I=1}^{p}(\lambda_I^0)_\alpha \Gamma_1^I,\end{aligned} \tag{4.15b}$$

where $K_n(\cdot)$ is the modified Bessel function of the second kind of the nth order.

Note that for a smooth function $F(\mathbf{x}) \equiv F(b_I, l_I^+, l_I^-)$ the use of chain rule gives

$$F_{,\alpha} \equiv \frac{\partial F}{\partial x_\alpha} = \frac{\partial F}{\partial b_I}\frac{\partial b_I}{\partial x_\alpha} + \frac{\partial F}{\partial l_I^+}\frac{\partial l_I^+}{\partial x_\alpha} + \frac{\partial F}{\partial l_I^-}\frac{\partial l_I^-}{\partial x_\alpha} \tag{4.16}$$

where the parameters b_I, l_I^+, l_I^- are related to $\mathbf{x}$ through

$$b_I = (v_\alpha^+ - x_\alpha)(\lambda_I^0)_\alpha, \tag{4.17a}$$

$$l_I^+ = (v_\alpha^+ - x_\alpha)(\eta_I^0)_\alpha, \tag{4.17b}$$

$$l_I^- = (v_\alpha^- - x_\alpha)(\eta_I^0)_\alpha, \tag{4.17c}$$

in which x_α, v_α^+ and v_α^- are, respectively, the coordinates of the points $\mathbf{x}, \mathrm{V}_I^+$ and V_I^- in the global coordinate system, and $(\lambda_I^0)_\alpha$ and $(\eta_I^0)_\alpha$ are the components of the unit base vectors $\boldsymbol{\lambda}_I^0$ and $\boldsymbol{\eta}_I^0$ in the global coordinate system.

It then follows from Eqs. (4.16) and (4.17a–c) that

$$F_{,\alpha} = -\frac{\partial F}{\partial b_I}(\lambda_I^0)_\alpha - (\frac{\partial F}{\partial l_I^+} + \frac{\partial F}{\partial l_I^-})(\eta_I^0)_\alpha, \tag{4.18a}$$

$$\begin{aligned}F_{,\alpha\beta} = &\frac{\partial^2 F}{\partial b_I^2}(\lambda_I^0)_\alpha(\lambda_I^0)_\beta + (\frac{\partial^2 F}{\partial b_I \partial l_I^+} + \frac{\partial^2 F}{\partial b_I \partial l_I^-})[(\lambda_I^0)_\alpha(\eta_I^0)_\beta + (\eta_I^0)_\alpha(\lambda_I^0)_\beta] \\ &+ [\frac{\partial^2 F}{\partial (l_I^+)^2} + \frac{\partial^2 F}{\partial (l_I^-)^2}](\eta_I^0)_\alpha(\eta_I^0)_\beta,\end{aligned} \tag{4.18b}$$

Using Eq. (4.18a, b) in Eq. (4.13) leads to

$$\langle G\rangle_{,\alpha\beta} = -\frac{1}{4\pi\mu}\sum_{I=1}^{p}\{\frac{\partial(\Lambda_1^I+\Gamma_1^I)}{\partial b_I}(\lambda_I^0)_\alpha(\lambda_I^0)_\beta + [\frac{\partial(\Lambda_1^I+\Gamma_1^I)}{\partial l_I^+}+\frac{\partial(\Lambda_1^I+\Gamma_1^I)}{\partial l_I^-}](\lambda_I^0)_\alpha(\eta_I^0)_\beta\},$$

(4.19a)

$$\langle G\rangle_{,\alpha\beta\gamma} = \frac{1}{4\pi\mu}\sum_{I=1}^{p}\{(\frac{\partial^2\Lambda_1^I}{\partial b_I^2}+\frac{\partial^2\Gamma_1^I}{\partial b_I^2})(\lambda_I^0)_\alpha(\lambda_I^0)_\beta(\lambda_I^0)_\gamma + [\frac{\partial^2(\Lambda_1^I+\Gamma_1^I)}{\partial b_I\partial l_I^+}+\frac{\partial^2(\Lambda_1^I+\Gamma_1^I)}{\partial b_I\partial l_I^-}]$$
$$[(\lambda_I^0)_\alpha(\lambda_I^0)_\beta(\eta_I^0)_\gamma + (\lambda_I^0)_\alpha(\eta_I^0)_\beta(\lambda_I^0)_\gamma] + [\frac{\partial^2(\Lambda_1^I+\Gamma_1^I)}{\partial(l_I^+)^2}+\frac{\partial^2(\Lambda_1^I+\Gamma_1^I)}{\partial(l_I^-)^2}]$$
$$(\lambda_I^0)_\alpha(\eta_I^0)_\beta(\eta_I^0)_\gamma\}.$$

(4.19b)

Inserting Eq. (4.19a,b) into Eqs. (4.8) and (4.9), respectively, yields the expressions for the four non-zero Eshelby tensor components as

$$S_{3131} = \frac{1}{4\pi}\sum_{I=1}^{p}\{\frac{\partial(\Lambda_1^I+\Gamma_1^I)}{\partial b_I}(\lambda_I^0)_1^2 + [\frac{\partial(\Lambda_1^I+\Gamma_1^I)}{\partial l_I^+}+\frac{\partial(\Lambda_1^I+\Gamma_1^I)}{\partial l_I^-}](\lambda_I^0)_1(\eta_I^0)_1\},$$

$$S_{3132} = S_{3231} = \frac{1}{4\pi}\sum_{I=1}^{p}\{\frac{\partial(\Lambda_1^I+\Gamma_1^I)}{\partial b_I}(\lambda_I^0)_1(\lambda_I^0)_2 + [\frac{\partial(\Lambda_1^I+\Gamma_1^I)}{\partial l_I^+}+\frac{\partial(\Lambda_1^I+\Gamma_1^I)}{\partial l_I^-}](\lambda_I^0)_1(\eta_I^0)_2\},$$

$$S_{3232} = \frac{1}{4\pi}\sum_{I=1}^{p}\{\frac{\partial(\Lambda_1^I+\Gamma_1^I)}{\partial b_I}(\lambda_I^0)_2^2 + [\frac{\partial(\Lambda_1^I+\Gamma_1^I)}{\partial l_I^+}+\frac{\partial(\Lambda_1^I+\Gamma_1^I)}{\partial l_I^-}](\lambda_I^0)_2(\eta_I^0)_2\}, \qquad (4.20a\text{-}c)$$

and the eight non-zero components of the fifth-order Eshelby-like tensor as

$$T_{31311}=\frac{L^2}{4\pi}\sum_{I=1}^{p}\{\frac{\partial^2(\Lambda_1^I+\Gamma_1^I)}{\partial b_I^2}(\lambda_I^0)_1^3+2[\frac{\partial^2(\Lambda_1^I+\Gamma_1^I)}{\partial b_I\partial l_I^+}+\frac{\partial^2(\Lambda_1^I+\Gamma_1^I)}{\partial b_I\partial l_I^-}](\lambda_I^0)_1^2(\eta_I^0)_1$$
$$+[\frac{\partial^2(\Lambda_1^I+\Gamma_1^I)}{\partial(l_I^+)^2}+\frac{\partial^2(\Lambda_1^I+\Gamma_1^I)}{\partial(l_I^-)^2}](\lambda_I^0)_1(\eta_I^0)_1^2\},$$

$$T_{31312}=T_{31321}=T_{32311}=\frac{L^2}{4\pi}\sum_{I=1}^{p}\{\frac{\partial^2(\Lambda_1^I+\Gamma_1^I)}{\partial b_I^2}(\lambda_I^0)_1^2(\lambda_I^0)_2$$
$$+[\frac{\partial^2(\Lambda_1^I+\Gamma_1^I)}{\partial b_I\partial l_I^+}+\frac{\partial^2(\Lambda_1^I+\Gamma_1^I)}{\partial b_I\partial l_I^-}][(\lambda_I^0)_1^2(\eta_I^0)_2+(\lambda_I^0)_1(\lambda_I^0)_2(\eta_I^0)_1]$$
$$+[\frac{\partial^2(\Lambda_1^I+\Gamma_1^I)}{\partial(l_I^+)^2}+\frac{\partial^2(\Lambda_1^I+\Gamma_1^I)}{\partial(l_I^-)^2}](\lambda_I^0)_1(\eta_I^0)_1(\eta_I^0)_2\},$$

$$T_{31322}=T_{32312}=T_{32321}=\frac{L^2}{4\pi}\sum_{I=1}^{p}\{\frac{\partial^2(\Lambda_1^I+\Gamma_1^I)}{\partial b_I^2}(\lambda_I^0)_1(\lambda_I^0)_2^2$$
$$+2[\frac{\partial^2(\Lambda_1^I+\Gamma_1^I)}{\partial b_I\partial l_I^+}+\frac{\partial^2(\Lambda_1^I+\Gamma_1^I)}{\partial b_I\partial l_I^-}](\lambda_I^0)_1(\lambda_I^0)_2(\eta_I^0)_2$$
$$+[\frac{\partial^2(\Lambda_1^I+\Gamma_1^I)}{\partial(l_I^+)^2}+\frac{\partial^2(\Lambda_1^I+\Gamma_1^I)}{\partial(l_I^-)^2}](\lambda_I^0)_1(\eta_I^0)_2^2\},$$

$$T_{32322}=\frac{L^2}{4\pi}\sum_{I=1}^{p}\{(\frac{\partial^2\Lambda_1^I}{\partial b_I^2}+\frac{\partial^2\Gamma_1^I}{\partial b_I^2})(\lambda_I^0)_2^3+2[\frac{\partial^2(\Lambda_1^I+\Gamma_1^I)}{\partial b_I\partial l_I^+}+\frac{\partial^2(\Lambda_1^I+\Gamma_1^I)}{\partial b_I\partial l_I^-}](\lambda_I^0)_2^2(\eta_I^0)_2$$
$$+[\frac{\partial^2(\Lambda_1^I+\Gamma_1^I)}{\partial(l_I^+)^2}+\frac{\partial^2(\Lambda_1^I+\Gamma_1^I)}{\partial(l_I^-)^2}](\lambda_I^0)_2(\eta_I^0)_2^2\},$$

(4.21a-d)

where

$$\frac{\partial\Lambda_1^I}{\partial b_I}=2[\tan^{-1}(\frac{l_I^+}{b_I})-\tan^{-1}(\frac{l_I^-}{b_I})],\quad \frac{\partial\Lambda_1^I}{\partial l_I^+}+\frac{\partial\Lambda_1^I}{\partial l_I^-}=\ln[b_I^2+(l_I^+)^2]-\ln[b_I^2+(l_I^-)^2],$$

$$\frac{\partial\Gamma_1^I}{\partial b_I}=\sum_{n=0}^{\infty}\frac{(-1)^{n+1}}{n!(2n+1)2^n}\frac{1}{b_I^{n+1}L^{n+1}}[b_IK_{n-1}(\frac{b_I}{L})+2LnK_n(\frac{b_I}{L})+bK_{n+1}(\frac{b_I}{L})]$$
$$[(l_I^+)^{2n+1}-(l_I^-)^{2n+1}],$$

$$\frac{\partial\Gamma_1^I}{\partial l_I^+}+\frac{\partial\Gamma_1^I}{\partial l_I^-}=2K_0(\frac{\sqrt{b_I^2+(l_I^+)^2}}{L})-2K_0(\frac{\sqrt{b_I^2+(l_I^-)^2}}{L}),\qquad (4.22a\text{-}d)$$

$$\frac{\partial^2\Lambda_1^I}{\partial b_I^2}=2[-\frac{l_I^+}{b_I^2+(l_I^+)^2}+\frac{l_I^-}{b_I^2+(l_I^-)^2}],\quad \frac{\partial^2\Lambda_1^I}{\partial b_I\partial l_I^+}+\frac{\partial^2\Lambda_1^I}{\partial b_I\partial l_I^-}=\frac{2b_I[-(l_I^+)^2+(l_I^-)^2]}{[b_I^2+(l_I^+)^2][b_I^2+(l_I^-)^2]},$$

$$\frac{\partial^2\Lambda_1^I}{\partial (l_I^+)^2}+\frac{\partial^2\Lambda_1^I}{\partial (l_I^-)^2}=\frac{2(l_I^+-l_I^-)(b_I^2-l_I^+l_I^-)}{[b_I^2+(l_I^+)^2][b_I^2+(l_I^-)^2]},$$

$$\frac{\partial^2\Gamma_1^I}{\partial (b_I)^2}=\sum_{n=0}^{\infty}\frac{(-1)^n}{n!(2n+1)2^{n+1}}\frac{1}{b_I^{n+2}L^{n+2}}[b_I^2K_{n-2}(\frac{b_I}{L})+4b_ILnK_{n-1}(\frac{b_I}{L})$$
$$+(2b_I^2+4L^2n+4L^2n^2)K_n(\frac{b_I}{L})+4b_ILnK_{n+1}(\frac{b_I}{L})+b_I^2K_{n+2}(\frac{b_I}{L})][(l_I^+)^{2n+1}-(l_I^-)^{2n+1}],$$

$$\frac{\partial^2\Gamma_1^I}{\partial b_I\partial l_I^+}+\frac{\partial^2\Gamma_1^I}{\partial b_I\partial l_I^-}=-\frac{2bK_1(\frac{\sqrt{b_I^2+(l_I^+)^2}}{L})}{L\sqrt{b_I^2+(l_I^+)^2}}+\frac{2bK_1(\frac{\sqrt{b_I^2+(l_I^-)^2}}{L})}{L\sqrt{b_I^2+(l_I^-)^2}},$$

$$\frac{\partial^2\Gamma_1^I}{\partial (l_I^+)^2}+\frac{\partial^2\Gamma_1^I}{\partial (l_I^-)^2}=-\frac{2l_I^+K_1(\frac{\sqrt{b_I^2+(l_I^+)^2}}{L})}{L\sqrt{b_I^2+(l_I^+)^2}}+\frac{2l_I^-K_1(\frac{\sqrt{b_I^2+(l_I^-)^2}}{L})}{L\sqrt{b_I^2+(l_I^-)^2}}. \qquad (4.22e\text{-}j)$$

Eqs. (4.20a-c) can be written as

$$S_{3\alpha 3\beta}=S_{3\alpha 3\beta}^C+S_{3\alpha 3\beta}^G, \qquad (4.23a)$$

where

$$S_{3\alpha 3\beta}^C=\frac{1}{4\pi}\sum_{I=1}^{p}\{(S_1^C)_I(\Theta_{\alpha\beta})_1^I+(S_2^C)_I(\Theta_{\alpha\beta})_2^I\}\equiv\frac{1}{4\pi}\sum_{I=1}^{p}[(S^C)_I][(\Theta_{\alpha\beta})^I]^T \qquad (4.23b)$$

with

$$(S_1^C)_I=\frac{\partial\Lambda_1^I}{\partial b_I},\quad (S_2^C)_I=(\frac{\partial\Lambda_1^I}{\partial l_I^+}+\frac{\partial\Lambda_1^I}{\partial l_I^-}), \qquad (4.23c)$$

$$[(S^C)_I]=[(S_1^C)_I,(S_2^C)_I], \qquad (4.23d)$$

$$[(\Theta_{\alpha\beta})^I]=[(\lambda_I^0)_\alpha(\lambda_I^0)_\beta,(\lambda_I^0)_\alpha(\eta_I^0)_\beta],, \qquad (4.23e)$$

and

$$S^G_{3\alpha 3\beta} = \frac{1}{4\pi}\sum_{I=1}^{p}\{(S_1^G)_I(\Theta_{\alpha\beta})_1^I + (S_2^G)_I(\Theta_{\alpha\beta})_2^I\} \equiv \frac{1}{4\pi}\sum_{I=1}^{p}[(S^G)_I][(\Theta_{\alpha\beta})^I]^T, \quad (4.23f)$$

with

$$(S_1^G)_I = \frac{\partial \Gamma_1^I}{\partial b_I}, \quad (S_2^G)_I = (\frac{\partial \Gamma_1^I}{\partial l_I^+} + \frac{\partial \Gamma_1^I}{\partial l_I^-}), \quad (4.23g)$$

$$[(S^G)_I] = [(S_1^G)_I, (S_2^G)_I]. \quad (4.23h)$$

Similarly, Eqs. (4.21a-d) can be rewritten as

$$T_{3\alpha 3\beta\gamma} = \frac{L^2}{4\pi}\sum_{I=1}^{p}\{T_1^I(\Xi_{\alpha\beta\gamma})_1^I + T_2^I(\Xi_{\alpha\beta\gamma})_2^I + T_3^I(\Xi_{\alpha\beta\gamma})_1^I\} \equiv \frac{L^2}{4\pi}\sum_{I=1}^{p}[T^I][(\Xi_{\alpha\beta\gamma})^I]^T, \quad (4.24a)$$

where

$$T_1^I = \frac{\partial^2(\Lambda_1^I + \Gamma_1^I)}{\partial b_I^2}, \quad T_2^I = \frac{\partial^2(\Lambda_1^I + \Gamma_1^I)}{\partial b_I \partial l_I^+} + \frac{\partial^2(\Lambda_1^I + \Gamma_1^I)}{\partial b_I \partial l_I^-},$$

$$T_3^I = \frac{\partial^2(\Lambda_1^I + \Gamma_1^I)}{\partial (l_I^+)^2} + \frac{\partial^2(\Lambda_1^I + \Gamma_1^I)}{\partial (l_I^-)^2}, \quad (4.24b)$$

$$[T^I] = [T_1^I, T_2^I, T_3^I], \quad (4.24c)$$

$$[(\Xi_{\alpha\beta\gamma})^I_\bullet] = [(\lambda_I^0)_\beta(\lambda_I^0)_\gamma(\lambda_I^0)_\alpha, (\lambda_I^0)_\beta(\lambda_I^0)_\alpha(\eta_I^0)_\gamma + (\lambda_I^0)_\beta(\eta_I^0)_\alpha(\eta_I^0)_\gamma, (\lambda_I^0)_\beta(\eta_I^0)_\alpha(\eta_I^0)_\gamma]. \quad (4.24d)$$

From Eqs. (4.23a,b,f) and (4.24a) it can be seen that all components of the Eshelby tensor **S** and the Eshelby-like tensor **T** can be represented by a position-dependent part related to the position of point **x** inside Ω_I and a direction-dependent basis related to the local coordinate system attached to Ω_I.

Equations (4.23a-h), (4.24a-d) and (4.15a,b) provide general expressions for all non-zero components of the Eshelby tensor **S** and the fifth-order Eshelby-like tensor **T** for an anti-plane strain inclusion with an arbitrary-shape polygonal cross section. All components of **T** will vanish when $L = 0$. Each of the four non-zero Eshelby tensor components can be separated into a classical part, $S^C_{3\alpha 3\beta}$, and a strain gradient part, $S^G_{3\alpha 3\beta}$. $S^C_{3\alpha 3\beta}$ depends on Λ only and involves no elastic constant, while $S^G_{3\alpha 3\beta}$ depends on Γ and is related to L. That is, $S_{3\alpha 3\beta}$ is material microstructure-dependent and can therefore capture the inclusion size effect. When $L = 0$, $S^G_{3\alpha 3\beta} = 0$, and Eqs. (4.20a-c) reduce to Eqs. (4.23a-c) which are $S_{3\alpha 3\beta} = S^C_{3\alpha 3\beta}$ (see Eq. (4.23a)). That is, the Eshelby tensor based on the SSGET is reduced to its counterpart based on classical elasticity when the strain gradient effect is not considered.

4.4 Averaged Eshelby tensor

For applications in homogenization analyses of fiber-reinforced composites, the average of the position-dependent Eshelby tensor over the cross sectional area of the polygonal inclusion is evaluated here.

The procedure for obtaining the averaged Eshelby tensor is similar to that used in the plane strain inclusion case discussed in Chapter III. The averaged Eshelby tensor, $\overline{S}_{3\alpha 3\beta}$, is given by

$$\overline{S}_{3\alpha 3\beta} = \frac{1}{A_\Omega}\{\sum_{N=1}^{p}\sum_{I=1}^{p}\iint_{\Omega_N}(S_N)_{3\alpha 3\beta}(b_I, l_I^+, l_I^-)dA\}, \tag{4.25}$$

where $(S_N)_{3\alpha 3\beta}$ is the Eshelby tensor at point **x** within the triangle Ω_N given by Eqs. (4.23a-h) and (4.15a,b), and Ω_N is the triangle area formed by the global coordinate system origin **O** and the two vertices on the *N*th edge of the polygon. The parameters involved in $(S_N)_{3\alpha 3\beta}$ can be determined as

$$b_I = (v_\alpha^{IN+} - x_\alpha^{IN})(\lambda_I^0)_\alpha^N = (v_\alpha^{IN-} - x_\alpha^{IN})(\lambda_I^0)_\alpha^N, \tag{4.26a}$$

$$l_I^+ = (v_\alpha^{IN+} - x_\alpha^{IN})(\eta_I^0)_\alpha^N, \tag{4.26b}$$

$$l_I^- = (v_\alpha^{IN-} - x_\alpha^{IN})(\eta_I^0)_\alpha^N, \tag{4.26c}$$

with (v_1^{IN+}, v_2^{IN+}), (v_1^{IN-}, v_2^{IN-}) and (x_1^{IN}, x_2^{IN}) being the coordinates of the two vertices on the *N*th edge and point **x** inside the triangle Ω_N in the local coordinate system (λ_N, η_N), and $(\lambda_I^0)_\alpha^N$ and $(\eta_I^0)_\alpha^N$ being the αth components of the unit base vectors $(\boldsymbol{\lambda}_I^0)^N, (\boldsymbol{\eta}_I^0)^N$ in the local coordinate system, (λ_N, η_N) .

Using Eqs. (4.26a-c) in Eq. (4.25) gives

$$\overline{S}_{3\alpha 3\beta} = \frac{1}{A_\Omega}\{\sum_{N=1}^{p}\sum_{I=1}^{p}\iint_{\Omega_N}(S_{NI})_{3\alpha 3\beta}[b_I(\lambda_N,\eta_N), l_I^+(\lambda_N,\eta_N), l_I^-(\lambda_N,\eta_N)]d\lambda_N d\eta_N\}, \tag{4.27}$$

which is applicable to an anti-plane strain inclusion with an arbitrary-shape polygonal cross section.

Note that $(S_{NI})_{3\alpha 3\beta}$ in Eq. (4.27) can be written as

$$(S_{NI})_{3\alpha 3\beta} = \frac{1}{4\pi}[(S)_{NI}[b_I(\lambda_N,\eta_N), l_I^+(\lambda_N,\eta_N), l_I^-(\lambda_N,\eta_N)]][(\Theta_{\alpha\beta})^I]^T, \tag{4.28}$$

where use has been made of Eqs. (4.23a,b) and $S_N = (S^C)_N + (S^G)_N$.

For an inclusion with a regular polygonal cross section, the direction-dependent array $[(\Theta_{\alpha\beta})^I]$ does not change with λ_N or η_N. Hence,

$$\sum_{N=1}^{p}[\iint_{\Omega_N}(S)_{N1}\,d\lambda_N d\eta_N] = \sum_{N=1}^{p}[\iint_{\Omega_N}(S)_{N2}\,d\lambda_N d\eta_N] = \cdots = \sum_{N=1}^{p}[\iint_{\Omega_N}(S)_{Np}\,\lambda_N d\eta_N] = [\Sigma], \quad (4.29)$$

and

$$\sum_{N=1}^{p}\sum_{I=1}^{p}\iint_{\Omega_N}(S_{NI})_{3\alpha 3\beta}[b_I(\lambda_N,\eta_N), l_I^{+}(\lambda_N,\eta_N), l_I^{-}(\lambda_N,\eta_N)]d\lambda_N d\eta_N = \frac{1}{4\pi}\sum_{I=1}^{p}[\Sigma][(\Theta_{\alpha\beta})^I]^T \quad (4.30)$$

Using Eqs. (4.29) and (4.30) in Eq. (4.27) yields

$$\overline{S}_{3\alpha 3\beta} = \frac{1}{4\pi A_\Omega}\sum_{I=1}^{p}[\Sigma][(\Theta_{\alpha\beta})^I]^T, \quad (4.31)$$

where $[\Sigma]$ can be obtained from Eq. (4.29).

It can be seen from Eq. (4.29) that the area integral of the position-dependent array for a sub-part of the Eshelby tensor $(S_I)_{3\alpha 3\beta}$ is *p*-fold rotationally symmetric for an anti-plane strain inclusion whose cross section is a *p*-sided regular polygon. Hence, only the area integral of one part of the Eshelby tensor (e.g., Eshelby tensor computed based on only the *I*th triangle) needs to be evaluated.

4.5 Numerical results

To demonstrate the Eshelby tensor and its area average derived in Sections 4.4 and 4.5, variations of ε_{31} and ε_{32} along the x_1 axis inside an anti-plane strain inclusion with regular polygonal cross section are provided here by directly applying Eqs. (4.7), (4.23a-h) and (4.15a,b). The eigenstrain gradient $\boldsymbol{\kappa}^*$ is set to be zero and the eigenstrain $\boldsymbol{\varepsilon}^*$ are prescribed to be $\varepsilon_{31}^* = \varepsilon_0$ and $\varepsilon_{32}^* = \varepsilon_0$. To illustrate the effect of the sides of the polygon of the non-zero components, the numerical results have been obtained for a series of regular polygons. Also, the inclusion size effect on ε_{31} and ε_{32} are analyzed by examining the results obtained for different inclusion sizes.

In the numerical examples presented below, Poisson's ratio v is taken to be 0.3 and the material length scale parameter is chosen to be 17.6 μm, as was done in chapters II and III. Five types of regular polygonal inclusions, i.e., triangular, square, hexagonal, octagonal and tetrakaidecagonal, are studied for comparison purposes. Each of the inclusions is inscribed in a circle with the radius R, and one vertex of each inclusion is placed on the positive x_1 axis, as shown in Fig. 4.2. Also, three different inclusion size (i.e., $R = 2L$, $R = 4L$, and $R = 6L$) are used to observe the inclusion size effect.

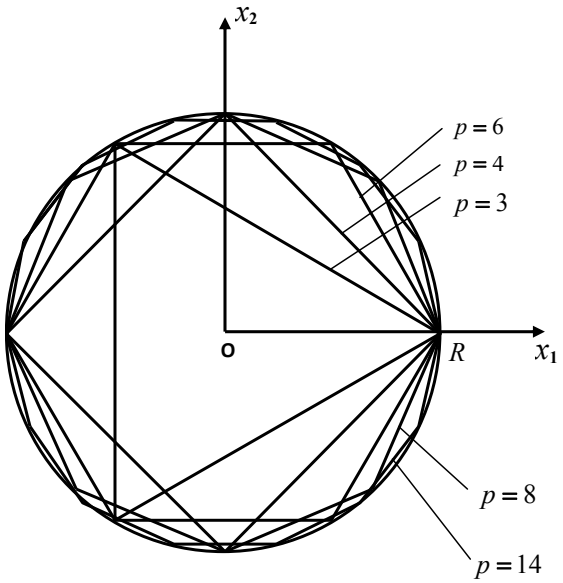

Fig. 4.2 Regular polygonal inclusions inscribed in a circle of radius R with one vertex on the positive x_1 axis for each inclusion.

The variations of the normalized strain component $\varepsilon_{31}/\varepsilon_0$ for the five types of inclusions along the x_1 axis are shown in Figs. 4.3-4.5 for three different inclusions sizes R. Also, the SSGET-based $\varepsilon_{31}/\varepsilon_0$ component for a circular inclusion of radius R is provided for comparison, which is obtained from the formulas derived in Gao and Ma (2011). To show the strain gradient effect, the results of the normalized classical part $(\varepsilon_{31}^C/\varepsilon_0 = S_{3131}^C \varepsilon_{31}^*/\varepsilon_0 + S_{3132}^C \varepsilon_{32}^*/\varepsilon_0)$ for the tetrakaidecagonal and circular inclusions are displaced in Figs. 4.3-4.5 as well.

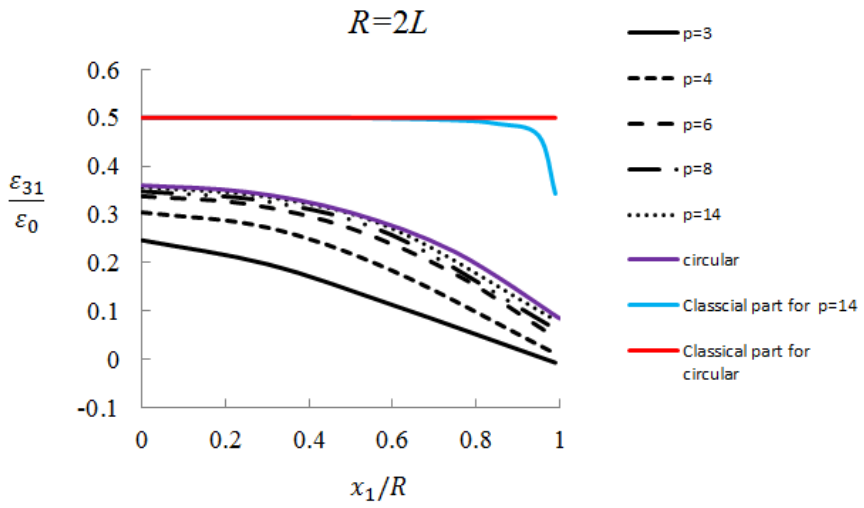

Fig. 4.3 Variations of $\varepsilon_{31}/\varepsilon_0$ along the x_1 axis inside each inclusions with $R = 2L$.

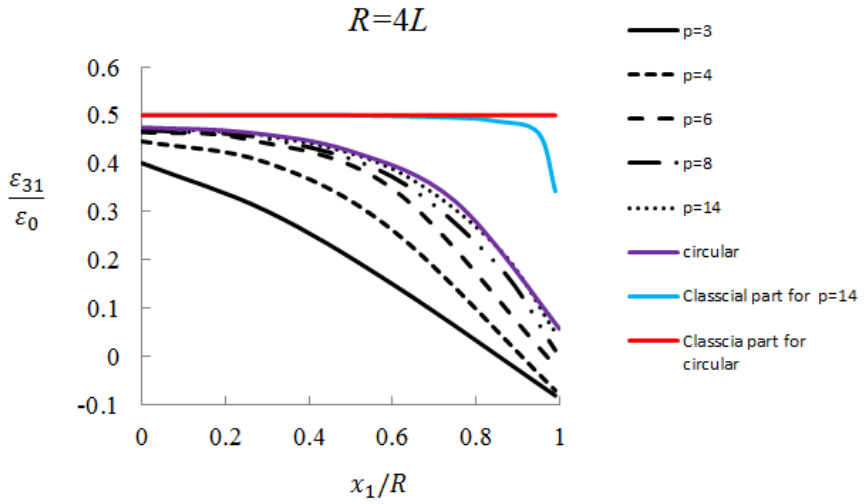

Fig. 4.4 Variations of $\varepsilon_{31}/\varepsilon_0$ along the x_1 axis inside each inclusion with $R = 4L$.

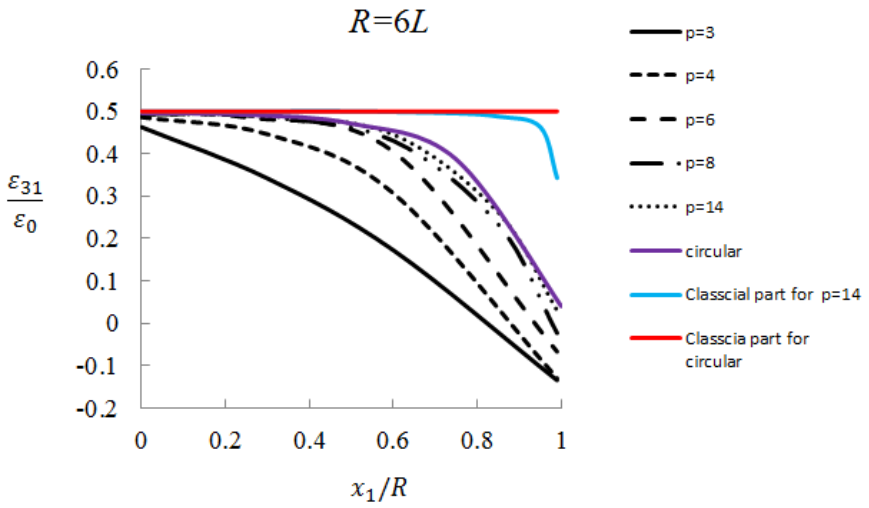

Fig. 4.5 Variations of $\varepsilon_{31}/\varepsilon_0$ along the x_1 axis inside each inclusion with $R = 6L$.

From Figs. 4.3-4.5 it can be seen that the value of classical part ε_{31}^C for the tetrakaidecagonal inclusion is not constant along the x_1 axis, unlike that for the circular inclusion which is uniform within the inclusion (with $\varepsilon_{31}^C/\varepsilon_0 = 0.5$). This confirms the Eshelby conjecture (e.g., Gao and Liu, 2011) in the case of tetrakaidecagonal inclusions. But the curve for the classical part for the 14-sided polygonal inclusion is very close to the line for the circular inclusion except for the boundary region. The values of $\varepsilon_{31}^C/\varepsilon_0$ for tetrakaidecagonal inclusion are the same at a given value of x_1/R for all inclusion sizes, and the same result can be observed for the classical part for the circular inclusion. This means that the Eshelby tensor based on classical elasticity are inclusion size-independent. However, Figs. 4.3-4.5 show that the SSGET-based Eshelby tensor give results that vary with both the position and the inclusion size. When $R = 2L$, it is seen from Figs. 4.3-4.5 that the difference between the $\varepsilon_{31}/\varepsilon_0$ and $\varepsilon_{31}^C/\varepsilon_0$ for the

tetrakaidecagonal inclusion is very significant and cannot be ignored. As the inclusion size increases, this difference becomes much smaller, although it is still considerably large near the boundary. For each value of R/L considered, the value of $\varepsilon_{31}/\varepsilon_0$ increases with the increase of p (i.e., the number of sides of the polygon) at a given position, approaching from below of the values of $\varepsilon_{31}/\varepsilon_0$ for the circular inclusion. As the inclusion size increases (i.e., as R/L goes up), the $\varepsilon_{31}/\varepsilon_0$ curve for each inclusion shape moves upward. When $p = 14$, the $\varepsilon_{31}/\varepsilon_0$ curve is almost coincident with the curve for the circular inclusion at all inclusion sizes, indicating that the SSGET-based Eshelby tensor components for a polygonal inclusion will approach those for a circular inclusion when the number of sides of the polygon is very large (e.g., $p = 14$ here) as expected. For both the circular and polygonal inclusions, the differences between the values given by the SSGET-based Eshelby tensor and those by the classical elasticity-based Eshelby tensor are very significant near the boundary for all values of R/L. This is due to the fact that the largest strain gradient exists near the inclusion boundary. Also, it suggests that an even larger inclusion size (e.g., $R/L = 12$) may be needed in order to be able to neglect the inclusion size effect.

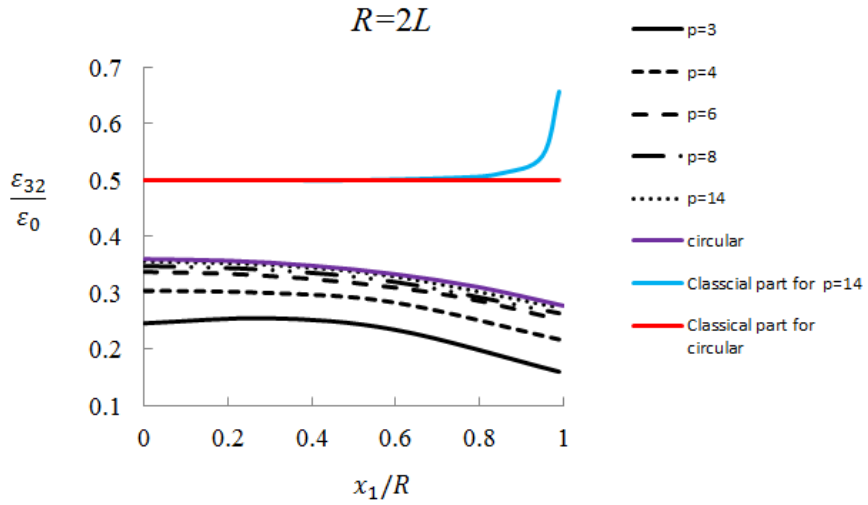

Fig. 4.6 Variations of $\varepsilon_{32} / \varepsilon_0$ along the x_1 axis inside each inclusion with $R = 2L$.

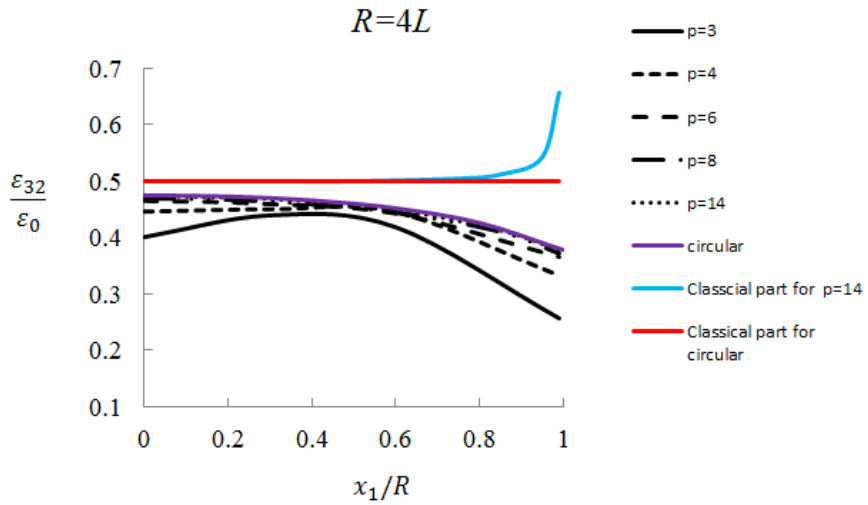

Fig. 4.7 Variations of $\varepsilon_{32} / \varepsilon_0$ along the x_1 axis inside each inclusion with $R = 4L$.

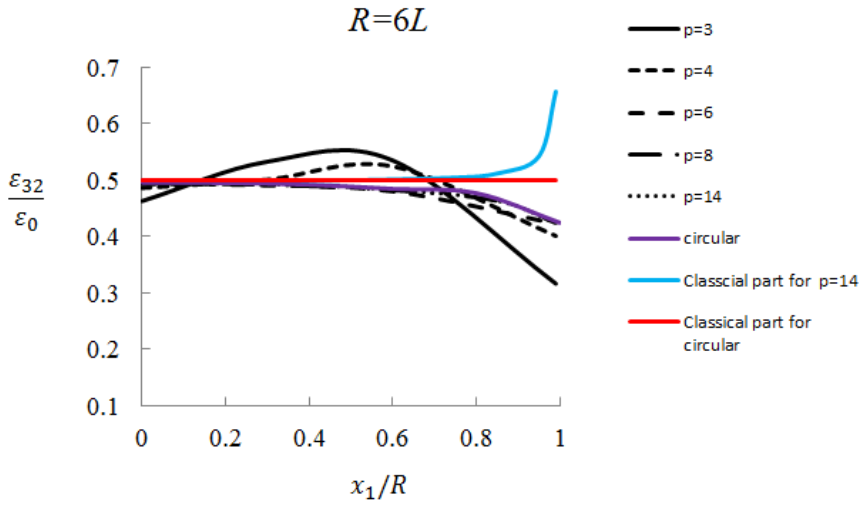

Fig. 4.8 Variations of $\varepsilon_{32}/\varepsilon_0$ along the x_1 axis inside each inclusion with $R = 6L$.

The variations of $\varepsilon_{32}/\varepsilon_0$ with the position and inclusion size for the five polygonal inclusion shapes and its counterpart $\varepsilon_{32}^C/\varepsilon_0$ for the tetrakaidecagonal inclusion are shown in Figs. 4.6-4.8, where, the curves for a circular inclusion are also provided for comparison. Obviously, the classical part $\varepsilon_{32}^C/\varepsilon_0$ is again uniform in a circular inclusion with a value of 0.5 for all the inclusion sizes, while the counterpart for the tetrakaidecagonal inclusion varies along the x_1 axis with a sudden jump near the boundary. Both of these two classical parts do not change with the inclusion size. The trends for the changes of $\varepsilon_{32}/\varepsilon_0$ with the inclusion size and the number of sides of the polygon are observed to be similar to those for the $\varepsilon_{31}/\varepsilon_0$ curves. For the inclusion sizes $R = 2L$ and $R = 4L$, the $\varepsilon_{32}/\varepsilon_0$ curve for a circular inclusion provides an upper bound to the curves for all the polygonal inclusions considered. When the number of sides of the polygon is large enough (i.e., p=14 here), the circular inclusion result can be well

approximated by such a polygonal inclusion. However, for the inclusion size $R = 6L$, irregular large values for the triangular and square inclusions are observed at around $x_1/R = 0.5$. This may be due to the non-symmetry of the triangular inclusion about the x_2 axis and the peculiarity of the square inclusion which has been found in 2D plane strain analysis of Kawashita and Nozaki (2001). Also, for both the circular and polygonal inclusions, the differences between the values given by the SSGET-based and classical elasticity-based Eshelby tensors are still very large near the boundary even for a large inclusion (i.e., R/L=6) because of the largest strain gradient near the inclusion boundary.

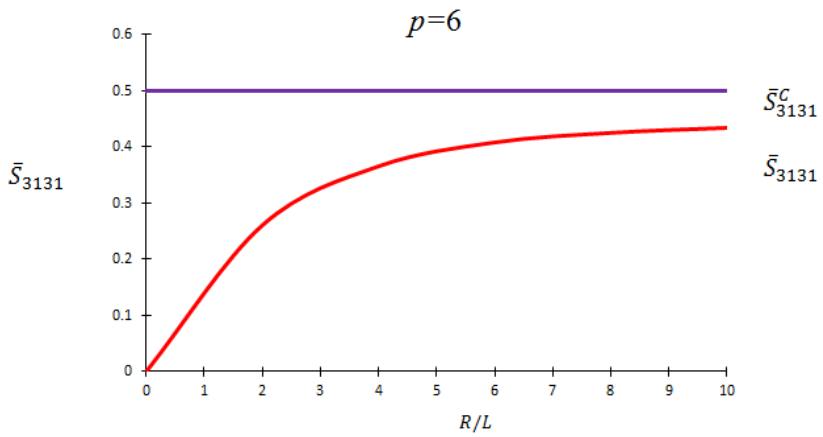

Fig. 4.9 Variation of $\bar{S}_{3131}$ with the inclusion size: (*a*) hexagonal, (*b*) octagonal, and (*c*) Tetrakaidecagonal.

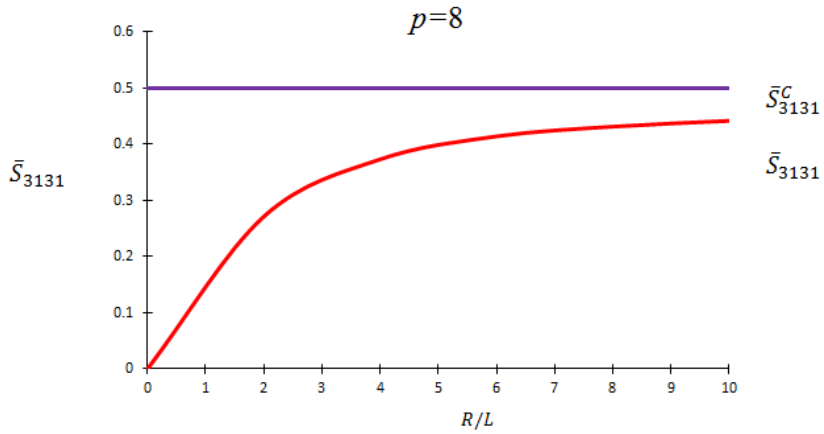

(*b*)

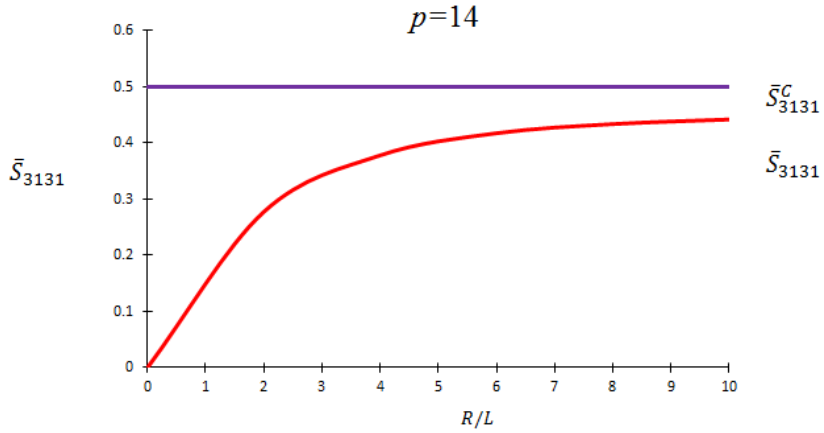

(*c*)

Fig. 4.9 Continued.

The results for the averaged Eshelby tensor component $\overline{S}_{3131}$ for three types of inclusions (i.e., hexagonal, octagonal and tetrakaidecagonal) have been obtained using Eqs. (4.31), (4.23a-e) and (4.15a,b) and displayed in Fig. 4.9. From Fig. 4.9 it can be concluded that for each polygonal inclusion, the classical part $\overline{S}^{C}_{3131}$ is a constant and equal to the value obtained for the circular inclusion. But the strain gradient part

$\overline{S}^{G}_{3131}(=\overline{S}_{3131}-\overline{S}^{C}_{3131})$ changes with the inclusion size. For all three types of inclusions, when inclusion is small, the difference between the SSGET-based value and the classical value is very large and cannot be neglected. However, when inclusion is large enough, the effect of the strain gradient part becomes insignificant and may be ignored. For the same value of R/L, $\overline{S}_{3131}$ increases with the number of sides of the polygonal inclusion. When R/L is sufficiently large (i.e., $R/L \geq 8$), this effect is very small and thus can be neglected.

4.6 Summary

The Eshelby tensor for an anti-plane strain inclusion with an arbitrary shape polygonal cross section is analytically derived using the simplified strain gradient elasticity theory (SSGET). The newly derived Eshelby tensor is separated into a classical part and a gradient part. The former does not depend on any material constant, while the latter is directly related to a material length scale parameter that enables the explanation of the inclusion size effect. The area average of the Eshelby tensor is also obtained in a general form.

To illustrate the Eshelby tensor and its area average, variations of the two non-vanishing strain components with the position and inclusion size are quantitatively studied for five types of regular polygonal inclusions. The results for an anti-plane strain circular inclusion based on the SSGET are also induced for comparison. The numerical result show that the disturbed strain components vary with the position in the inclusion and change with the inclusion size. The size effect is very significant when inclusion is

small. For large inclusions, the size effect becomes much smaller and may be ignored. When the number of sides of the polygon increases, the curves of components for the regular polygonal inclusions approach from below the curve for the circular inclusion, which provides an upper bound. The numerical results for the averaged Eshelby tensor components at different inclusion sizes reveal that the size effect may be neglected only when the inclusions size is very large.

CHAPTER V

CONCLUSIONS

The Eshelby-type problems of a polygonal or a polyhedral inclusion of arbitrary shape embedded in an infinite homogeneous isotropic elastic body are analytically solved by using a simplified strain gradient elasticity theory (SSGET) that contains a material length scale parameter. The SSGET-based Eshelby tensors are derived in general forms in terms of three potential functions for both the polyhedral and plane strain polygonal inclusions, and two potential functions for the anti-plane polygonal inclusion. Each of the newly obtained Eshelby tensors is separated into a classical part and a gradient part. The gradient part contains a material length scale parameter, which enables the interpretation of the inclusion size effect. This gradient part vanishes and the Eshelby tensor reduces to its counterpart based on classical elasticity when the material length scale parameter is zero. The each SSGET-based volume or area average of Eshelby tensor over the polyhedral inclusion domain or over the polygonal cross section is also obtained for homogenization analyses of composites containing polyhedral or polygonal inclusions.

For the polyhedral inclusion problem the numerical results show that the classical part of the Eshelby tensor varies with the position within the polyhedral inclusion but does not depend on the inclusion size, while, the newly obtained Eshelby tensor changes with both the position and inclusion size. When the inclusion is small, the gradient part contributes significantly and should not be ignored. This size effect becomes small as the

inclusion size increases. Also, it is observed that the components of the volume averaged Eshelby tensor become smaller when the inclusion size gets smaller. Hence, the inclusion size effect may be neglected for large polyhedral inclusions in some cases.

For the plane strain polygonal inclusion problem, the similar trends have been observed. Also, it has been found that the area averaged Eshelby tensor increase with the number of sides of the polygonal inclusion and the difference between the averaged values of different polygonal inclusions can be neglected when the inclusion size is sufficiently large.

The solution for the Eshelby-type problem of an anti-plane strain inclusion with an arbitrary polygonal cross-sectional shape is also analytically derived using the SSGET. Both the Eshelby tensor and its area average over the polygonal cross section are obtained in general forms. Five types of regular polygonal inclusions are quantitatively studied by applying the general expressions of the Eshelby tensor obtained. For each of the inclusion shapes, the disturbed strain components based on classical elasticity are seen to vary with the position but not change with the inclusion size. However, the components of the disturbed strain evaluated using the newly obtained Eshelby tensor based on the SSGET change with not only the position but also the inclusion size. When the inclusion size is small, the contribution of the gradient part is significantly large and should not be neglected. As the number of the sides of the polygonal inclusion increases, the components of the disturbed strain approach from below the values of those for the circular inclusion. Also, it is found that when the inclusion is small, the averaged Eshelby tensor components strongly depend on the

inclusion size: the smaller the inclusion, the smaller the component values. Therefore, the inclusion size effect may be ignored only for large polygonal inclusions undergoing anti-plane strain deformations. In addition, the number of sides of the polygonal inclusion affects the averaged Eshelby tensor, which increases with the number of sides. This effect will vanish for a considerably large inclusion size.

REFERENCES

Ammari, H., Capdeboscq, Y., Kang, H., Lee, H., Milton, G.W. and Zribi, H., 2010. Progress on the strong Eshelby's conjecture and extremal structures for the elastic moment tensor. Journal de Mathématiques Pures et Appliqués. 94, 93–106.

Chiu, Y.P., 1977. On the stress field due to initial strains in a cuboid surrounded by an infinite elastic space. ASME J. Appl. Mech. 44, 587–590.

Cho, J., Joshi, M.S. and Sun, C.T., 2006. Effect of inclusion size on mechanical properties of polymeric composites with micro and nano particles. Compos. Sci. Tech. 66, 1941–1952.

Cheng, Z.-Q. and He, L.-H., 1995. Micropolar elastic fields due to a spherical inclusion. Int. J. Eng. Sci. 33, 389–397.

Cheng, Z.-Q. and He, L.-H., 1997. Micropolar elastic fields due to a circular cylindrical inclusion. Int. J. Eng. Sci. 35, 659–668.

Eshelby, J.D., 1957. The determination of the elastic field of an ellipsoidal inclusion, and related problems. Proc. R. Soc. Lond. A 241, 376–396.

Eshelby, J.D., 1959. The elastic field outside an ellipsoidal inclusion. Proc. R. Soc. Lond. A 252, 561–569.

Eshelby, J.D., 1961. Elastic inclusions and inhomogeneities. Progress in Solid Mechanics (Ed. I. N. Sneddon and R. Hill), Vol. 2, pp. 89–140. North-Holland, Amsterdam.

Gao, X.-L., 1996. A mathematical analysis of the elasto-plastic anti-plane shear problem of a power-law material and one class of closed-form solutions. Int. J. Solids Struct. 33, 2213-2223.

Gao, X.-L. and Li, K., 2005. A shear-lag model for carbon nanotube-reinforced polymer composites. Int. J. Solids Struct. 42, 1649-1667.

Gao, X.-L. and Ma, H.M., 2009. Green's function and Eshelby's tensor based on a simplified strain gradient elasticity theory. Acta Mech. 207, 163–181.

Gao, X.-L. and Ma, H.M., 2010a. Solution of Eshelby's inclusion problem with a bounded domain and Eshelby's tensor for a spherical inclusion in a finite spherical matrix based on a simplified strain gradient elasticity theory. J. Mech. Phys. Solids 58, 779–797.

Gao, X.-L. and Ma, H.M., 2010b. Strain gradient solution for Eshelby's ellipsoidal inclusion problem. Proc. R. Soc. A 466, 2425-2446.

Gao, X-L. and Ma, H.M., 2011. Strain gradient solution for the Eshelby-type anti-plane strain inclusion problem. Manuscript to be submitted to Acta Mech.

Gao, X.-L. and Park, S.K., 2007. Variational formulation of a simplified strain gradient elasticity theory and its application to a pressurized thick-walled cylinder problem. Int. J. Solids Struct. 44, 7486–7499.

Gao, X.-L. and Rowlands, R. E., 2000. Hybrid method for stress analysis of finite three-dimensional elastic components. Int. J. Solids Struct. 37, 2727–2751.

Glas, F., 2001. Elastic relaxation of truncated pyramidal quantum dots and quantum wires in a half space: an analytical calculation. J. Appl. Phys. 90, 3232-3241.

Jhaver, R. and Tippur, H., 2009. Processing, compression response and finite element modeling of syntactic foam based interpenetrating phase composite (IPC). Mater. Sci. Eng. A 499, 507-517.

Kawashita, M. and Nozaki, H., 2001. Eshelby tensor of a polygonal inclusion and its special properties. J of elasticity 64, 71-84.

Kiris, A. and Inan, E., 2006. Eshelby tensors for a spherical inclusion in microstretch elastic fields. Int. J. Solids Struct. 43, 4720–4738.

Kuvshinov, B.N., 2008. Elastic and piezoelectric fields due to polyhedral inclusions. *Int.* J. Solids. Struc. 45, 1352–1384.

Le Quang, H., He, Q.-C. and Zheng, Q.-S., 2008. Some general properties of Eshelby's tensor fields in transport phenomena and anti-plane elasticity. Int. J. Solids Struct. 45, 3845-3857.

Lee, J.K. and Johnson, W.C., 1978. Calculation of the elastic strain field of a cuboidal precipitate in an anisotropic matrix. Phys. Stat. Sol. (a) 46, 267–272.

Li, K., Gao, X.-L. and Roy, A.K., 2003. Micromechanics model for three-dimensional open-cell foams using a tetrakaidecahedral unit cell and Castigliano's second theorem. Compos. Sci. Tech. 63, 1769–1781.

Li, K., Gao, X.-L. and Subhash, G., 2006. Effects of cell shape and strut cross-sectional area variations on the elastic properties of three-dimensional open-cell foams. J. Mech. Phys. Solids 54, 783–806.

Li, X.F. and Lee, K.Y., 2004. Electroelastic behavior of a rectangular piezoelectric ceramic with an antiplane shear crack at arbitrary position. Eur. J. Mech. A Solids 23, 645–658.

Li, S., Sauer, R. and Wang, G.., 2005. A circular inclusion in a finite domain I. The Dirichlet-Eshelby problem. Acta. Mech. 179, 67–90.

Li, S. and Wang, G.., 2008. Introduction to Micromechanics and Nanomechanics. World Scientific, Singapore.

Liu, L.P., 2008. Solutions to the Eshelby conjectures. Proc. R. Soc. A 464**,** 573–594.

Liu, X.N. and Hu, G.K., 2004. Inclusion problem of microstretch continuum. Int. J. Eng. Sci. 42, 849–860.

Liu, S. and Wang, Q., 2005. Elastic fields due to eigenstrains in a half-space. ASME J. Appl. Mech. 72, 871–878.

Lubarda, V.A., 2003. Circular inclusions in anti-plane strain couple stress elasticity. Int. J. Solids Struct. 40, 3827-3851.

Lubarda, V.A. and Markenscoff, X., 1998. On the absence of Eshelby property for non-ellipsoidal inclusions. Int. J. Solids Struct. 35, 3405–3411.

Ma, H.M. and Gao, X.-L., 2010a. Eshelby's tensors for plane strain and cylindrical inclusions based on a simplified strain gradient elasticity theory. Acta Mech. 211, 115–129.

Ma, H.M. and Gao, X.-L., 2011. Strain gradient solution for a finite-domain Eshelby-type plane strain inclusion problem and Eshelby's tensor for a cylindrical inclusion in a finite elastic matrix. Int. J. Solids Struct. 48, 44–55.

Ma, H.S. and Hu, G.K., 2006. Eshelby tensors for an ellipsoidal inclusion in a micropolar material. Int. J. Eng. Sci. 44, 595–605.

Ma, H.S. and Hu, G.K., 2007. Eshelby tensors for an ellipsoidal inclusion in a microstretch material. Int. J. Solids Struct. 44, 3049–3061.

Marcadon, V., Herve, E. and Zaoui, A., 2007. Micromechanical modeling of packing and size effects in particulate composites. Int. J. Solids Struct. 44, 8213–8228.

Markenscoff, X. 1998a. On the shape of the Eshelby inclusions. J. Elasticity 49, 163–166.

Markenscoff, X. 1998b. Inclusions with constant eigenstress. J. Mech. Phys. Solids 46, 2297–2301.

Michelitsch, T.M., Gao, H. and Levin, V.M., 2003. Dynamic Eshelby tensor and potentials for ellipsoidal inclusions. Proc. R. Soc. Lond. A 459, 863–890.

Mura, T., 1987. Micromechanics of Defects in Solids, 2nd ed. Martinus Nijhoff, Dordrecht.

Nemat-Nasser, S. and Hori, M., 1999. Micromechanics: Overall Properties of Heterogeneous Materials, 2nd ed. Elsevier Science, Amsterdam.

Nenashev, A.V. and Dvurechenskil, A.V., 2010. Strain distribution in quantum dot of arbitrary polyhedral shape: analytical solution. J. Appl. Phys. 107, 064322-1~8.

Nozaki, H., Horibe, T. and Taya, M., 2001. Stress field caused by polygonal inclusion. JSME Int, J. Series A 44, 472-482.

Nozaki, H. and Taya, M., 1997. Elastic fields in a polygonal-shaped inclusion with uniform eigenstrain. Jour. Appl. Mech. 64, 495-502.

Nozaki, H. and Taya, M., 2001. Elastic fields in a polyhedral inclusion with uniform eigenstrains and related problems. ASME J. Appl. Mech. 68, 441–452.

Pan, E., 2004. Eshelby problem of polygonal inclusions in anisotropic piezoelectric full and half plane. Jour. Mech. Phys. Solids 52, 567-589.

Pearson, G.S. and Faux, D.A., 2000. Analytical solutions for strain in pyramidal quantum dots. J. Appl. Phys. 88, 730–736.

Polyzos, D., Tsepoura, K.G., Tsinopoulos, S.V., and Beskos, D.E., 2003. A boundary element method for solving 2D and 3D static gradient elastic problems Part I: Integral formulation. Comp. Methods Appl. Mech. Engr. 192, 2845-2873.

Poniznik, Z., Salit, V., Basista, M. and Gross, D., 2008. Effective elastic properties of interpenetrating phase composites**.** Comput. Mater. Sci. 44, 813–820.

Rodin, G.J., 1996. Eshelby's inclusion problem for polygons and polyhedra. J. Mech. Phys. Solids 44, 1977-1995.

Rowlinson, J.S., 1989. The Yukawa potential. Physics. A 156, 15-34.

Ru, C.Q., 1999. Analytical solution for Eshelby's problem of an inclusion of arbitrary shape in a plane or half-plane. J. Appl. Mech. 66, 315-322.

Ru, C.Q., 2000. Eshelby's problem for two-dimensional piezoelectric inclusions of arbitrary shape. Proc. R. Soc. Lond. A 456, 1051-1068.

Timoshenko, S.P. and Goodier, J.N., 1970. Theory of Elasticity, 3rd ed. McGraw-Hill, New York.

Tsukrov, I. and Novak, J., 2004. Effective elastic properties of solids with two-dimensional inclusions of irregular shapes. Int. J. Solids. Struct. 41, 6905-6924.

Vollenberg, P.H.T. and Heikens, D., 1989. Particle size dependence of the Young's modulus of filled polymers: 1. Preliminary experiments. Polymer 30, 1656–1662.

Waldvogel, J., 1979. The Newtonian potential of homogeneous polyhedra. *Z. A. M. P.* 30, 388-398.

Wang, J., Michelitsch, T.M., Gao, H. and Levin, V.M., 2005. On the solution of the dynamic Eshelby problem for inclusions of various shapes. Int. J. Solids Struct. 42, 353–363.

Xu, B.X. and Wang, M.Z., 2005. Special properties of Eshelby tensor for a regular polygonal inclusion. Acta. Mech. Sinica. 21, 267-271.

Xu, B.X. and Wang, M.Z., 2007a. The arithmetic mean property for rotational symmetrical inclusions with rotational symmetrical eigenstrains. Z. Angew. Math. Mech. 87, 59-69.

Xu, B.X. and Wang, M.Z., 2007b. The arithmetic mean theorem for the *N*-fold rotational symmetrical inclusion in anti-plane elasticity. Acta Mech. 194, 233–242.

Zheng, Q.-S. and Zhao, Z.-H., 2004. Green's function and Eshelby's fields in couple-stress elasticity. Int. J. Multiscale Comput. Eng. 2, 15–27.

Zheng, Q.S., Zhao, Z.H. and Du, D.X., 2006. Irreducible structure, symmetry and average of Eshelby's tensor fields in isotropic elasticity. J. Mech. Phys. Solids 54, 368-383.

Zou, W.N., He, Q.C., Huang, M.J. and Zheng, Q.S., 2010. Eshelby's problem of non-elliptical inclusions. J. Mech. Phys. Solids. 58, 346-372.

VITA

Mengqi Liu received her Bachelor of Engineering degree in mechanical engineering from Beijing Institute of Technology, China, in 2004. She received her Master of Science degree in mechanical engineering from Southern Methodist University in 2007 and doctoral degree in mechanical engineering from Texas A&M University in 2011. Her research interests include micromechanics, finite element analysis and composites.

She may be reached at shuailang2010@gmail.com or Department of Mechanical Engineering, Texas A&M University, 3123 TAMU, College Station, Texas 77843-3123, United States of America.